UNIVERSITY OF CALIFORNIA,
IRVINE

# Water evaporation during methane hydrate combustion

THESIS

submitted in partial satisfaction of the requirements
for the degree of

MASTER OF SCIENCE

in Mechanical and Aerospace Engineering

by

Joan Santacana Vall

Thesis Committee:
Professor Derek Dunn-Rankin, Chair
Associate Professor Jack Brouwer
Adjunct Professor Vincent McDonell

2014

## TABLE OF CONTENTS

# LIST OF FIGURES

# LIST OF TABLES

# ACKNOWLEDGMENTS

I would like to thank my advisor during the master thesis, Professor Derek Dunn-Rankin for all the help, guidance and productive discussions about the research that made me grow as a student, researcher and also as a person.

Also I am grateful to Dr. Sunny Karnani and Michela Vicariotto for sharing their knowledge and work with me during all the project and experiments; it has been a great experience working with them. I have to thank all my LFA lab-mates for the suggestions and support during all the time we have been working together.

My gratitude to the W.M. Keck Foundation for financing the project. Finally I would like to thank the Balsells Fellowship program and Peter Balsells for giving me the financial support and the opportunity to do my studies and research in the University of California Irvine.

# ABSTRACT OF THE THESIS

Water evaporation during methane hydrate combustion

by

Joan Santacana Vall

Master of Science in Mechanical and Aerospace Engineering

University of California, Irvine, 2014

Professor Derek Dunn-Rankin, Chair

Methane hydrates are ice-like non-stoichiometric crystalline solids composed of water cages that are stabilized by the presence of a guest methane molecule. They occur naturally in the permafrost and in deep ocean sediments. They represent a potential mega-resource of energy and, at the same time, they can have a substantial potential impact on the environment.

This project studies experimentally the formation and direct combustion of methane hydrates. Formation of methane hydrates samples is a complex process that needs precise control due to fragile stability of the hydrates at high pressure within narrow time and temperature ranges. Heat from the combustion process dissociates the hydrate into water and methane, which feeds the methane-air diffusion flame. In this thesis, uniform, repeatable and high quality samples were successfully formed with a clathration of 81.82 ±3.39%. Another achievement was that the samples burned completely and they had three different regimes, an initial one of 1 second based on the propagation of the flame, a second one between 1 and 5 second with a bright and high flame and finally the quasi-steady state regime after 5 seconds until the end of the process. The accomplishment of reaching this

quasi-steady state regime permitted the determination of key properties of the combustion behavior. The results show that the burning rate at this regime is 2.5 mg/s*cm$^2$, a flame temperature estimated between 1550 and 2050 K and the novelty of determining the water vapor content versus methane in the flame, which is between 0.5 and 1.5 by molar ratio. Finally the energy balance model showed that 25% of the heat is needed for dissociation of the hydrate and the remaining heat produces approximately 470 kW/m$^2$.

# INTRODUCTION

## Description of methane hydrates/clathrates

Methane hydrates (also called methane clathrates) consist of a cage like crystalline water structure with a guest methane molecule trapped inside. The methane molecule gets captured and sealed inside the surrounding water molecule structure by supporting the hydrogen-bonded water in a thermodynamically stable configuration.

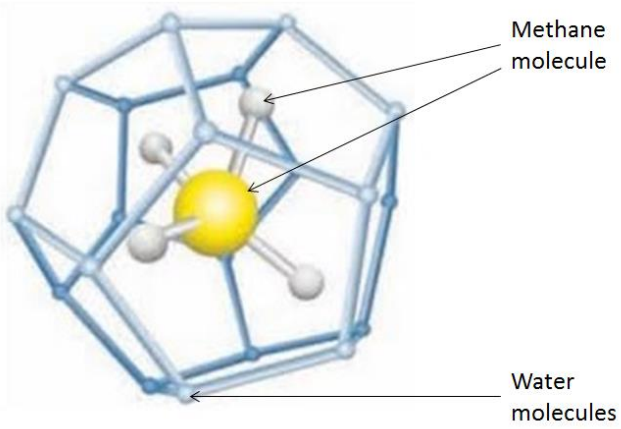


**Figure 1. Methane clathrate structure [1].**

As seen in Figure 1, the methane molecule, consisting of one carbon atom and four hydrogen atoms, gets trapped by hydrogen-bonded water molecules. Clathrates are, therefore, composed of crystalline solids made of ice and gas [2]. Form a sample requires the thermodynamic conditions that encourage hydrate formation, with gas molecules inside ice, in crystalline form, and it is also necessary to create sufficient interaction surface for the process to develop on a reasonable timescale. It is known that gas hydrates are formed at an elevated pressure and low temperature when the gas concentration exceeds the solubility limit [4-5], and various authors have explored methods to increase the rate of hydrate formation [3, 6-8].

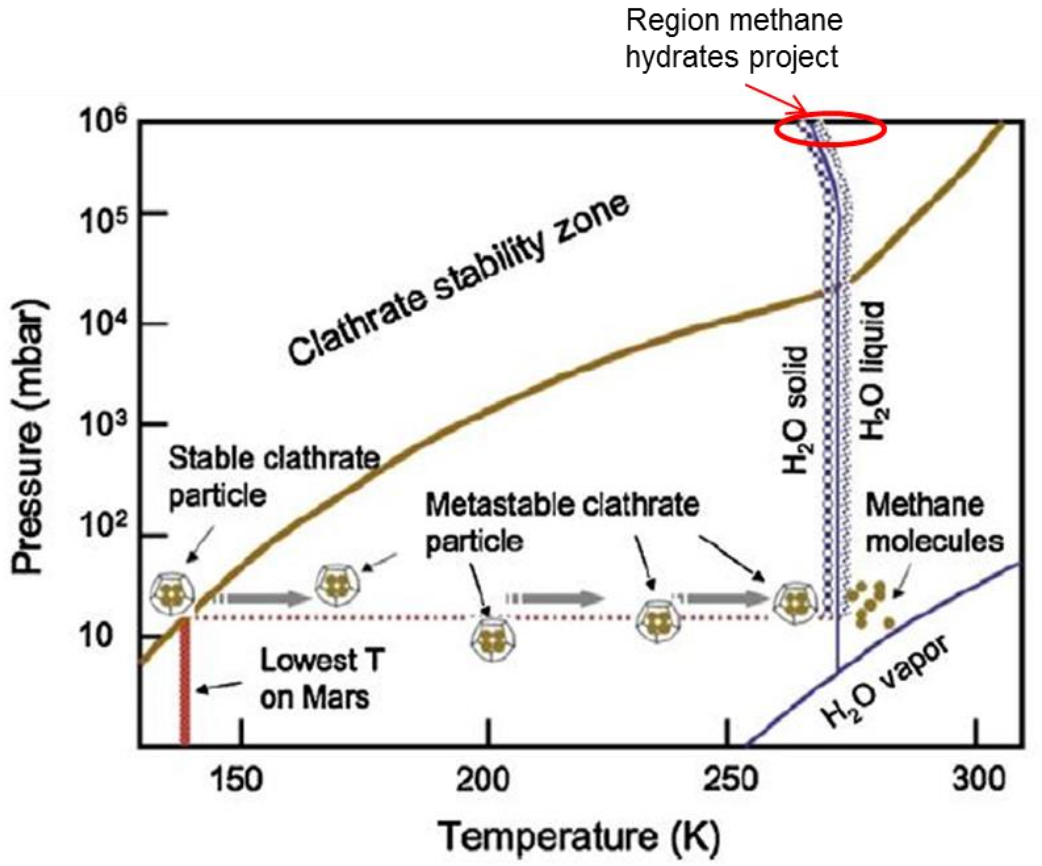


**Figure 2. Phase diagram of methane clathrate and water [9]. with the condition of the project indicated in red.**

In Figure 2 it is possible to see the phase diagram of methane hydrates and their stability line marked in brown. Marked in red is the region where the samples are formed in the present work and experiments. This region is between 1100 and 1500 psi (75 and 100 bar), and a temperature around the melting point of water (273 K).

In this project the guest molecule will be methane but it is possible to form a sample with ethane, propane or carbon dioxide, as well. Carbon dioxide hydrates in particular are interesting for their potential in greenhouse gas sequestration [39], but that subject is beyond the scope of this thesis. Based on the structure I hydrates of pure methane, explained in section below, the molar ratio of methane to water would be approximately 1:5.75, for an ideally saturated methane hydrates [2]. It is this value against which the level of clathration achieved in the experiments is compared. A piece of a natural methane

hydrate can be seen in Figure 3. Methane hydrates need to be formed with other materials or within sediments of the sea floor to be stable because pure hydrates have lower density than seawater and would therefore buoyantly rise. Methane is an attractive energy source because it is less carbon intensive than other hydrocarbons, such as oil or coal. Its combustion yields 44% less $CO_2$ than coal per each unit of energy released and 29% less compared to oil.

**Figure 3. Natural methane hydrate at the deep ocean [22].**

Researchers are studying methane hydrates for a wide variety of applications, ranging from chemical separations to mass and energy storage. Using methane hydrates as gas storage is very interesting since they permit compact storage space even at much lower pressure than their formation, improving the safety conditions. In this case the energy density is equivalent to that of a highly compressed gas, and it requires less energy to create than liquified gas since the temperature is warmer and pressure lower. The possibility of using methane hydrates as an alternative source of energy and natural gas is based on different estimations of the potential reserves that range from $7.6 \times 10^{18}$ $m^3$ [34] to $3.1 \times 10^{15}$ $m^3$ [35]. More detailed studies showed the potential resources to be closer to $1.5 \times 10^{16}$ $m^3$ [36].

In the mid-late 1990's, some thought was given to the possibility that methane clathrates would be the next step in green energy conversion; in 1995 was the first Ocean Drilling

Program (ODP) along the South Carolina coast. Then in 2000 the U.S. government signed a bill for research and development of methane clathrates [1]. Regardless of the large amount of methane available in hydrate form, their extraction from seafloor mounds and outcroppings is difficult, and currently only a small part can be extracted. In addition, there is a potential for disruption of seafloor ecosystems that depend on these deposits.

Methane is a strong greenhouse; therefore hydrates represent a substantial potential impact to the environment when methane is released in an uncontrolled manner. For example, it is highly probable that the disassociation of marine sedimentary methane hydrates induced episodes of rapid climate change warming through greenhouse forcing by atmospheric methane at various times in the geologic past [37].

**Hydrate structure**

The structure of methane hydrates is based in two important features: crystal structure and cavities [2]. Hydrate structures are composed of five polyhedrals formed by hydrogen-bonded water molecules. These cavities vary with temperature, pressure and guest composition. They are expanded relative to a pure ice structure, and are prevented from collapse by the repulsive presence of the guest molecule either in the cavity itself or in a large percentage of the neighboring cavities.

There are three main crystal structures of natural gas hydrates: cubic structure I, cubic structure II, or hexagonal structure H. The structure is formed by water molecules bonded by hydrogen in a solid lattice. Methane hydrate has a cubic structure I, since the diameter of the molecule is between 4.2 and 6 Angstrom. In this structure there are only 46 water molecules, and eight polyhedrals within the cube, two pentagonal dodecahedron ($5^{12}$) and six ($5^{12}6^2$) cavities.

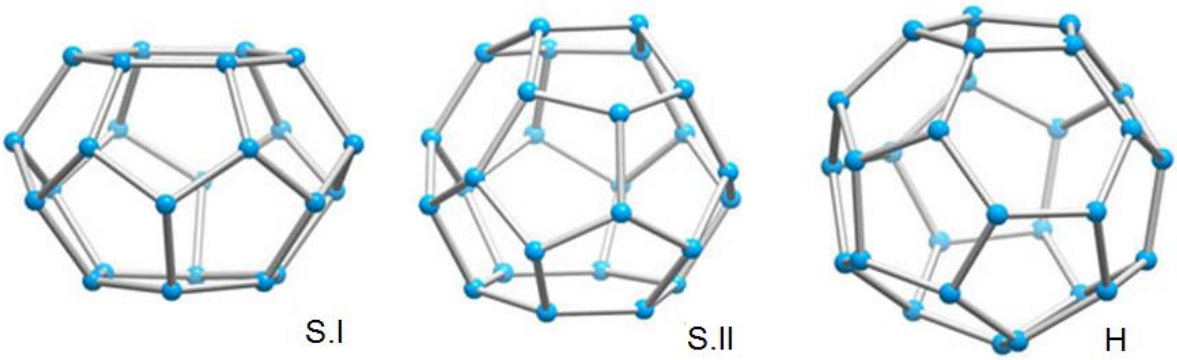


**Figure 4. Hydrate structures [38].**

**Literature review of the combustion of methane hydrates**

Methane hydrates are being considered an alternative source of energy, even though there have been only few studies on the direct combustion of this ice-like fuel. The internet has many photographs and videos of methane hydrates burning, commonly named as “burning ice”. Figure 5 shows a typical sample image that demonstrates the flammability of hydrates but contain no information about the important characteristics of the combustion.

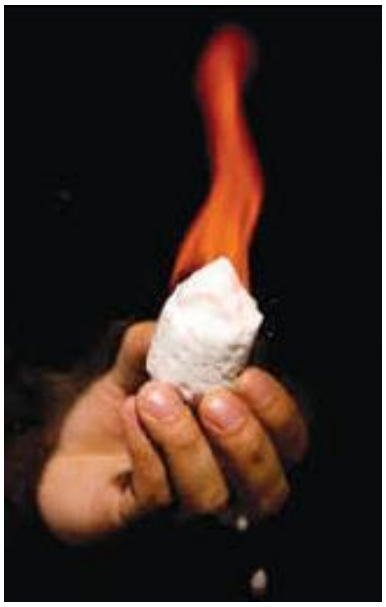

**Figure 5. Image of methane hydrate burn [25].**

There are some papers from researchers in Japan who tried to explain, using the classic Emmons problem configuration, some fundamental information on hydrate combustion

[26-29]. They found that under flat-plate combustion conditions hydrates exhibit a self-healing process that is very similar to that seen in hydrates warmed in other ways [30-31]. The phenomena of self-healing appears during combustion in the boundary layer flow because, when there is no methane, water is cooled past the solidus boundary through contact with the sub-cooled solid hydrate layers below. Another group of researchers in Russia described hydrate combustion as a porous media, including internal hydrate temperature but their work had no measurements of flame temperature or burning rates [32-33].

**Aims of the thesis**

In the present project, the formation process of methane hydrate samples is improved from previous work [11, 13] to achieve reproducibility and high quality hydrates. A differential weight experiment is designed to measure the mass of hydrate, water melted, and gas released. The gas released is studied to determine the species composition of the flame. Further calculations were done to determine key properties of the combustion behavior. For the first time, the water content inside the flame is determined during the combustion process of a methane hydrate. Dissociation rates, burning rates, molar ratios of water evaporated versus methane, heat flow to the hydrate and surroundings, heat of combustion, regression rate and flame temperatures are some properties calculated from the data collected in the experiments. The main goals of the present thesis are:

- Formation in the laboratory of uniform, equal and reproducible samples.
- Determine the natural dissociation of methane hydrates.
- Explain physically the combustion process of methane hydrates.
- Design an experimental setup for differential weight measurements during combustion.
- Calculate and determine the key characteristics of the combustion behavior.
- Water vapor content of the flame.
- Energy model of the combustion.

# DESIGN

## Design of the experiment

The combustion experiment design consists of differential weight measurements of the hydrate sample and the water melted during combustion. The design is based on two load cells, a mesh where the sample burns, a beaker for the water melted, an isolation system to reduce vibrations and the data acquisition control. Figure 6 shows the set up for a sample being examined during burning.

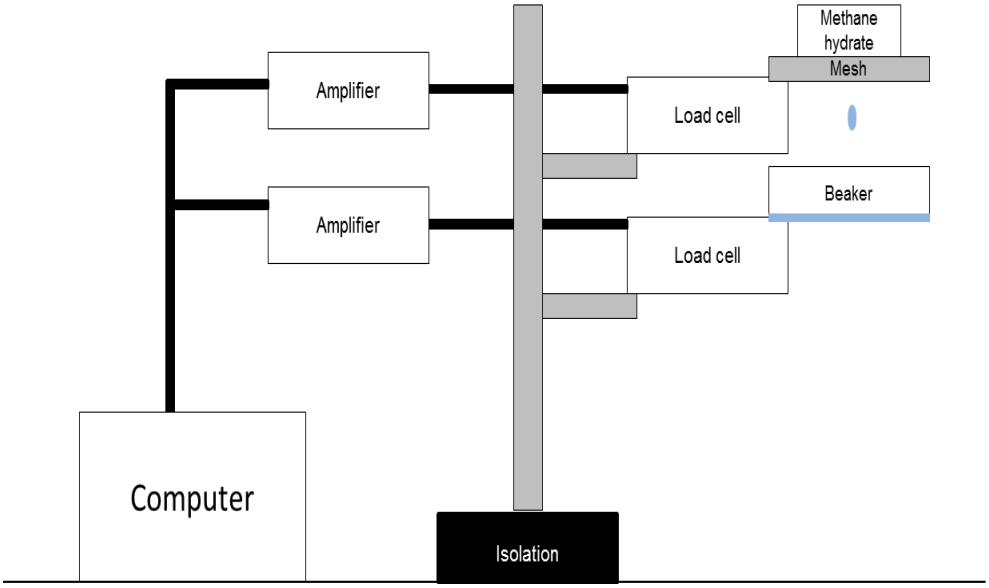


**Figure 6. Schematic of the differential weight measurement setup.**

The load cells installed are the Platform Load cell 1004 from Sensor Techniques, of 300g and 1500g capacity. The mesh is made of stainless steel with square holes of 2 mm. The size of the mesh is 11.5 x 11.5 cm, fixed in a ring platform of 9 cm diameter. To collect the water, a flat PYREX glassware beaker of 100 ml capacity is place just under the mesh. Finally all the structure is held by two bars on an optical table. At the base of the bars, there are 4 cylindrical sorbothane bumpers that absorb approximately 50% of the vibration of the table and improve the accuracy of the readings, based on the specifications of the manufacturer and proved in different tests.

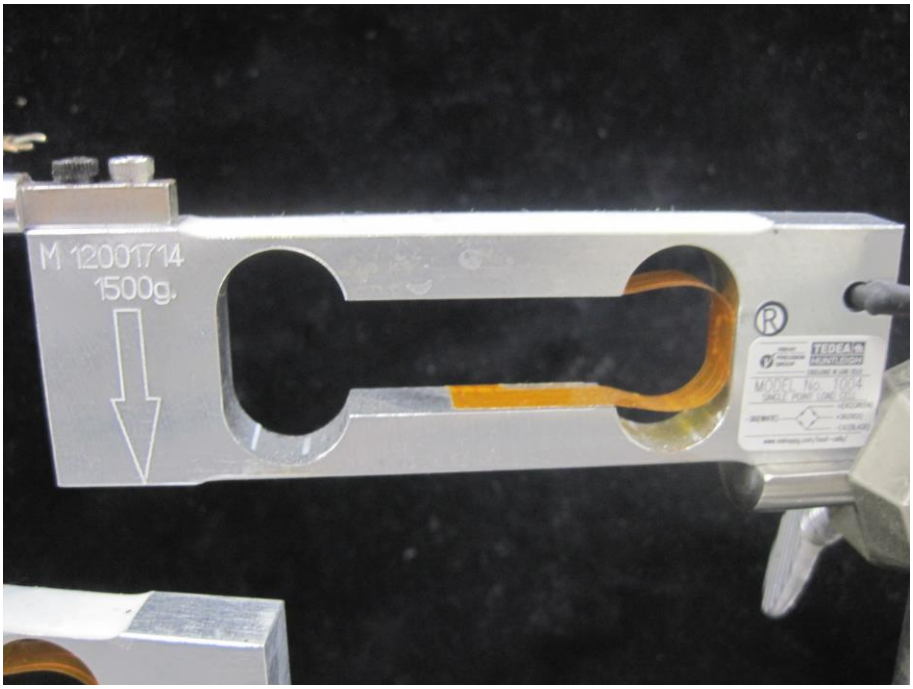


**Figure 7. Platform Load cell 1004.**

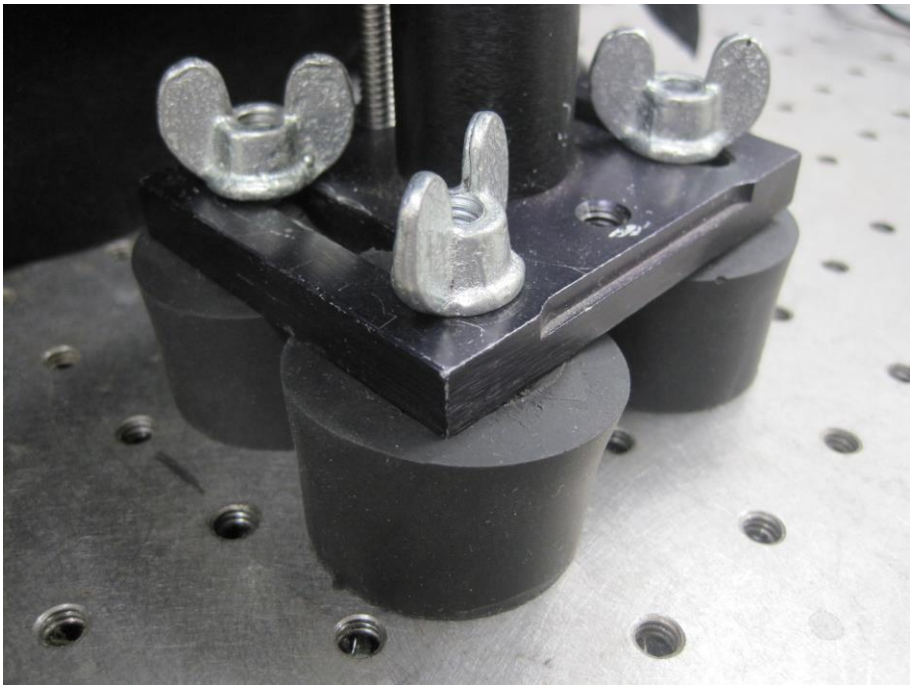

**Figure 8. Sorbothane bumpers for isolation.**

**Load cells**

A load cell is a transducer that converts force into a measurable electrical output. This

conversion is indirect and occurs in two stages. By a mechanical device, the force to be measured deforms a strain gauge. The strain gage converts the deformation into electrical signals. A load cell usually includes four feeler gages connected in a Wheatstone bridge-type configuration. Table 1 shows the main characteristics of the load cells.

**Table 1. Load cell specifications.**

| | |
|---|---|
| Capacity | 0.3 and 1.5 kg |
| Dimensions | 10x33x110 (width x height x length) mm |
| Excitation | 10 VDC (15 max) |
| Rated output | 0.9mv/V |
| Resolution | 0.01g |
| Save Overload | 150% capacity (450g and 2250g) |

The electrical signal output is typically on the order of a few millivolts and must be amplified by an instrumentation amplifier before it can be used. For the present project, a high precision load cell amplifier LDU 69.1 and the unit adaptor UA77 for LDU series, from Sensor Techniques are used for the signal conversion. The output of the transducer is processed through an algorithm to calculate the force applied in it.

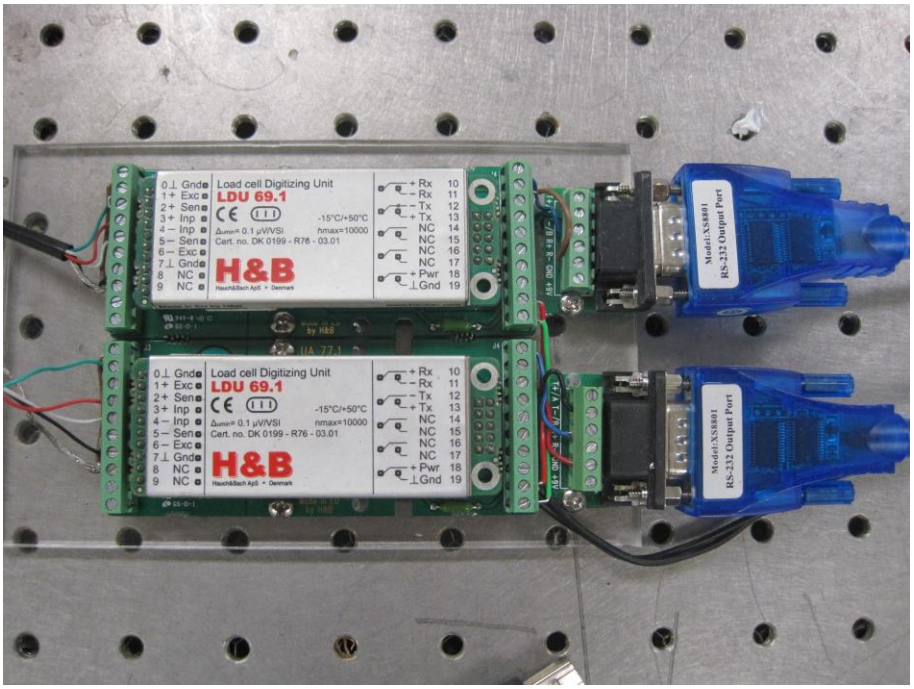


**Figure 9. High precision load cell amplifier LDU 69.1.**

**Control load cells**

To meet the requirements of the measurement, several factors must be taken into account.

1. Load cell accuracy: There are some specifications that must be taken into account for a correct performance of the load cells. The most important ones are the nonlinearity and hysteresis. Nonlinearity is the maximum curve deviation from the straight line of the load cell calibration, this error is maximum at full weight, and for the present load cell is 0.01% of the rated output. On the other side, hysteresis, is the difference between two load cells readings for the same applied load, in this case is also 0.01%. Other important characteristics are the creep, which is the change on output occurring with time under load and the temperature effect on the output, based on the change with variation in the ambient temperature.
2. Load factors: The way the load is applied to the load cell is crucial to determine the type of load cell more suitable to the system. For accurate weighing, the load cells alone must support all the weight to be measured. The load must be correctly aligned and twisting loads must be avoided.

3. Environmental factors: Forces like wind loading, shock loading, vibration, large temperature changes or pressure differentials, can produce errors in the load cell signal. It is important to ensure that only the weight force is transmitted to the load cell.
4. Interference with signal transmission: In addition to ensuring that the load cells measure only the desired weight, it is important to ensure that the weight controller measures only the load cell electrical signal. Radio frequency interference, electromechanical interference, and moisture can interfere with this electrical signal.

The calibration of the load cells is done using the software program from Hauch & Bach "Device Operating Program 4 (DOP 4)". Using commercial weights, Figure 10, the load cells are adjusted to real weight every time before the experiment to avoid the non-linearity and hysteresis problems explained before.

**Figure 10. Calibration weight.**

A Labview data acquisition VI is used to read the load cells signals. This program reads the load cell data every 0.1 seconds with a resolution of 1mg. After each experiment the program exports the data in an Excel file for further manipulation. Figure 11 shows the program during one experiment. The red curve is the weight of the methane hydrate sample

and the white one is the weight of the water collected.

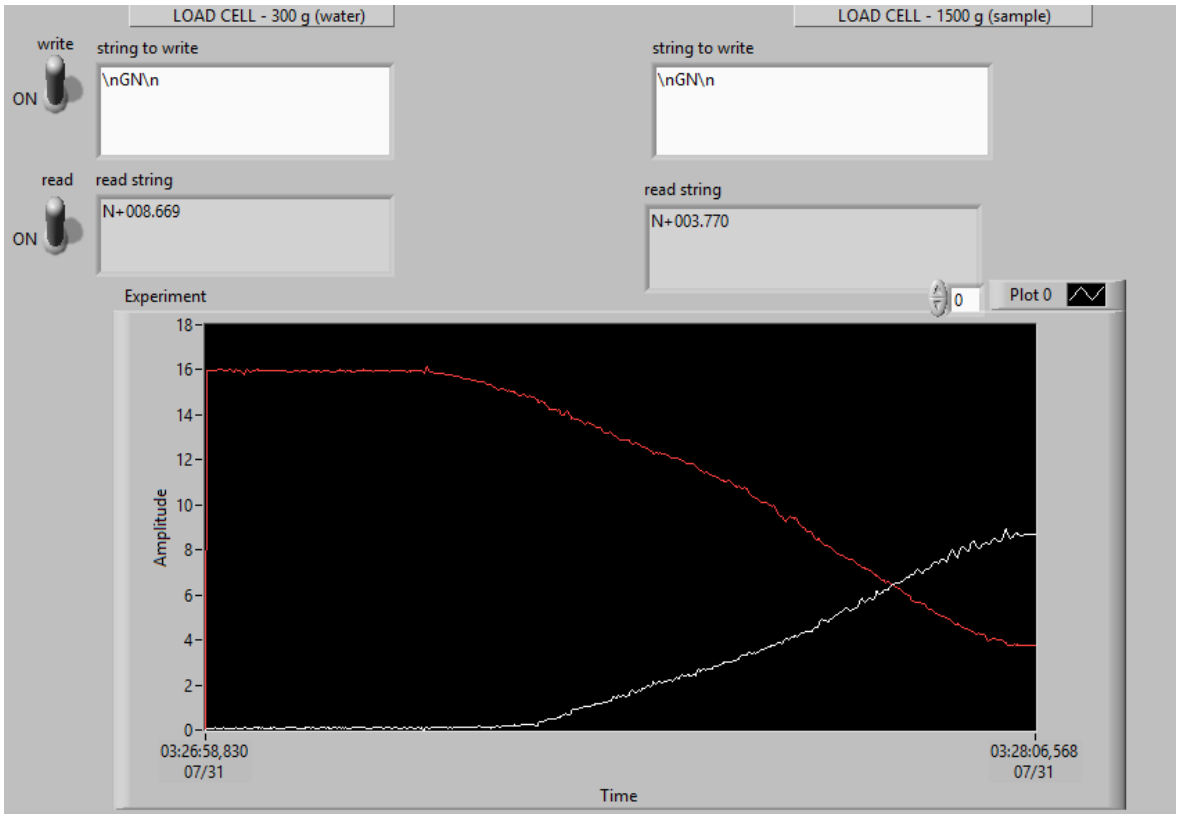


**Figure 11. Labview data acquisition program.**

## PRODUCTION OF METHANE HYDRATES

The first objective of the methane hydrate combustion experiment is to form uniform and repeatable samples. In previous work [11, 13] water with sodium dodecyl surfactant, pressurized in methane, was used for making clathrates but the results showed the need for improvement to achieve higher clathration and quality of samples. Better reproducibility, compact shape and higher clathration, had been achieved by starting with ice rather than liquid water. Although starting with ice is theoretically slower, the group that is working in the formation can form samples in 4-5 hours using liquid water [24] , because the formation would require the methane to diffuse into the ice crystal, spread the bonds, and enter the cage to prop up the new structure, experiments showed better results. It is not completely clear how the formation proceeds beginning with ice but it appears that methane diffuses into the porous ice powder and then as the temperature rises to near melting, the cages form. The purpose of this first phase of the experiment was to understand which elements influence hydrate formation and then combustion in order to form repeatable samples. From the literature, it is known that the size of the ice powder forming the hydrate base plays an important role in the formation rate [3, 21] as does the temperature rate increase needed to promote rapid formation [3]. Another important factor is the time taken in the process.

The hydrates in this study are produced using a modified version of the Stern group approach [3]. Figure 12 explains the process for the formation of samples and the modification is shown in red. Starting at low temperatures, approximately 255-260K, the chamber is first pressurized to between 1100-1500 psi with methane, to be sure that they can burn at different formation pressures. At this point, the temperature is increased at a constant rate of 5 K/hour and then held at 281 K for 8-12 hours. Note from Figure 2 that this condition is very close to the stability line of the hydrate. Then, the sample is cooled down to 265K so that it can be depressurized without instant decomposition of the hydrate. In fact, one of the interesting challenges of the experiment is that the sample further cools during depressurization to a degree that is difficult to predict. This additional cooling can give rise to slightly different ignition behavior as well as to differences in early

decomposition and combustion.

The details of the steps involved in the formation of the hydrate samples follows:

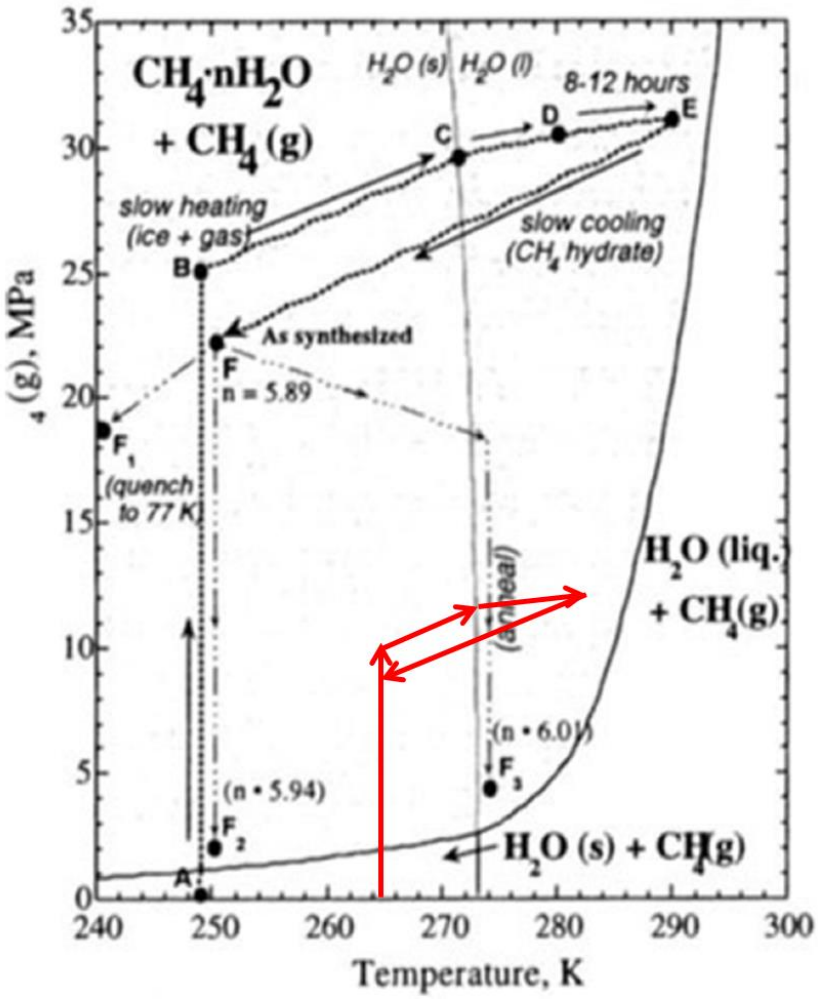


**Figure 12. Methane hydrate phase diagram and process description of the formation of samples [3].**

**Preparing the powder ice**

The first step required to form a methane hydrate sample is preparing the ice powder.

1. A burette with 50 ml of DI water is used to release droplets into a container full of liquid nitrogen to create uniform but large ice droplets.

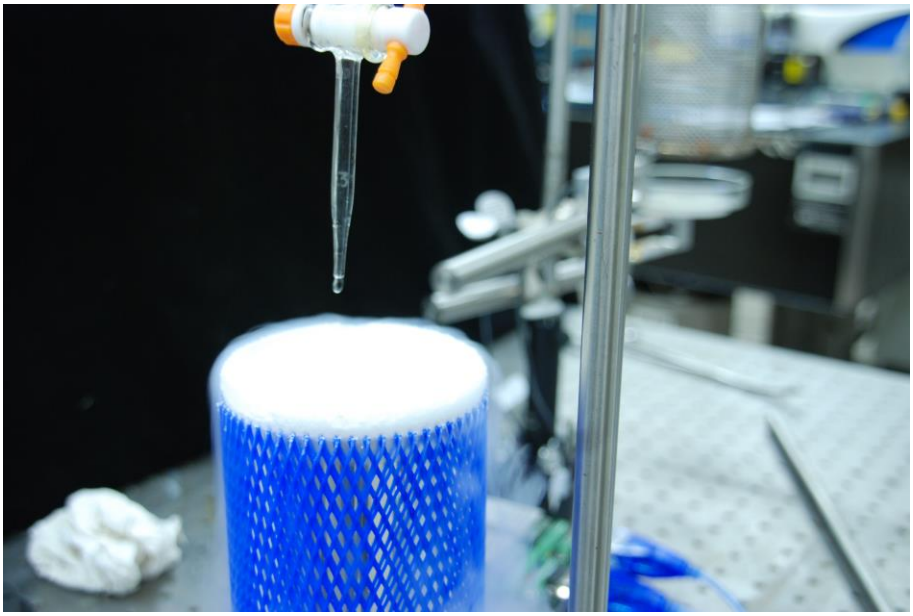

**Figure 13. Liquid water droplets into liquid nitrogen.**

2. The liquid nitrogen is poured onto a mesh to filter the liquid and leave behind only the ice droplets. The mesh is covered with isolation foam to avoid heat losses and melting of the ice.

**Figure 14. Pour liquid nitrogen onto the mesh.**

**Figure 15. Ice drops.**

3. The ice droplets are ground with a chilled coffee blender for 25 seconds to have seed ice of approximately 300 μm size.

**Figure 16. Blend the ice droplet in a coffee blender.**

4. The seed ice is introduced into a mold. This mold consists of a hollow split-cylinder that can be filled with a measured mass of water ice to approximately 40% porosity. The

porosity between the ice grains provides space for a molar ratio of methane to water well in excess of that required for complete reaction (clathration). A disk on the bottom of the mold prevents ice displacement during the process.

**Figure 17. Put seed ice into the cylinder.**

5. Before the sample is placed into the pressure vessel, the mass of ice is measured.

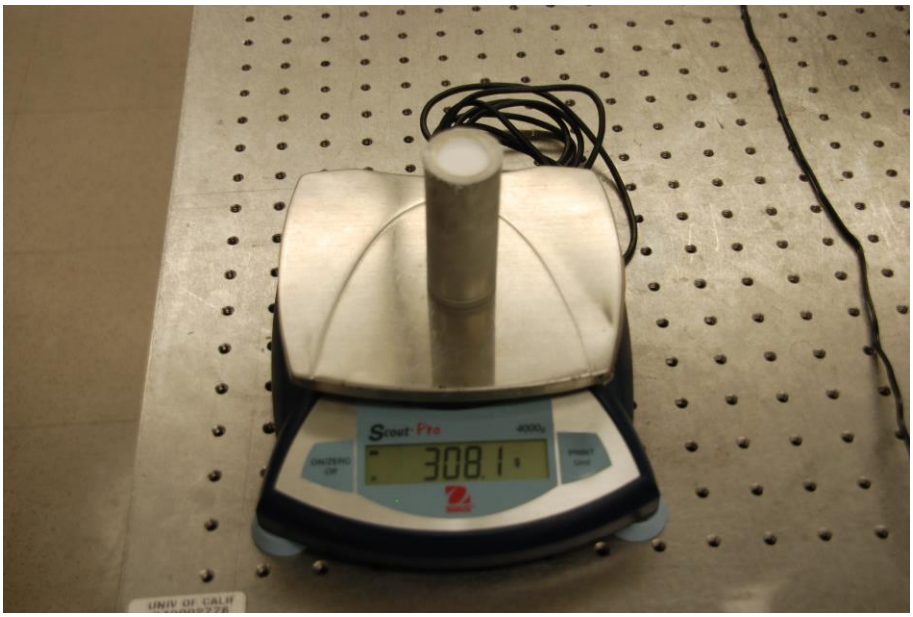


**Figure 18. Measure weight cylinder.**

6. The cylinder is placed inside a 1 liter stainless steel pressure cell (4611 Pressure vessel Parr Instruments). The vessel is sealed with a built-in Teflon gasket and split-ring assembly, which clamps the vessel head to the cylinder body using an array of cap screws.

**Figure 19. Place cylinder inside the vessel.**

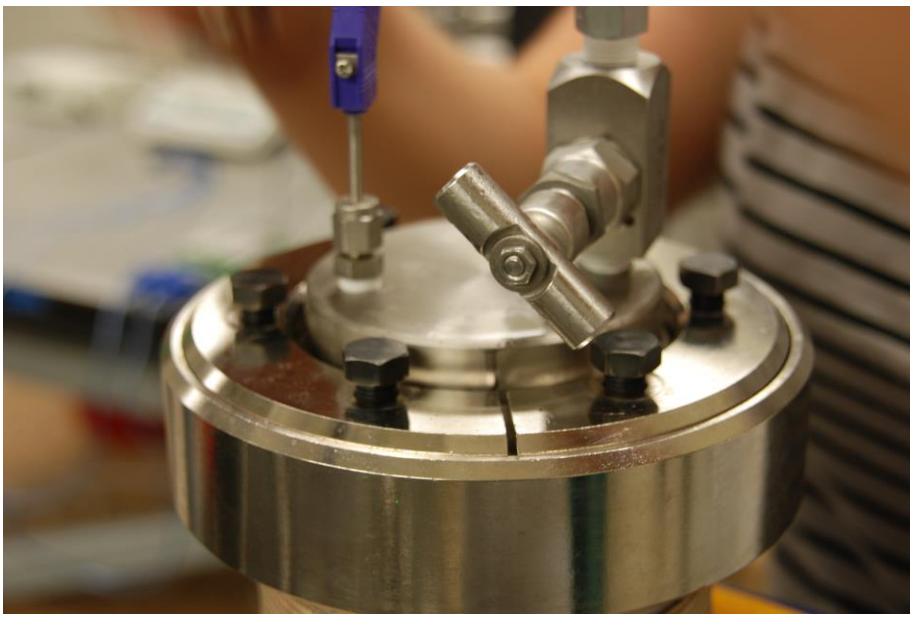

**Figure 20. Close the lid of the vessel.**

7. The vessel is then positioned in a freezer. The temperature is controlled by a six-

foot long, 120 VAC-heating tape wrapped around the pressure cell. By controlling the voltage delivered to the heating tape, the internal temperature of the pressure cell can be adjusted using a mounted E-type thermocouple as a feedback sensor.

**Figure 21. Pressure cell inside the freezer.**

**Formation of the methane hydrate**

The second phase of the formation process is the pressurization of the vessel and the formation of the methane hydrate. Figure 22 shows a schematic of the experimental setup inside the freezer and the hydraulic system used to pressurize the methane inside the pressure cell. Component A is the air line, PCV is the pressure control valve of the methane bottle, P is the pressure gauge of the line to the pressure vessel, PR is the pressure gauge of the vessel, TR is the thermocouple and V the voltage of the heating tape.

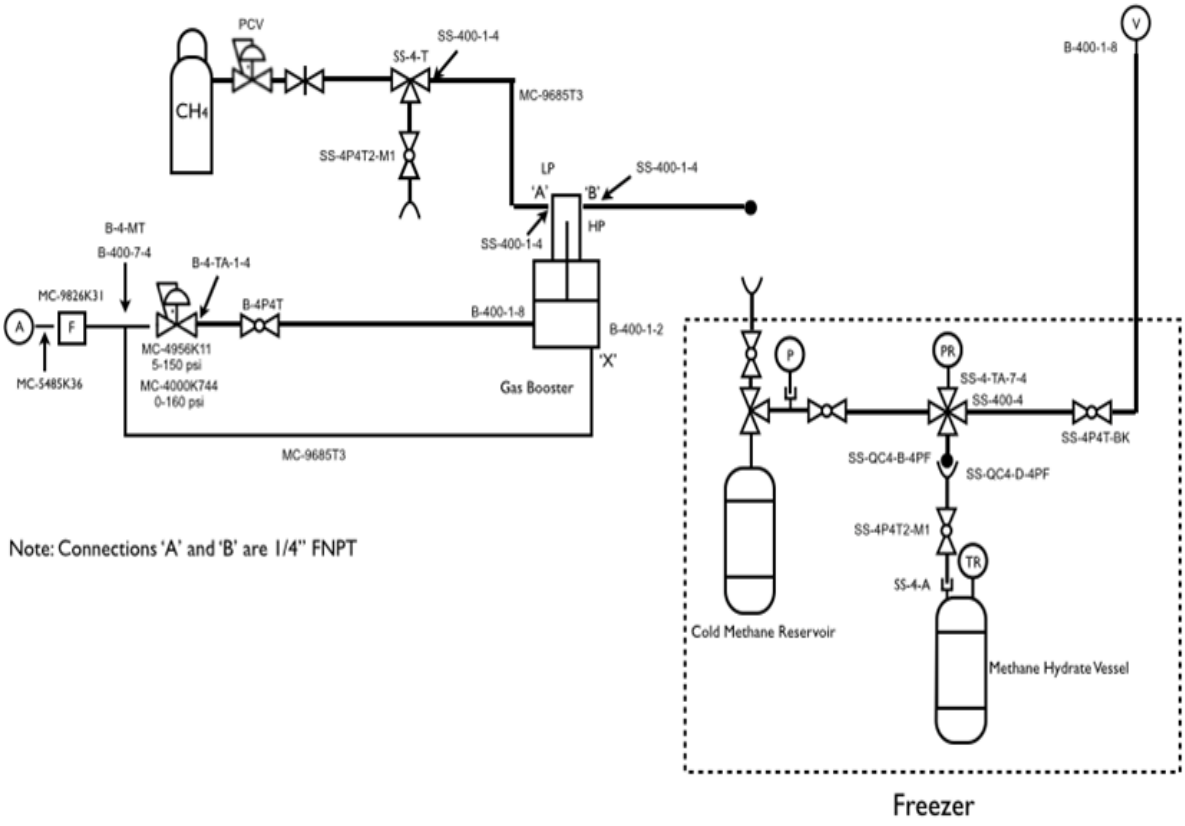


**Figure 22. Schematic of the system to produce methane hydrate samples.**

A commercial bottled methane gas cylinder with a maximum delivery pressure of 2500 psi is used to provide the methane. The inlet valve of the cylinder is opened and the gas flows to a Maximator air driven gas booster pump. This pump can pressurize to gas at the desired pressure. The methane pump is used to maximize the use of methane before new source bottles are needed.

1. The air inside the pressure cell is evacuated with the vacuum pump and the methane is opened to charge the vessel to ~1500 psi (between 1100 and 1600 psi). An Omegadyne PX-309 pressure transducer monitors the pressure throughout the hydrate growth, and a PID control loop is controlling the temperature. Note that the pressure transducer is inside the freezer and the thermocouple is measuring the temperature of the pressure cell and not the hydrate.
2. While pressurizing, the temperature increases to around 273 K so that, two hours of cooling are needed to chill the hydrate to 260K. At that point the heater is activated and

the sample and gas are warmed up at a rate of 5 K/h to 281K. Up to 273 K, methane gas pressure increases approximately linearly with increasing temperature, following a slope governed by the equilibrium thermal expansion of free methane in the system. The clathration begins approximately at 273K, around the melting point of ice, and the consumption of methane gas by the hydrate formation slows the rate of pressure increase. With the Labview data-acquisition software the pressure-temperature, pressure-time, temperature-time curve are recorded throughout each experiment.

3. Once the temperature is 281 K the heater holds the system steady at this temperature for 8-12 hours to achieve nearly complete clathration. Following clathration, the heater is turned off, and the hydrate slowly cools to 265K.
4. Finally, for removing the sample, the pressure cell is slowly depressurized to atmospheric pressure and opened to further use the methane hydrate sample.

Clathration and, therefore the amount of methane trapped as a hydrate can be estimated by measuring the overall temperature corrected pressure drop inside the pressure cell as methane molecules are tightly packed into the clathrate structure. The pressure falls because the average specific volume of the consumed methane gas and initial ice volume is larger than the specific volume of the produced methane hydrate.

Figure 23 shows a typical pressure-temperature curve of the formation process. The oscillations are due to the temperature cycle of the freezer; the overall pressure drop is 15-20 psi.

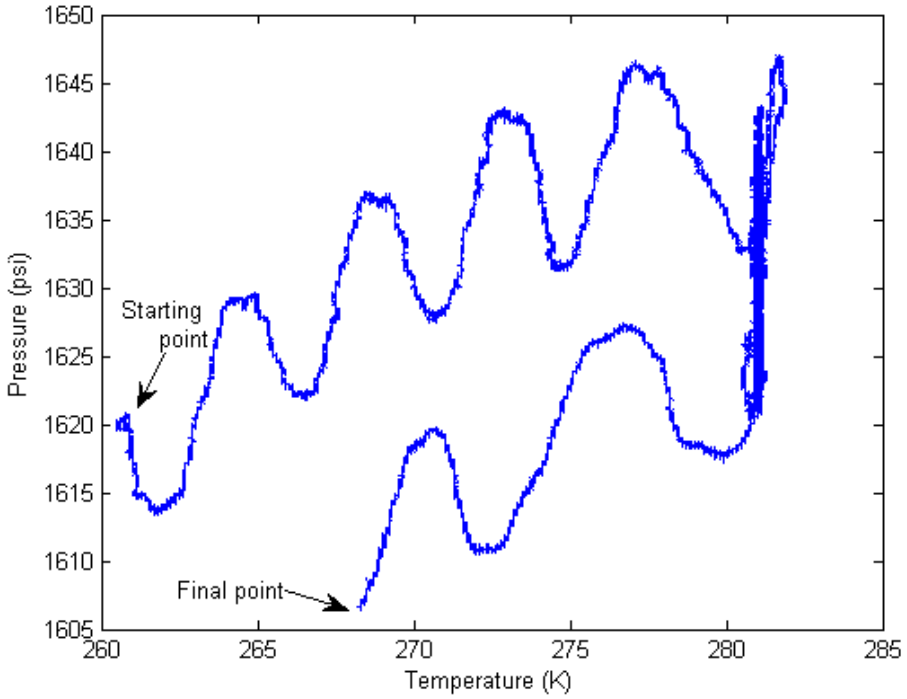


**Figure 23. Pressure-temperature curve during hydrate formation.**

This pressure drop is more noticeable in Figure 24 and Figure 25 when, during the temperature constant period, the peak of pressure drops around 15 psi. Also the change of slope can be seen during the first 4 hours of the temperature increase.

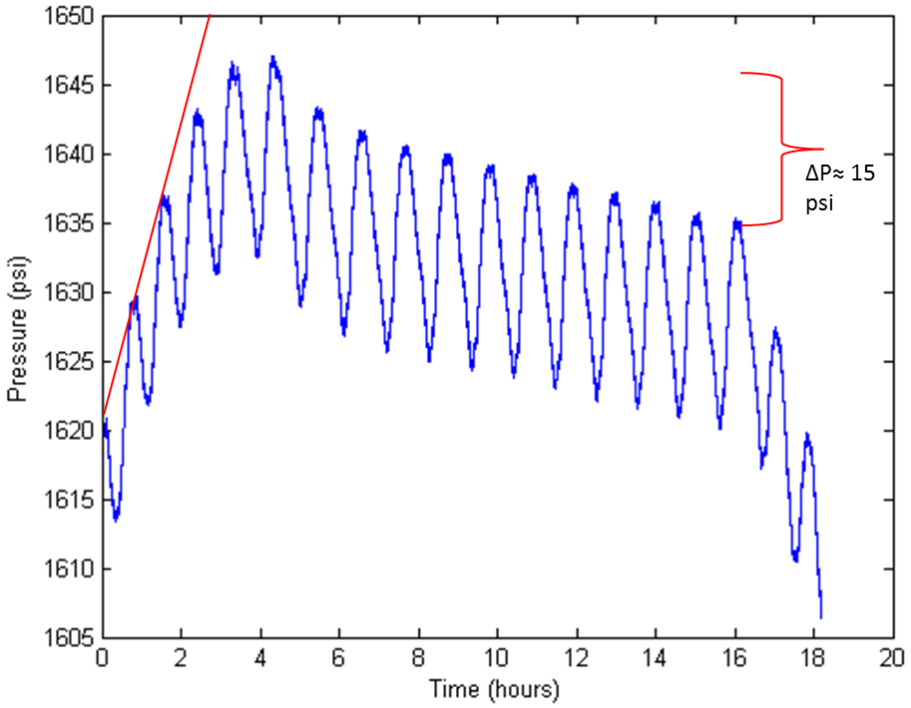


**Figure 24. Pressure time history during hydrate formation.**

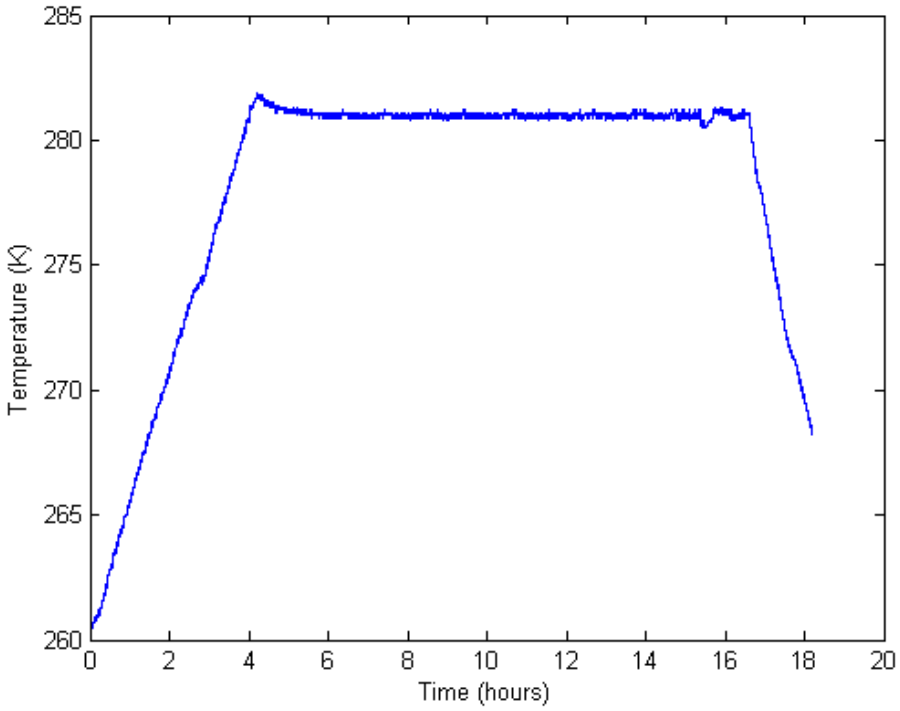


**Figure 25. Temperature time history during hydrate formation.**

**Clathration**

Methane hydrates are non-stoichiometric compounds. That means that the ratio of methane to water can vary. Hence, determining the real composition and the amount of methane introduced is important to know the quality of the sample and further calculations. As mentioned earlier, when the hydrate is saturated, the maximum amount of methane trapped inside the clathrate structure has an effective molar composition of $CH_4*5.75H_2O$, or 87% water and 13% methane on a mass basis. If the methane hydrate is saturated, the clathration achieved is 100%. Therefore, the amount of methane trapped can be described as the percentage of clathration of the sample.

To measure the clathration during formation it is possible to use the technique explained above, i.e., by measuring the temperature corrected pressure drop. It is also possible to do a direct mass balance. This technique consists of measuring the difference of the sample weight and the weight of water left after the sample has been melted. This difference of mass is the methane gas of the hydrate (and evaporated water, which is negligible at these temperatures). There are other techniques also available, like directly measuring the volumetric methane gas loss from the hydrate or letting the sample dissociate while the mass is recorded continuously, assuming that any difference is the mass of the methane gas. There is no technique better than the other and the reason for using the initial and final mass is for convenience of the experiment. Table 2 shows the different results using the initial/final mass balance technique for several samples formed. The results show good reproducibility and fairly high levels of clathration. It is important to note that the measurement of the initial clathrate weight is done approximately 3 minutes after starting the process of depressurization, losing a small quantity of methane similar throughout the experimets. The clathrate is dissociating during this 3 minutes so the clathration achieved at the end of the formation process is higher than the results show. It is not possible, unfortunately, to avoid this loss. Actually, the measurement accurately characterizes the initial state of the hydrate to be burned. The results show that the clathration is between 75% and 90% when the sample is ready for combustion. This level indicates a very high quality that certifies the repeatability and effectiveness of the formation process.

**Table 2. Clathration results.**

| Initial weight [g] | Final weight [g] | Methane weight [g] | Mass % of methane | Clathration (%) |
|---|---|---|---|---|
| 14.8 | 16.8 | 2 | 11.90 | 87.3 |
| 14.6 | 16.6 | 2 | 12.04 | 88.49 |
| 14.6 | 16.4 | 1.8 | 10.97 | 79.64 |
| 15.2 | 17.2 | 2 | 11.62 | 85 |
| 15.5 | 17.3 | 1.8 | 10.40 | 75.02 |
| 15.5 | 17.5 | 2 | 11.42 | 83.35 |
| 14.5 | 16.2 | 1.7 | 10.49 | 75.74 |
| 14 | 15.6 | 1.6 | 10.25 | 73.83 |
| 14.2 | 16.4 | 2 | 12.19 | 89.72 |
| 14.6 | 16.4 | 1.8 | 10.97 | 79.64 |
| 15.5 | 17.5 | 2 | 11.42 | 83.35 |
| 15.6 | 17.4 | 1.8 | 10.34 | 74.54 |
| 14.9 | 17 | 2.1 | 12.35 | 91.05 |
| Average | | | 11.29 ±0.44 | 81.82 ±3.39 |

With a 95% of confidence the mass of methane is 11.29 ±0.44% and the clathration level is 81.82 ±3.39%. These results indicate a very high quality that certifies the repeatability and effectiveness of the formation process.

# DISSOCIATION

In this section, the dissociation of the methane hydrate is studied without igniting it, and two experiments are analyzed to understand the properties and consequences for the combustion. The first experiment is done just after taking the sample from the cold formation pressure vessel, and the second one is after the sample has been sitting for 30 minutes inside dry ice with a surface temperature of 200K.

Dissociation is the process where the methane hydrate breaks its bonds between the ice structure and the methane molecule. Hence the methane escapes from the cage and the water changes to liquid or stays as ice without the molecule inside. Once the pressure of the vessel drops below the stability line of the methane hydrate the dissociation process starts, and quantifying the amount of methane that is released during this period before the experiment starts is essential to confirm the real quality of the hydrate before depressurizing and to determine the natural dissociation rate of the hydrate at standard conditions: atmospheric pressure (1 atm) and room temperature (293 K).

**Natural dissociation**

The first experiment consists of placing the sample of 15 grams onto a load cell right after measuring its weight, and then measuring the mass continuously until it is completely melted. Data is collected every second. It is considered that all the gas released is methane because the heat from the environment is changing a very small portion of the liquid water into gas, and the water is drained.

$$Methane\ released\ (t) = Mass\ sample\ (t_0) - Mass\ sample\ (t) - water\ drained(t)$$

Figure 26 is the time history of the methane released during the experiment. The sample dissociates completely in 70 minutes, although in 8 minutes the sample lost approximately 50% of the methane (1 gram), and in 30 minutes it had lost 95% of the methane. The methane released can be fit with an exponential function, and during the first seconds after leaving the hydrate at room conditions there is a significant level of methane is released. It is possible that part of this loss is trapped methane gas but in any case the delay time of starting the experiment should be minimized.

In this sample the total methane lost estimated is 2.1g; that represents 14% of the mass of the hydrate sample (15 grams), which is more than 100% clathration (13.41%). Hence, in the losses of the sample that were assumed to be methane only, there is very few water and/or there is a little bit of trapped methane gas from the hydrate that was measured as guest molecule methane released.

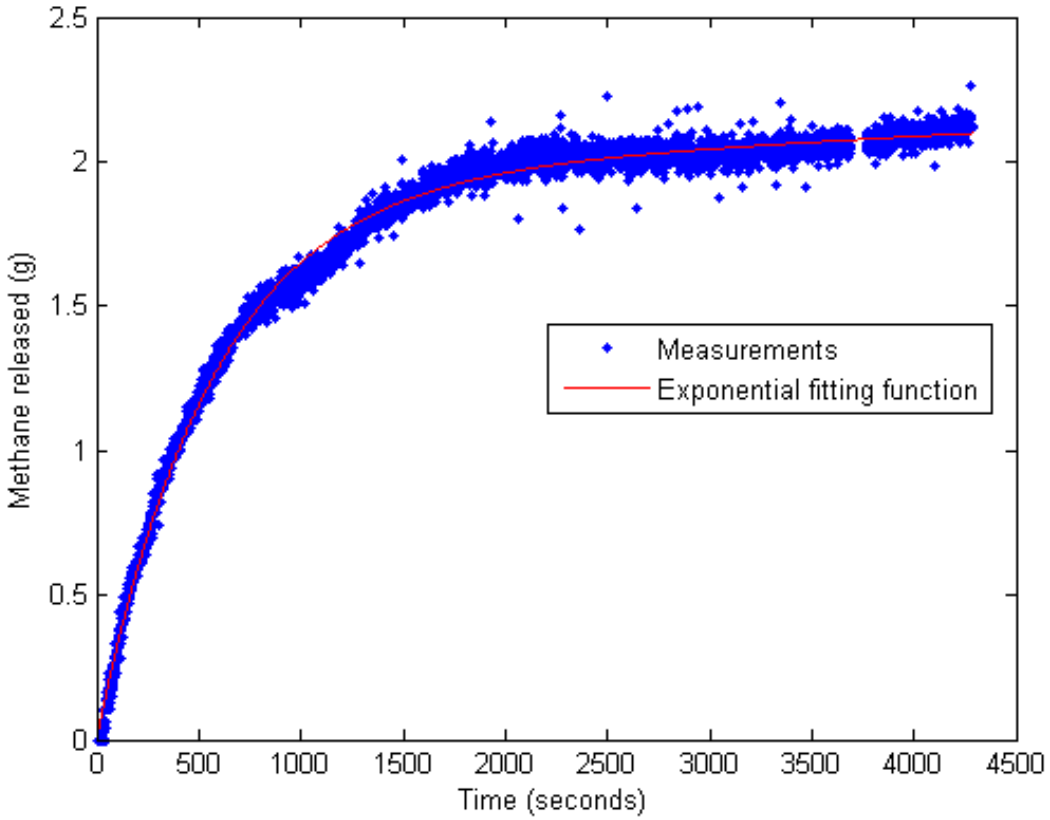


**Figure 26. Methane released during natural dissociation.**

However, the important conclusion of the experiment is the rate at which the methane is released and this value can be calculated by the derivative of the exponential fitting function of the methane mass curve as shown in Figure 27.

$$Flow\ rate\ methane\ released\ \left({}^{g}/_{s}\right) = \frac{d(Methane\ released\ (t))}{dt}$$

There is a maximum flow rate of 3.4 mg/s at the start of the experiment.

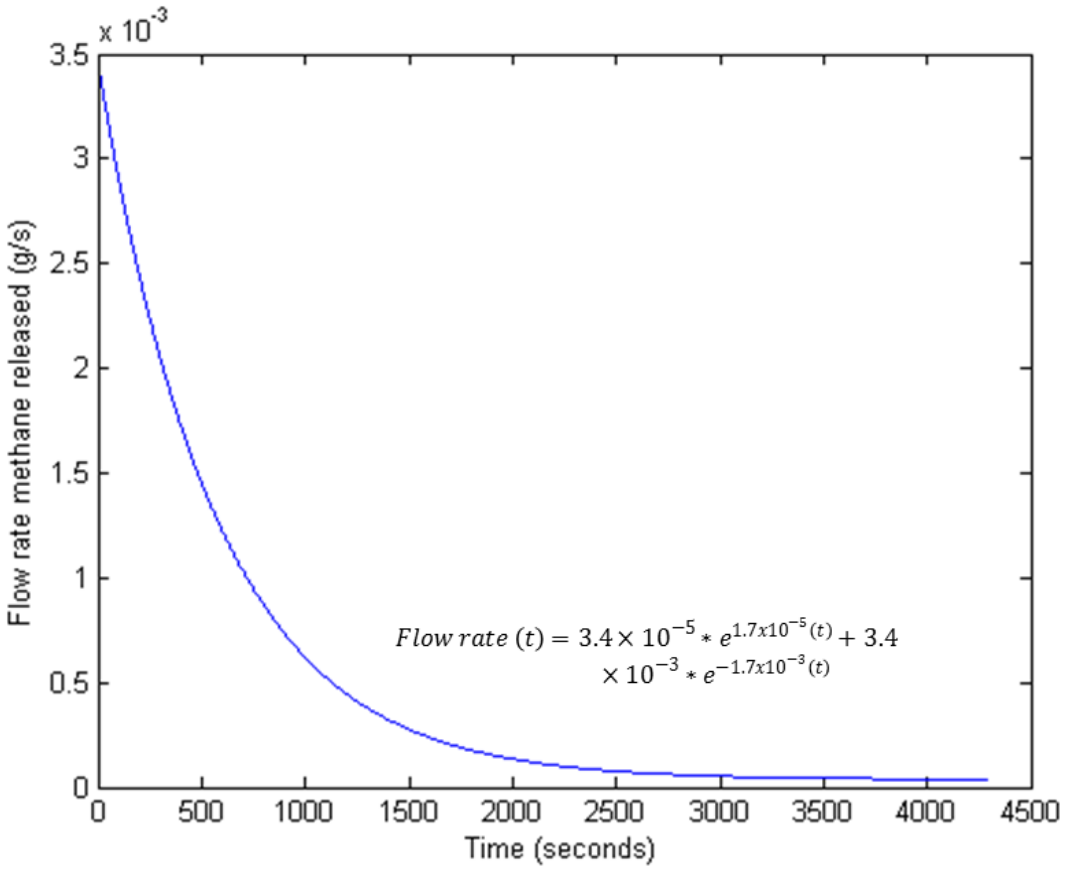


**Figure 27. Flow rate methane released in natural dissociation.**

Another property of the hydrate that is measured during this experiment is the surface temperature. Images of the dissociation process are taken every 0.1 Hz using a FLIR SC620 IR camera. The parameters of the camera to determine the temperature are adjusted to be snow, because it has similar optical properties to the hydrate.

Figure 28 shows the initial state of the hydrate when is positioned on the mesh, with an initial average temperature of -10.2ºC (263.2 K). The temperature increases to -4ºC (269 K) in only 2 minutes, and after 5 minutes it reaches the constant temperature of around -3.3º C (269.7 K), as can be seen in Figure 29. Hence is very difficult to determine the initial surface temperature of the hydrate, because when it is exposed to the environment it increases very rapidly. For this reason the initial surface temperature of the hydrate is estimated to be the temperature when is pulled out from the vessel, -14.3ºC (258.7 K).

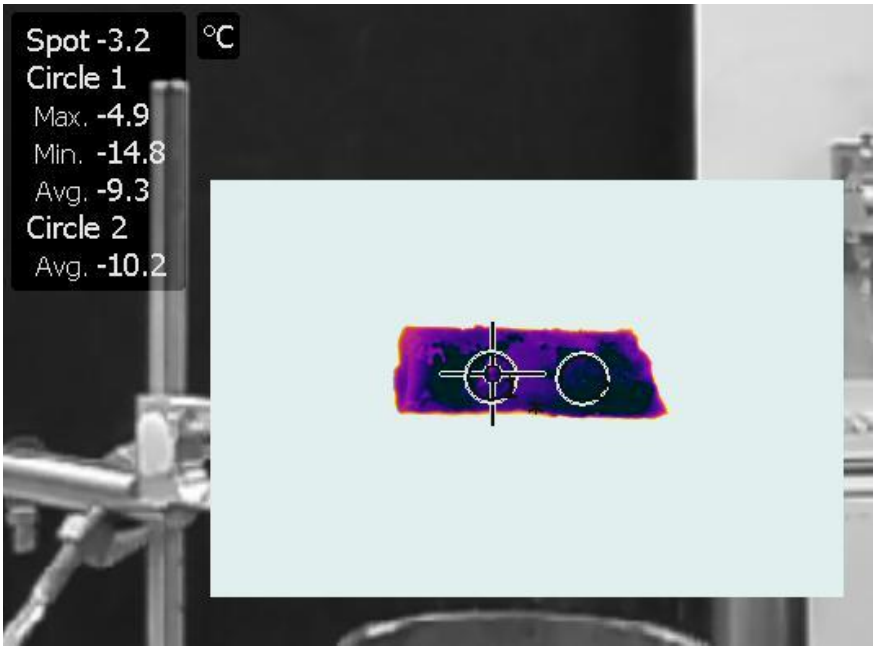


**Figure 28. Initial measurement of the methane hydrate temperature.**

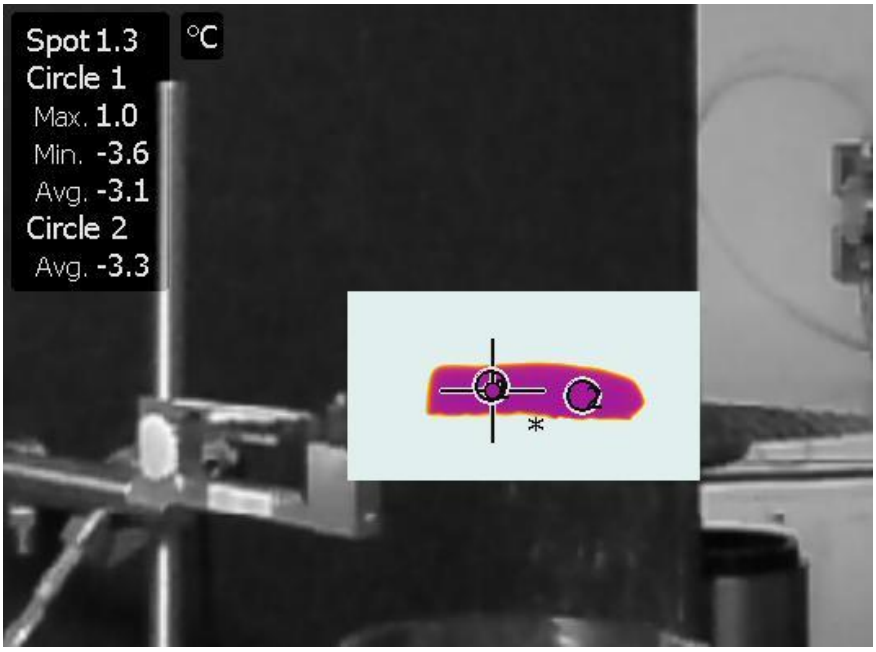


**Figure 29. Measurement of methane hydrate temperature after 20 minutes.**

**Dry ice dissociation**

A second experiment was designed to determine if it is possible to conserve the hydrate without dissociation if it is cooled down to 250K after depressurization. This experiment

consists of placing a 15 gram hydrate sample inside a freezer full of dry ice to keep it cold. After 30 minutes, the sample is taken out and placed on the mesh to start the experiment. From Figure 30 it can be seen that in the first 4 minutes there are no mass losses from the sample, therefore the main purpose of the experiment is accomplished and the methane hydrate samples are conserved without dissociating inside the dry ice.

After these 4 minutes the hydrate dissociates approximately linearly at a rate of 2.6 mg/s. At this point the methane is almost released completely and only water remains. The noise at the end of the experiment is due to a bad signal of the load cells, but it does not affect the results.

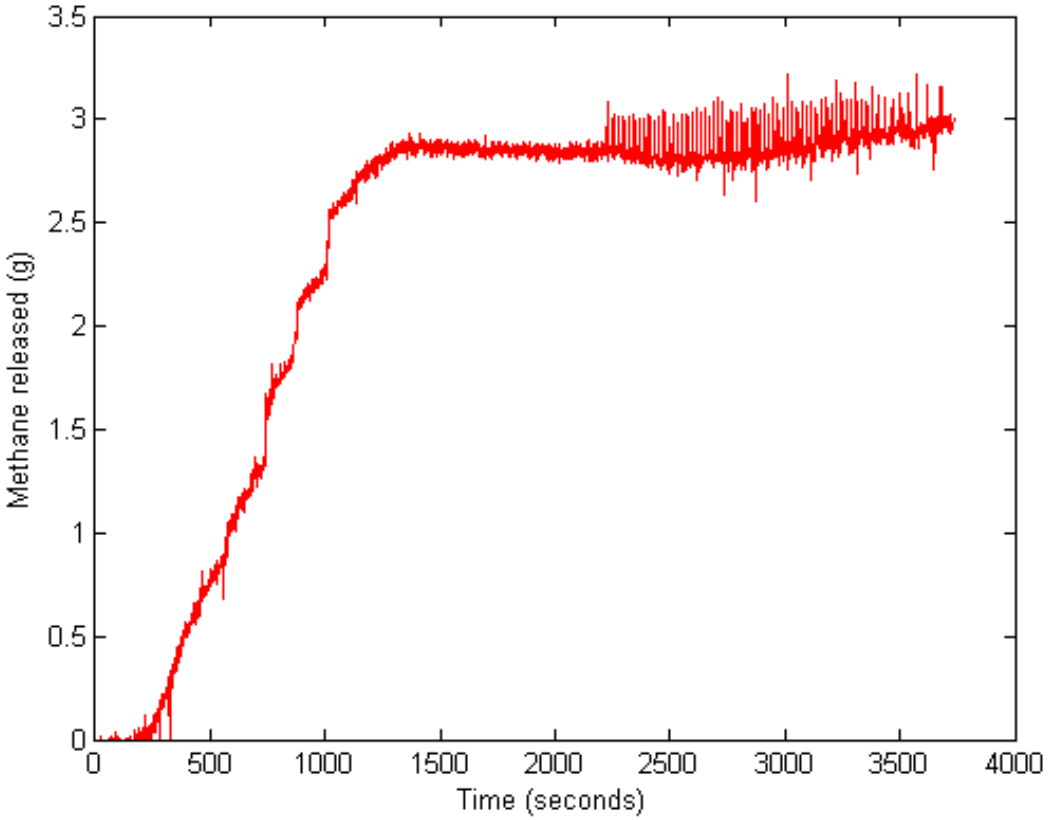


**Figure 30. Methane released during the dry ice chilled dissociation experiment.**

The temperature is also measured with the IR camera. Figure 31 shows the initial state of the hydrate when is positioned on the mesh, with an initial average temperature of -35ºC (238 K). The temperature increases rapidly to -25ºC (248 K) in 1 minute, -20ºC in 2 minutes, and -10ºC in 4 minutes. After 6 minutes it reaches the constant temperature of

around -4º C (269 K) as it can be seen in Figure 32. The final temperature is the same as in the non-chilled case indicating no deep core influence.

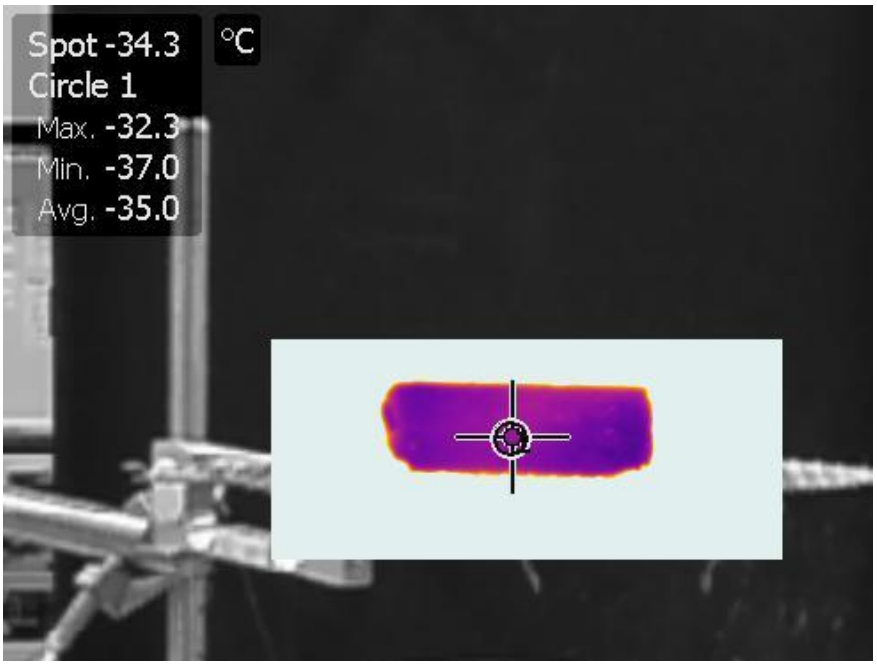


**Figure 31. Initial measurement of the methane hydrate temperature.**

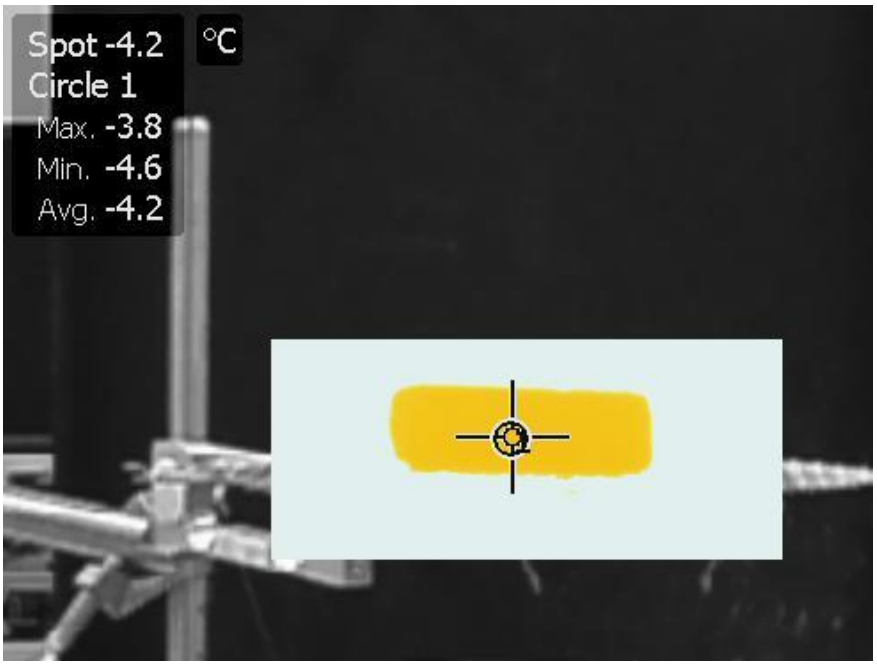


**Figure 32. Measurement of methane hydrate temperature after 25 minutes.**

## COMBUSTION

The combustion process consists of igniting the hydrate to be able to melt the outer layer then, the methane caged in that surface layer is released and this gas proceeds to feed the flame, and the heat of the flame melts the next layer of hydrate. The moment when the methane is released occurs when it is possible to see a flame expansion flame from the hydrate cake. During this process of evaporation, not only the methane is released, there is also water evaporation as it joins the fuel gas mixture and some of it remains as liquid water and drips down from the surfaces of the hydrate and filters through the mesh into the container.

Figure 33 shows a simplified notional diagram of the hydrate burning process where heat from the flame dissociates the hydrate, allowing methane gas to bubble through the liquid and travel to the reaction zone and some evaporated water also flows into the flame.

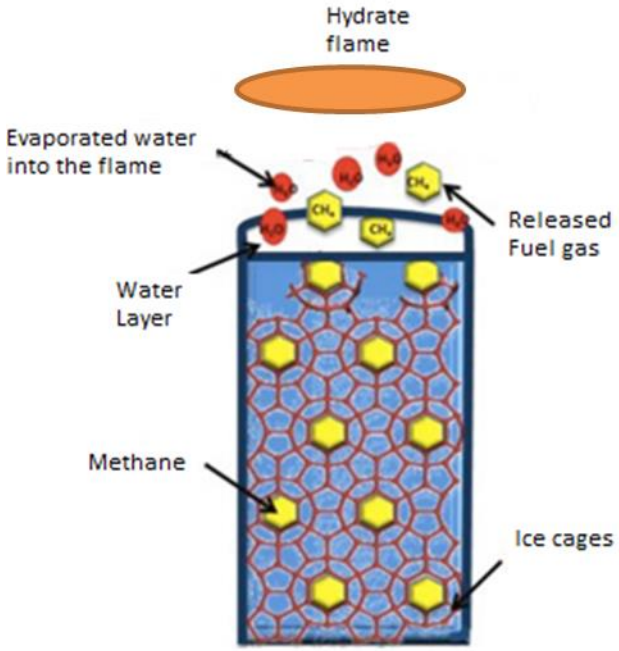


**Figure 33. Schematic of the hydrate burning process [11].**

During the combustion process it is possible to appreciate different regimes with specific characteristics. The initial regime is the ignition and propagation of the flame. The hydrate is ignited using a small propane torch from one side of the cylindrical sample. The flame

surrounds the entire circumference shape and starts propagating along the cylinder column. At the same time, the height of the flame increases rapidly and in 0.3 seconds it reaches the highest peak at 25 cm from the mesh. After 0.6 seconds the flame is propagated along the entire cylinder enclosing the hydrate as shown in Figure 34. Therefore, the bulk flame spread velocity of the hydrate is 0.1 m/s. This velocity is comparable to that found in hydrate flame spread studies of others [29].

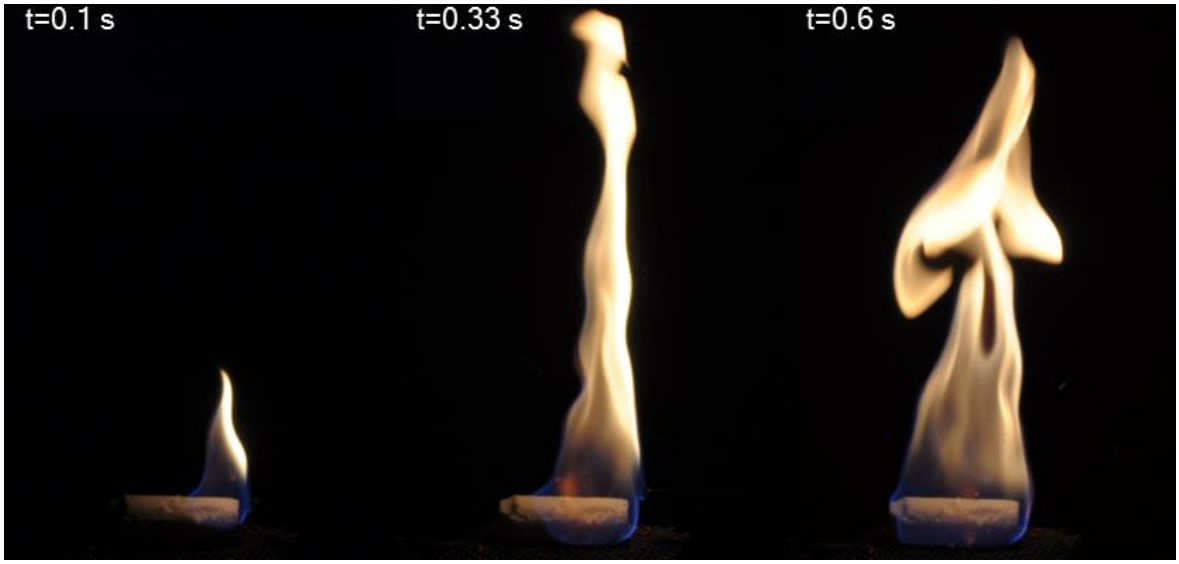


**Figure 34. Ignition and propagation of the hydrate flame.**

After the propagation, there is a second regime of the combustion starting at approximately 0.8 seconds and lasting until 5 seconds. The flame is characterized by a bright yellow color and unsteadiness due to the jets of methane released that induce an expansion of the flame. The height of the flame is variable and determined by these jets, although it is similar to the height during the ignition and flame spread regime. By the end of the regime, the brightness of the flame diminishes and it is more blue in color, but it still conserves some bright yellow flame, as shown in Figure 35.

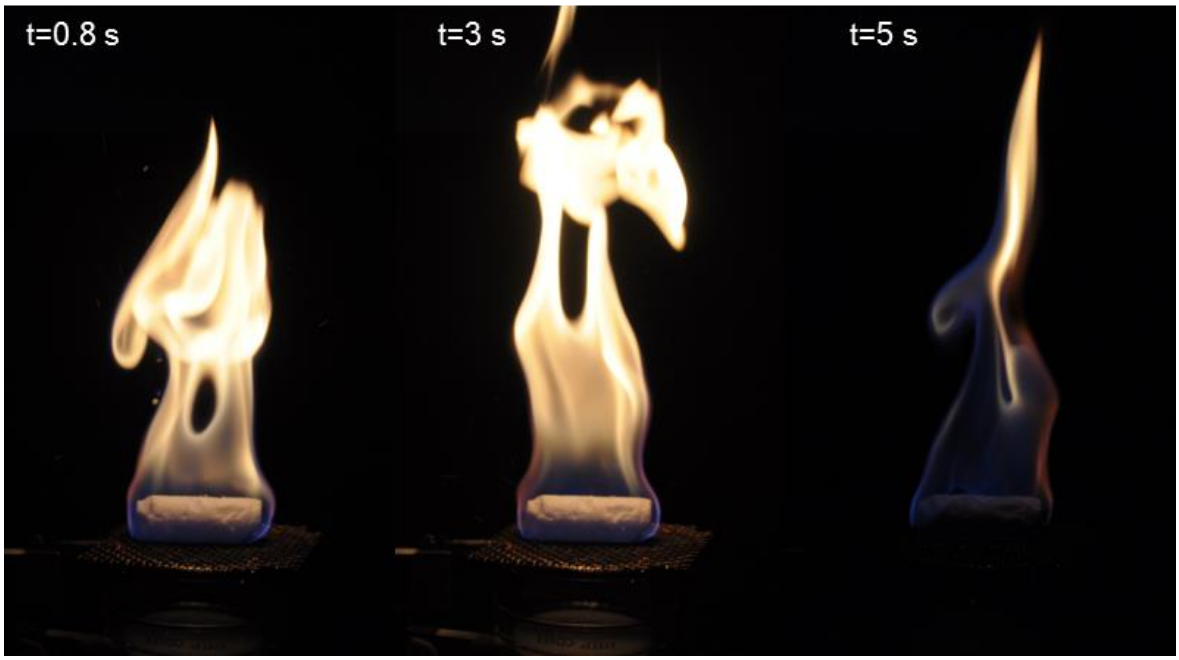


**Figure 35. Second regime of combustion.**

The third regime of the combustion starts approximately 5 seconds into the combustion process. During this regime the flame recedes toward the top of the clathrate sample and the bright color disappears. This is the longest phase and it is considered to be the quasi-steady state since the flame is similar throughout the regime, as shown in Figure 36. From the different photographs of Figure 36 it is possible to see the reduction of the diameter of the hydrate sample as a consequence of its dissociation. The length of the cylinder decreases very slowly which means that the flame is primarily heating the top of the sample. Heat is transport from the flame to the hydrate mainly due to of diffusion and not radiation, and that is the main reason of the linear regression of the diameter of the sample and not the length.


**Figure 36. Third and quasi-steady regime of combustion.**

The last regime of the combustion process starts when the cylinder changes shape into a flat rectangular hydrate that still contains some methane but is variable throughout the different samples due to the inhomogeneity of the methane hydrates and the caged methane distribution. At the end, the flame of the sample decreases until all the methane is released and there is no heat to maintain the flame so that it extinguishes.

What is remarkable about this final process is that the sample burns completely and no residual ice is left on the mesh, only the melted water trapped that was not drained. This behavior represents a significant improvement with respect to previous works [11, 13] where the uniformity of the samples did not allow the methane hydrate samples to burn completely.


**Figure 37. Extinction regime of combustion.**

## DIFFERENTIAL WEIGHT EXPERIMENTS DURING COMBUSTION

With the preliminary and qualitative results described above, it is now possible to develop a quantifiable measurement of the level of water evaporated into the hydrate flame during combustion. As described earlier, the first objective of the experiments was to form uniform, equal and reproducible samples to be able to compare the different experiments and have a better understanding of the combustion. In previous works done in the lab [11, 13] combustion of methane hydrates and preliminarily measurement were achieved, but not with precise control, uniformity and reproducibility. This objective was achieved. The next set of experiments focus on the differential weight measurement during hydrate combustion. It is important, therefore, to reiterate the process.

The methane hydrate formation is completed after 20-22 hours of starting the process. At this point, the vessel is depressurized slowly to atmospheric pressure. When the pressure is low enough to cross the stability line of the methane hydrate, the sample starts dissociating and it is possible to hear some cracking inside, meaning that some methane is being released. For this reason the samples are removed quickly to avoid excessive methane loss. After weighing the sample, the split mold parts are taken out of the cylinder and the methane hydrate sample is placed horizontally on the mesh of the experimental setup, as is seen in Figure 38. The time of all the depressurizing process, from starting depressurizing the vessel until the sample is taken out from the cylinder, is controlled to know the methane loss before burning. This time is around 3 minutes for all the samples presented (Table 3).

Once the sample is placed on the mesh, the Labview program is started and the hydrate is ignited with a torch. While the program records the weights, the combustion is monitored using a digital video camera (Canon SD1200 IS). In addition, photographs of the key periods of the burn are taken with a Nikon D90 digital SLR camera.

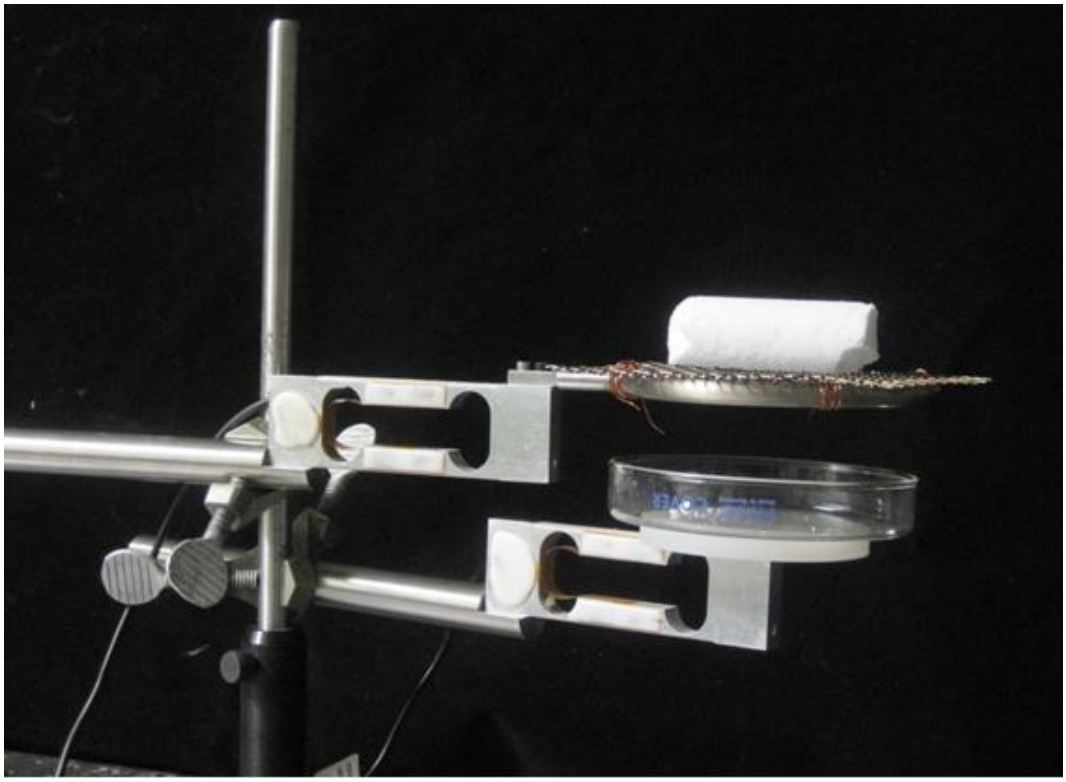

**Figure 38. Methane hydrate sample in the experimental setup.**

The first 10 experiments were a test to find the process to form hydrates. During these test cases some samples did not burn, some had very low amount methane trapped, others were not compact or had other defects and the timing for taking them out was too long (>4 min). Once the process was controlled, all the samples had the same cylindrical shape, similar quality (level of clathration) and could burn completely. It is valuable to remark that although the process and conditions to form samples was always similar, the complexity of the hydrates made them difficult to reproduce without fail, and occasionally the combustion behavior was not sufficiently robust to provide useful information. This random quality of hydrate formation is a commonly recognized challenge in the field.

There were a total of 30 experiments in the full measurement campaign, but for the reason explained above, the results and calculations of the experiments only consider 7 of the total which had the desirable characteristics needed to draw conclusions. Those are cases that had a complete combustion, good level of clathration little gas popping. The important properties that determine the quality of the samples are shown in Table 3.

**Table 3. Conditions of the valid experiments.**

| Experiment | Initial pressure (psi) | Ramp (K/hr) | Time to remove sample |
|---|---|---|---|
| Experiment 1 | 1640 | 5.1 | 2 min 52 sec |
| Experiment 2 | 1603 | 5.3 | 3 min 15 sec |
| Experiment 3 | 1149 | 4.4 | 3 min 5 sec |
| Experiment 4 | 1025 | 4.75 | 4 min |
| Experiment 5 | 1461 | 5.4 | 2 min 45 sec |
| Experiment 6 | 1232 | 4.94 | 3 min 22 sec |
| Experiment 7 | 1268 | 5 | 3 min 8 sec |
| Average | 1339.71 ±233.22 | 4.98 ±0.34 | 3 min 12 sec ±24 sec |

**Molar ratio of the methane hydrates**

Table 4 shows the masses of the samples as measured in each experiment, the mass percentage of methane content inside and the molar ratio of water to methane. These are the key features to determine the quality of the methane hydrates.

**Table 4. Masses hydrate and molar ratio.**

| Experiment | Initial ice mass (g) | Final hydrate mass (g) | % Mass methane | Molar ratio hydrate |
|---|---|---|---|---|
| Experiment 1 | 13.6 | 15.4 | 11.69 | 6.73 |
| Experiment 2 | 18.9 | 21.4 | 11.68 | 6.73 |
| Experiment 3 | 22.3 | 25.3 | 11.86 | 6.62 |
| Experiment 4 | 22.9 | 25.8 | 11.24 | 7.03 |
| Experiment 5 | 14.5 | 16.2 | 10.49 | 7.59 |
| Experiment 6 | 14.6 | 16.4 | 10.98 | 7.22 |
| Experiment 7 | 22.3 | 24.4 | 8.61 | 9.45 |
| Average | | | 10.9 ±1.13 | 7.34 ±0.99 |

The content of methane inside the hydrate is measured by the difference of mass between at the beginning and end of the formation process. The ideal saturated molar ratio of water and methane is 5.75, which means that all the cages of the hydrate contain a methane molecule. In the laboratory, it is very difficult to achieve this ideality and, therefore the clathration is determined experimentally. The clathration is the percentage of methane trapped in the hydrate related to that in the saturated case; it gives the quality of the sample.

$$Mass\ of\ CH_4\ left\ to\ be\ saturated\ (g) = \frac{Mass\ of\ H_2O\ (g)}{Ideal\ mass\ ratio} - Mass\ of\ CH_4\ (g)$$

$$Clathration\ (\%) = \left(\frac{Mass\ of\ CH_4\ left\ to\ be\ saturated\ (g)}{Mass\ of\ CH_4\ left\ to\ be\ saturated\ (g) + Mass\ of\ CH_4\ (g)}\right) * 100$$

As shown in Figure 39, clathration varies from 60.83% to 86.9%, with an average of 79.41% which is a very high quality. Considering that this is not the real clathration after

the formation, because during the process of taking out the samples, some methane is lost and the samples started dissociating. Therefore, the clathration of the methane hydrates during the formation is higher than 85% in all cases.

Clathration during the formation process could be monitored by measuring the pressure drop inside the cell as the methane gas is being absorbed inside the recrystallizing ice. The clathration is then estimated from the original mass of the ice and the overall temperature corrected pressure drop. For this project, measurement of clathration with pressure drop was not used because it is focused in the combustion of hydrates and not in the formation, as other group of the project is working [24] In addition, the results from the pressure drop calculations are, however, very similar to the mass balance findings.

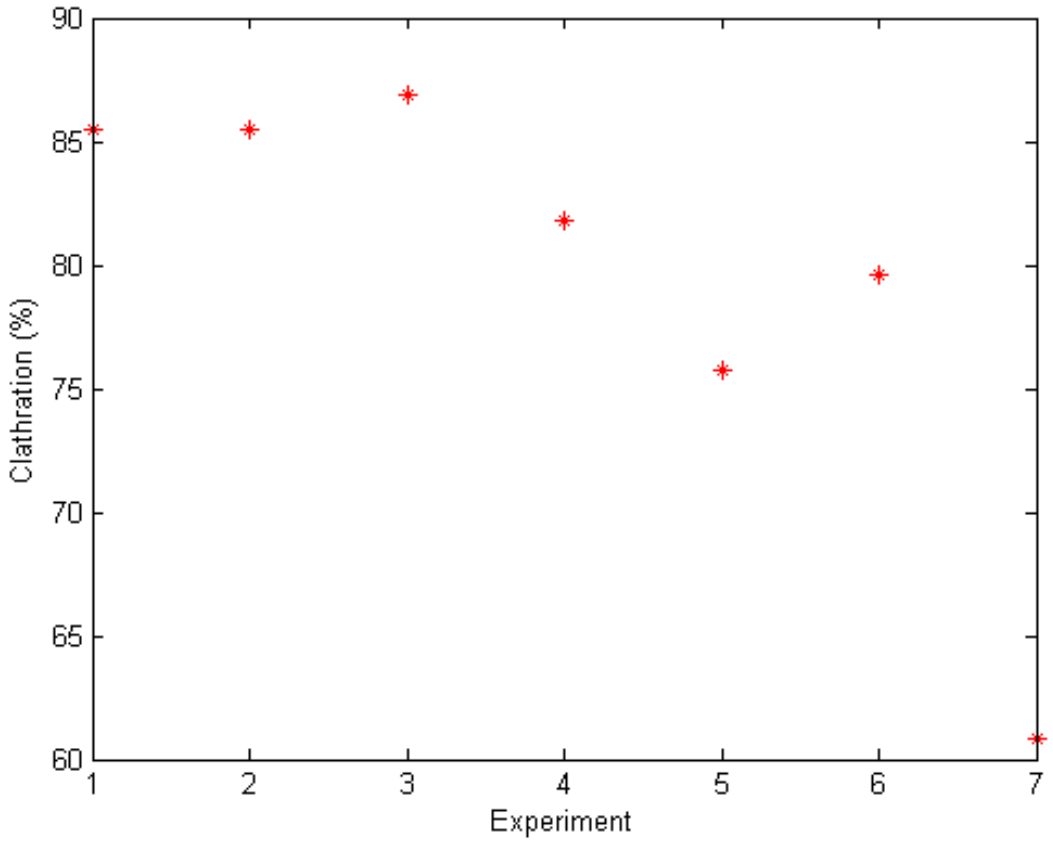


**Figure 39. Percentage of clathration of the experiments.**

**Time history**

During the experiments, what it is measured with the load cells and the Labview program is

the weight of the sample and the weight of the water melted during all the combustion time. Figure 41 shows the time history of the different experiments. They all have the same shape (cylindrical), but they vary in size and mass content.

Is it possible to appreciate the noise of the signal from the load cells readings, but with the sorbothane bumpers, explained in the design section above, vibration of the table was reduced so that the maximum error is reduced to ±0.15g (0.5-1% of the total mass).

One challenge of the measurements is that the reading of the water drained is delayed because the water gets trapped between the holes of the mesh and stays there for a time, as can be seen in Figure 40.

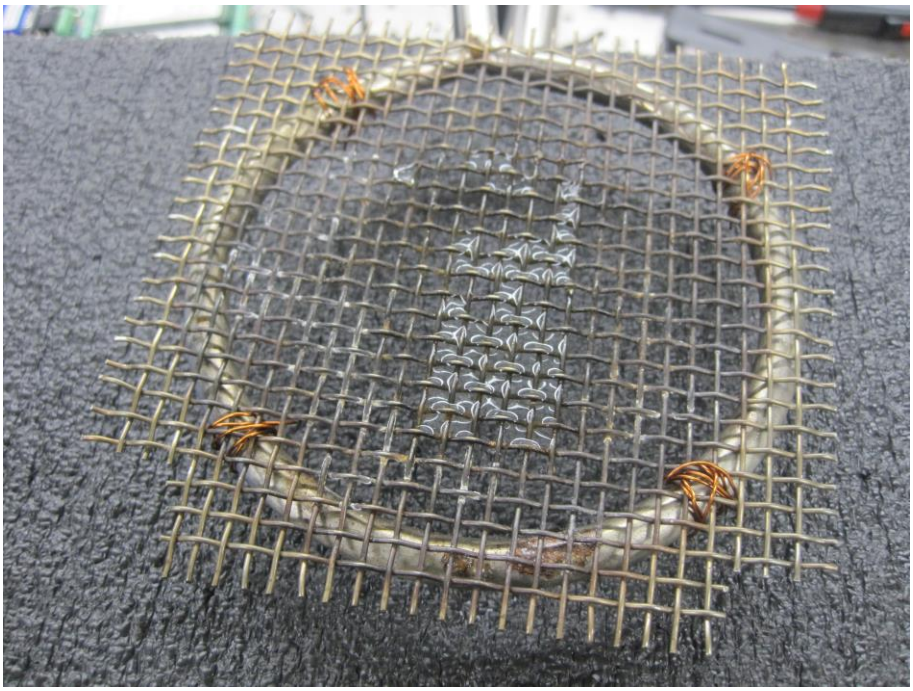

**Figure 40. Water trapped in the mesh.**

For determining the delay time, and in order to adjust the measurements to the real drain time, a linear integration is computed for the water drained measured in order to determine the delay. This is possible because the experiments show that the water drained is approximately constant. The final reading of the sample is the water that gets trapped in the mesh, and it is assumed that this is the water needed to start the draining. Therefore the time delay is calculated and the water drained can be shifted to estimate the experiment in

real time:

$$time\ delay\ water\ drained\ (s) = \frac{Mass\ trapped\ water\ (g)}{Slope\ linear\ integration\ (\frac{g}{s})}$$

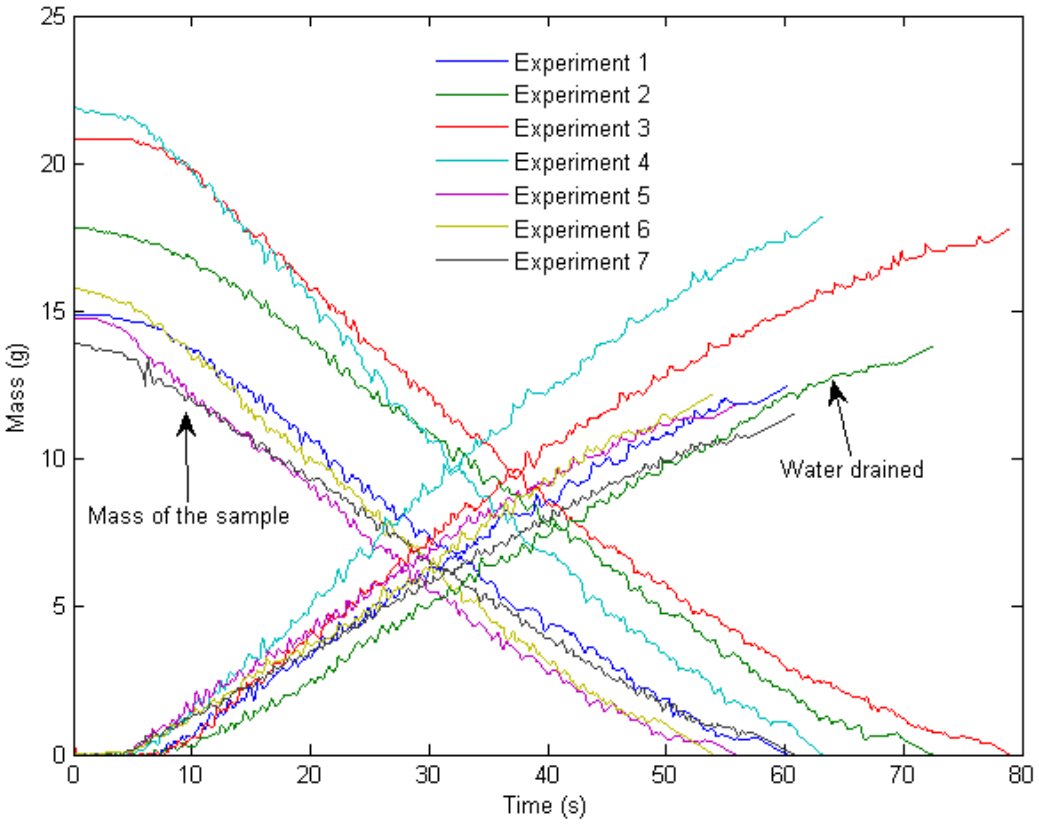


**Figure 41. Time history measurements of the experiments.**

With the readings of the weights, the water drained and the mass of the sample are calculated with a polynomial interpolation of third order to smooth the noise and simplify the calculations.

The gas released, which is the methane released from the hydrate and water evaporated due to the heat of the flame, is calculated by the difference between the initial mass of the sample minus the two readings of the load cells. The polynomial function and the gas released are shown in Figure 42.

$$gas\ released\ (t) = initial\ mass\ sample\ (t_0) - mass\ sample(t) - water\ drained\ (t)$$

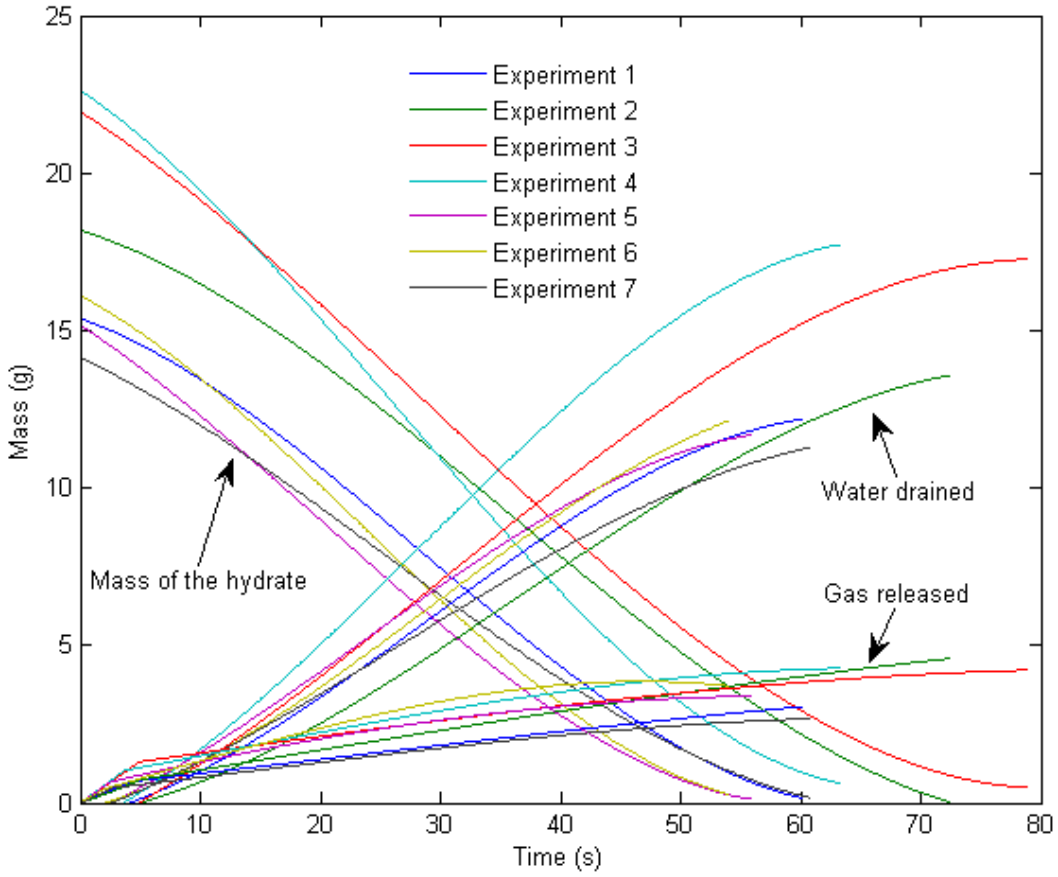


**Figure 42. Time history using polynomial fitting functions.**

From Figure 41 and Figure 42 it is possible to see that there is a starting stage (0-5 seconds) where a small amount of the hydrate is dissociated, and a quasi-steady-state stage (after 5 seconds) with constant dissociation, draining and gas released.

To be able to compare samples with different mass, the experiments are transformed to dimensionless units dividing all the masses by the initial mass of the methane hydrate, having this initial mass as unity.

$$Dimensionless\ mass\ sample\ (t) = \frac{Mass\ sample\ (t)}{Initial\ mass\ sample\ (t_0)}$$

$$Dimensionless\ water\ melted\ (t) = \frac{Water\ melted(t)}{Initial\ mass\ sample\ (t_0)}$$

$$Dimensionless\ gas\ released\ (t) = \frac{Gas\ released(t)}{Initial\ mass\ sample\ (t_0)}$$

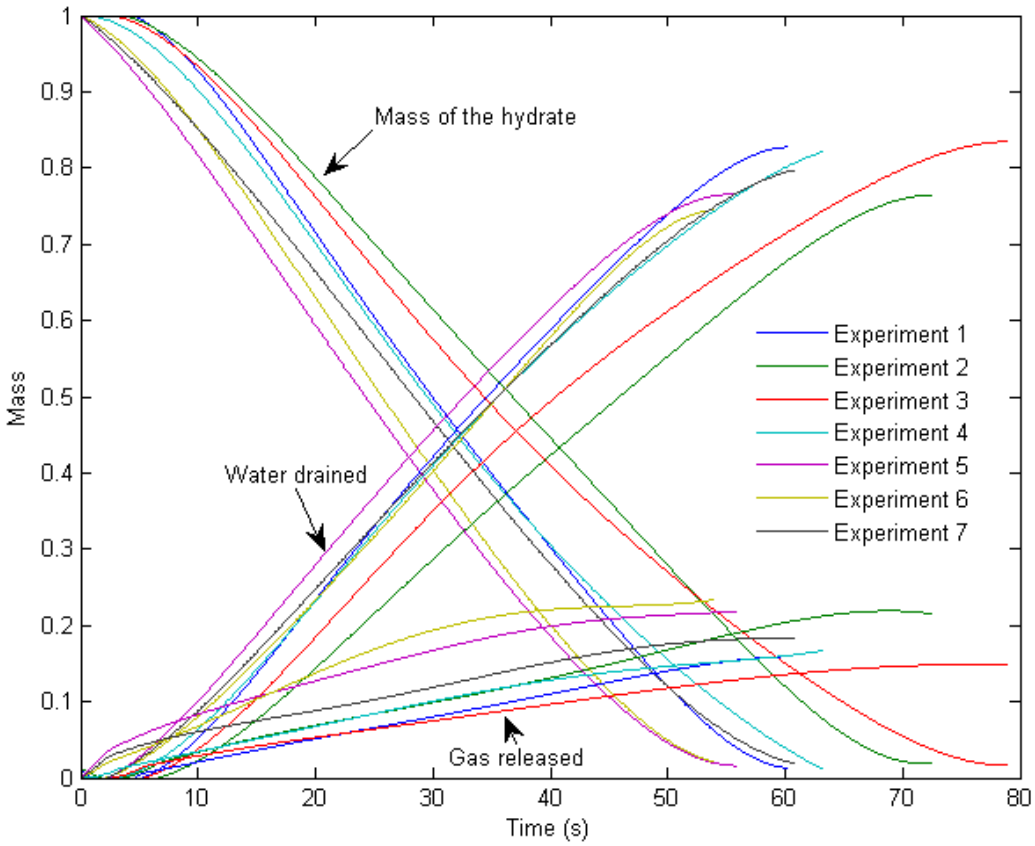


**Figure 43. Time history dimensionless measurements and dimensionless gas released.**

As seen in Figure 43, the experiments have the same history shape and the quasi-steady state is shown from approximately 10 seconds until the end.

**Water drained and gas released**

One of the important features of the combustion is to determine the amount of water evaporated that is contained in the flame; therefore the mass percentage of water drained and gas released can explain the mass percentage of the total water evaporated.

$$Total\ mass\ percentage\ water\ evaporated = 100\% - percentage\ mass\ water\ drained - percentage\ mass\ content\ methane$$

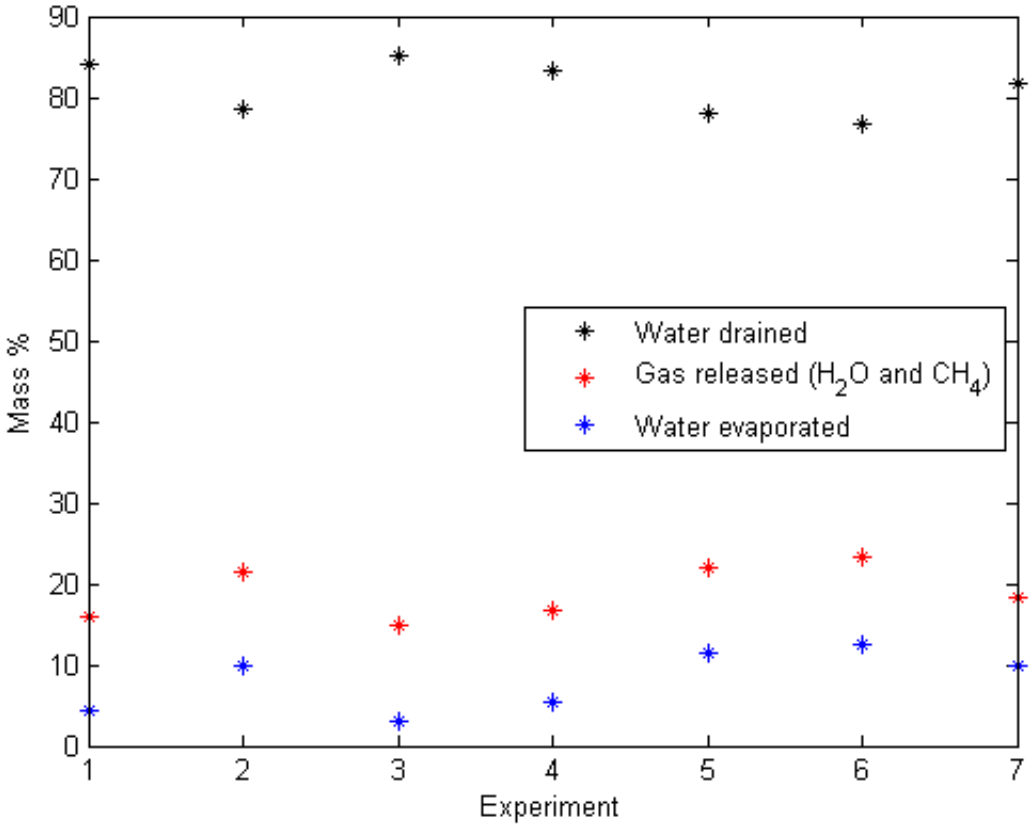


**Figure 44. Water melted, water evaporated and gas released mass percentages.**

The mean value of water evaporated and methane released is 18.95% ±3.31, with 81.05% ±3.31 of water melted and 8.01% ±3.71 of water evaporated. This means that on average for every unit of mass loss, 81% is liquid water drained, 8% is water evaporated, and 11% is methane.

**Time combustion**

The combustion time, Figure 45, is the time the flame exists. The time indicates how fast the methane clathrate dissociates. There is no clear pattern between the methane content and the time, and the reason for lasting longer is related to the combustion behavior of the flame; since in each experiment the flame burns at different places of the hydrate surface at the end of the combustion. In addition, the end of combustion is a very long period where relatively little mass is lost leading to larger variation in the overall time relative to the steady burning rate and evaporation fraction.

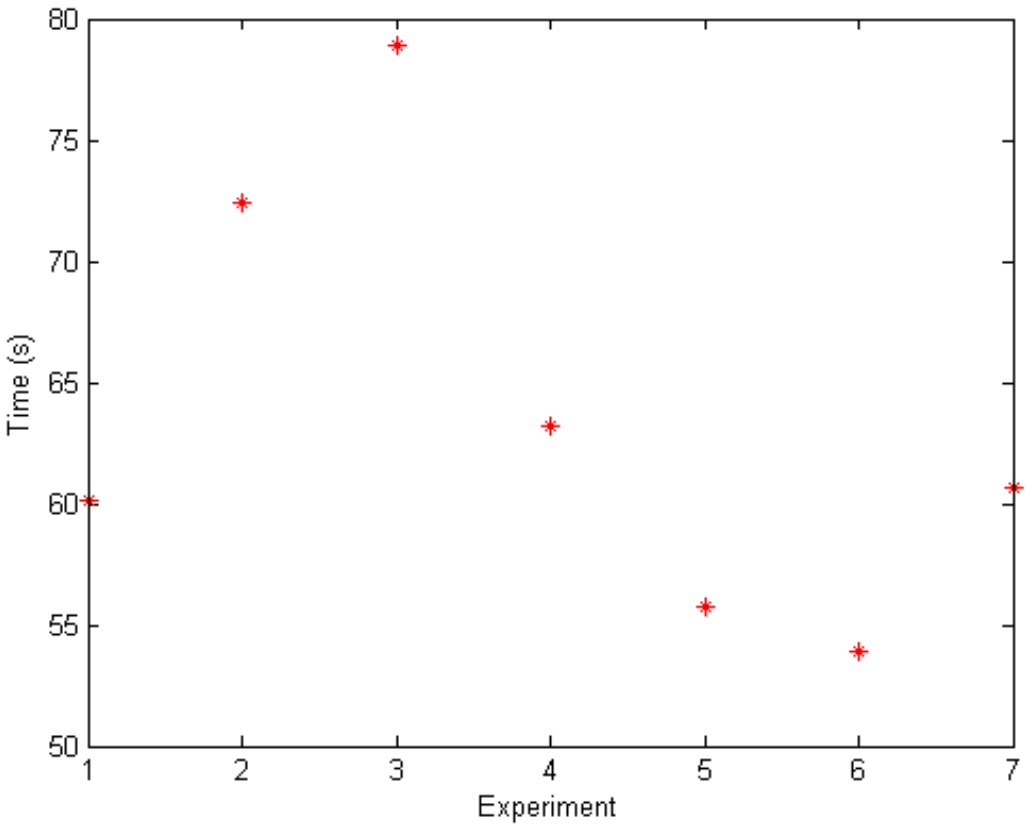


**Figure 45. Combustion time of the experiment.**

**Hydrate dissociation rate**

During combustion, the hydrate is dissociating into liquid water, vapor water and the methane released.

$$Mass\ dissociated\ (t) = Initial\ mass\ (t_0) - Liquid\ water(t) - Vapor\ water\ (t) - methane\ released\ (t)$$

In the experiment, the dissociation is calculated by the difference of mass between the initial mass of the sample and the mass of the sample at real time.

$$mass\ hydrate\ dissociated\ (t) = initial\ mass\ hydrate(t_0) - mass\ sample\ (t)$$

Once the dissociation is known, the velocity rate of dissociation is calculated by:

$$Dissociation\ rate\ \left({}^{g}/_{s}\right) = \frac{d(Mass\ dissociated\ (t))}{dt}$$

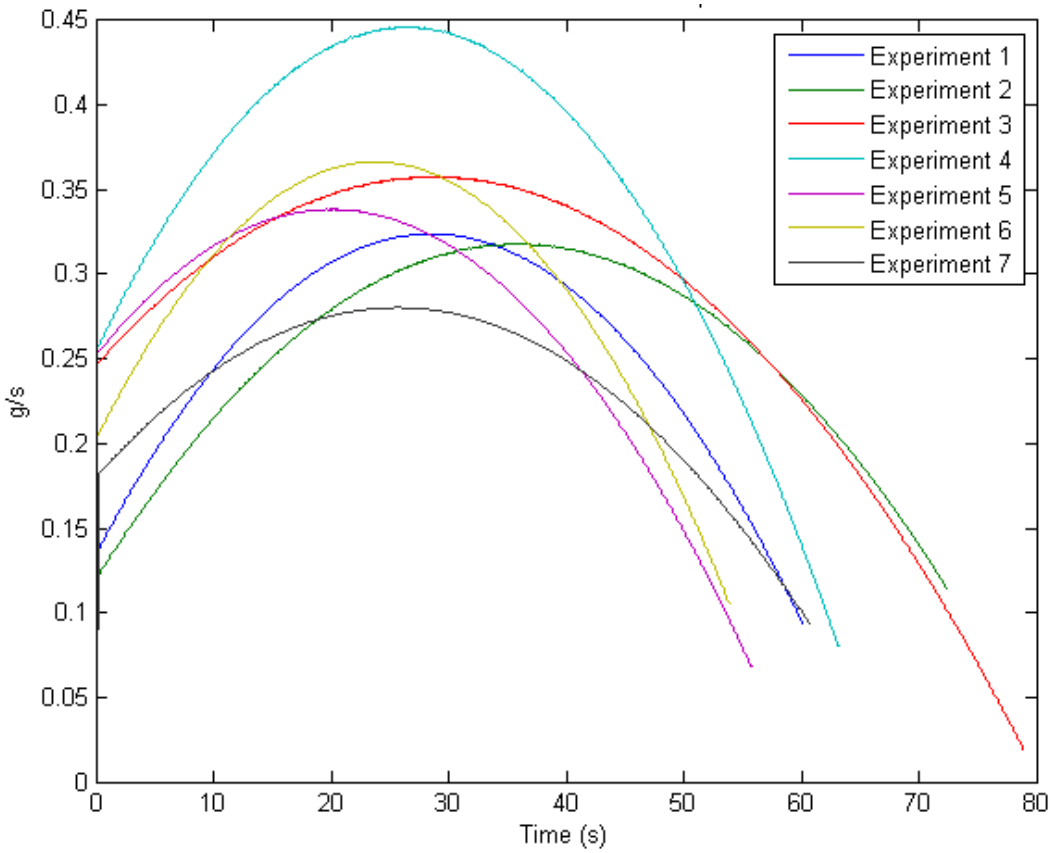


**Figure 46. Dissociation rate of methane hydrates.**

As seen in Figure 46, there is a first stage between 0 and 20 seconds where the dissociation velocity increases rapidly to its peak, a second stage where this velocity either stays steady or decreases slowly and the final stage where it dissociates at a low rate until the sample is gone.

For comparing the results, it is useful to use the dimensionless units as in the time history explained above. In Figure 47 it is possible to see the variability of the samples, while in 5 experiments the quasi-steady state is 2% $s^{-1,}$ one is at 4% $s^{-1}$ and another one at 5% $s^{-1}$. This difference in the last two experiments is due to a higher amount of water in the hydrate sample. It is important to point out that the combustion time depends directly on the dissociation rate, and therefore a higher dissociation rate also means faster combustion and shorter burning time.

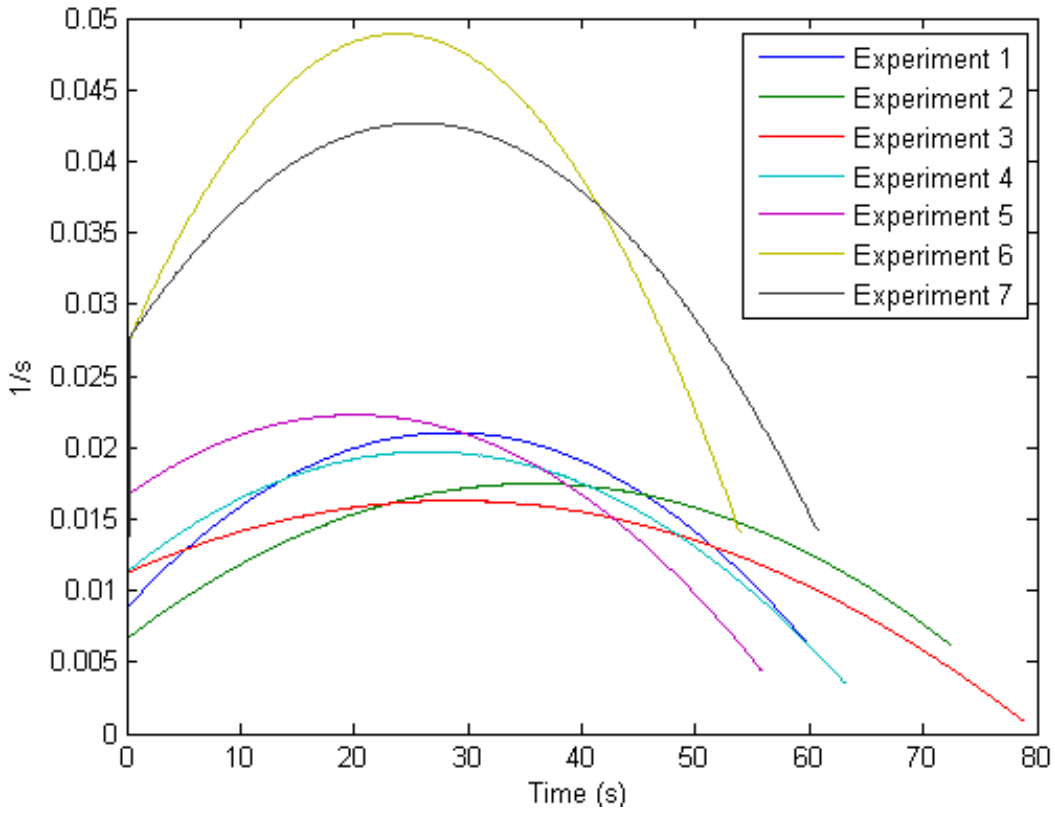


**Figure 47. Dimensionless dissociation rate.**

**Burning rate**

The burning rate, Figure 48, is the velocity at which the gas is released from the hydrate. This gas is composed of the methane released and the water evaporated. It is calculated by the derivative of time of the gas released.

$$Burning\ rate\ \left({}^{g}/_{s}\right) = \frac{d(Gas\ released\ (t))}{dt}$$

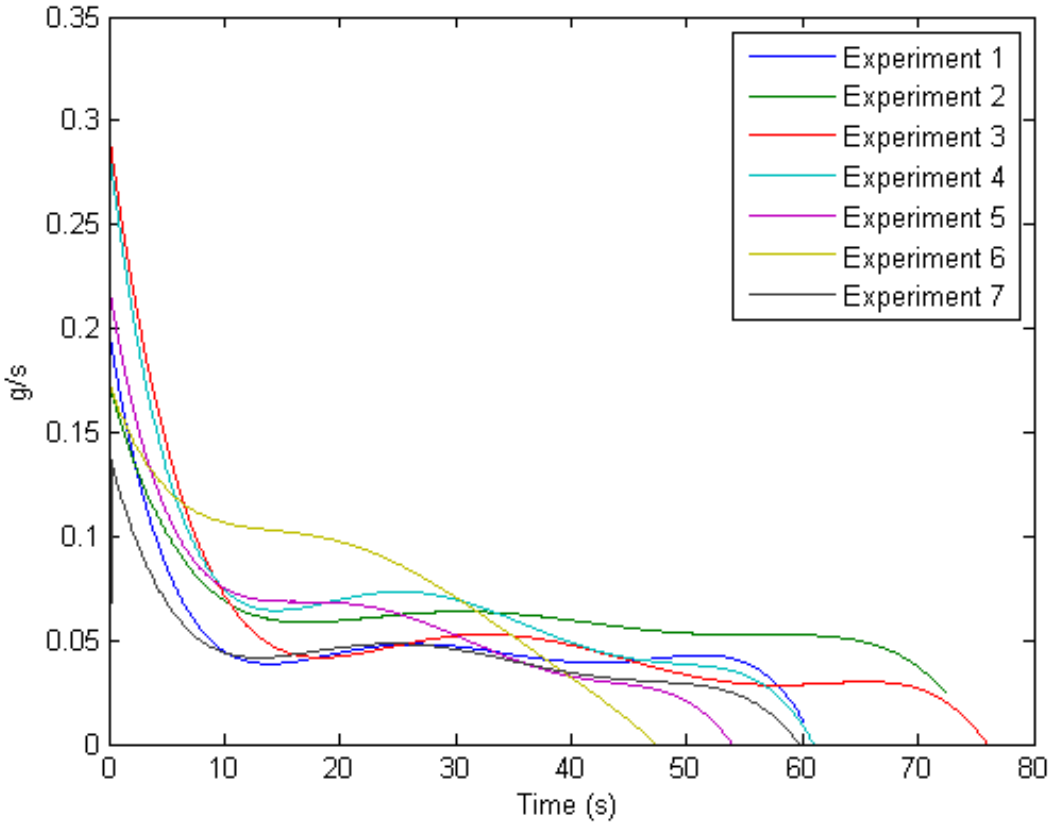


**Figure 48. Burning rate.**

The burning rate has two different regimes. At the beginning of the combustion this burning rate fluctuates in a range between 0.15 and 0.3 g/s, but during the firsts instants of the combustion the burning rate is higher because the outer layer of the hydrate is evaporating faster before it reaches the steady-steady state. This regime coincides with the second regime of the combustion process explained before with a bright flame and more heat transfer.

After 5-10 seconds, the burning rate stabilizes at around 0.05 g/s at the quasi-steady state until the end of the combustion. This parameter is important to prove that it is possible to have steady burning of the hydrates and determines their fuel consumption rate. The upturn in rate is probably an artifact of the curve fits.

Figure 49 shows the dimensionless burning rate to make it easier to compare between the experiments.

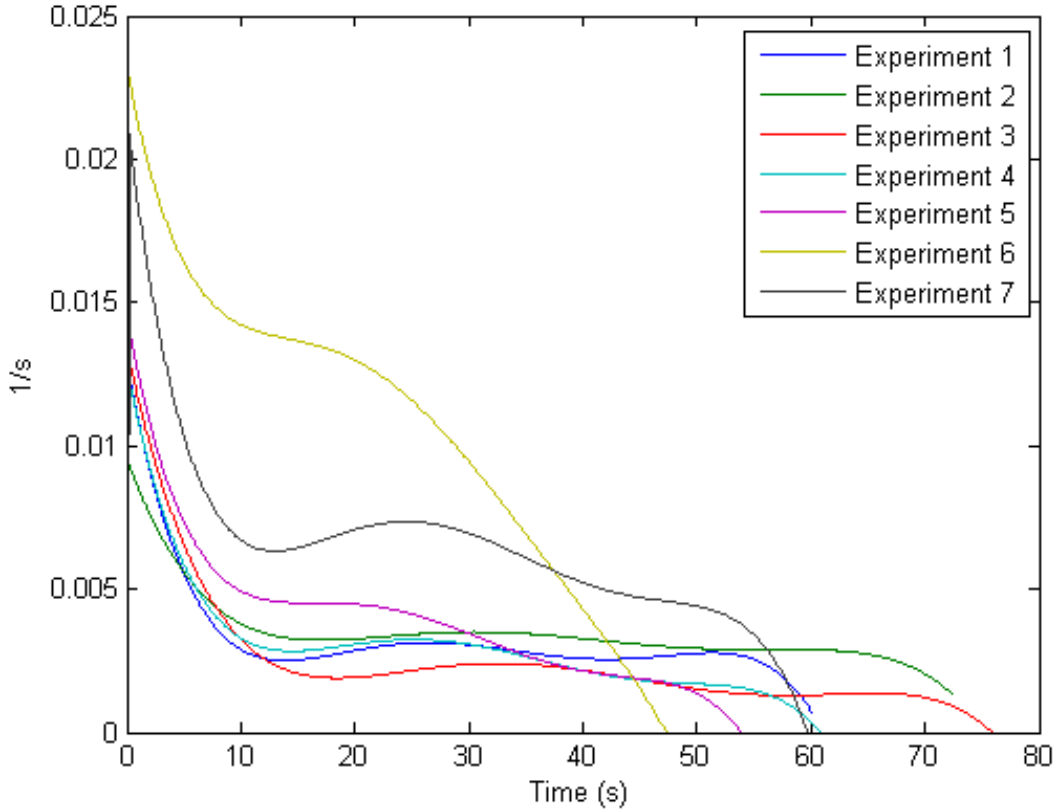


**Figure 49. Dimensionless burning rate.**

**Draining rate**

The draining rate, Figure 50, is the velocity at which the liquid water is drained through the mesh and collected in the beaker. It is assumed that the liquid collected is composed only of liquid water and no other components, although it might be interesting to analyze the composition of the liquid. It is calculated by the derivative with time of the water drained.

$$Burning\ rate\ \left({}^{g}/_{s}\right) = \frac{d(Water\ drained\ (t))}{dt}$$

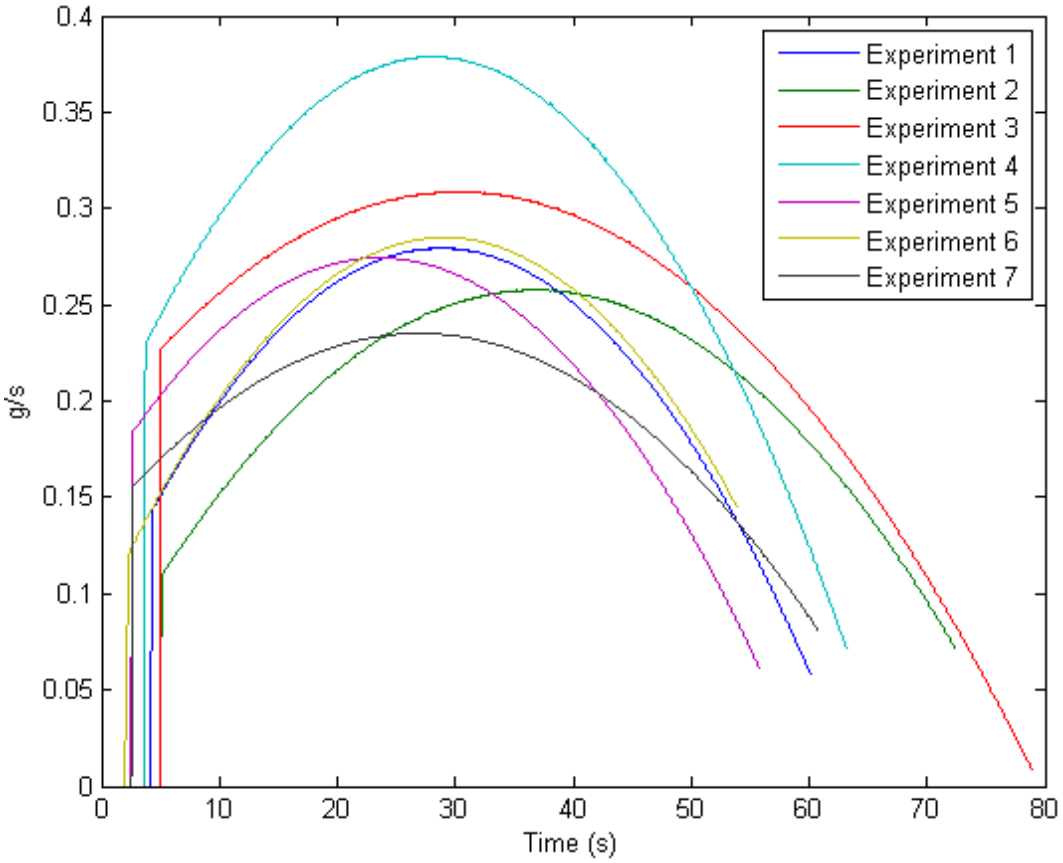


**Figure 50. Draining rate.**

It can be seen that at the beginning there is no water melting until 2-6 seconds, depending on the experiment. The physical explanation is that the flame does not melt the outer layer of the hydrate immediately, it needs time to heat it and also the liquid layer must flow from the top of the hydrate to the mesh. Even though there is a shifting of the delay of the mesh to try to avoid it, it is impossible to know it exactly and this affects the first stage of the draining rate and the difference between experiments.

As in the dissociation and burning rate, after around 10 seconds, the quasi-steady state is plausible until the end. The same pattern occurs, with the experiments that have a higher draining rate, shown in the dimensionless version of Figure 51, also being the ones with shorter combustion time. In conclusion, the three parameters of the combustion are in concordance with the existence of a quasi-steady state of combustion during a majority of the burn. The two outliers experiments with higher draining rate is because the percentage

of water is bigger, therefore more water needs to be drained.

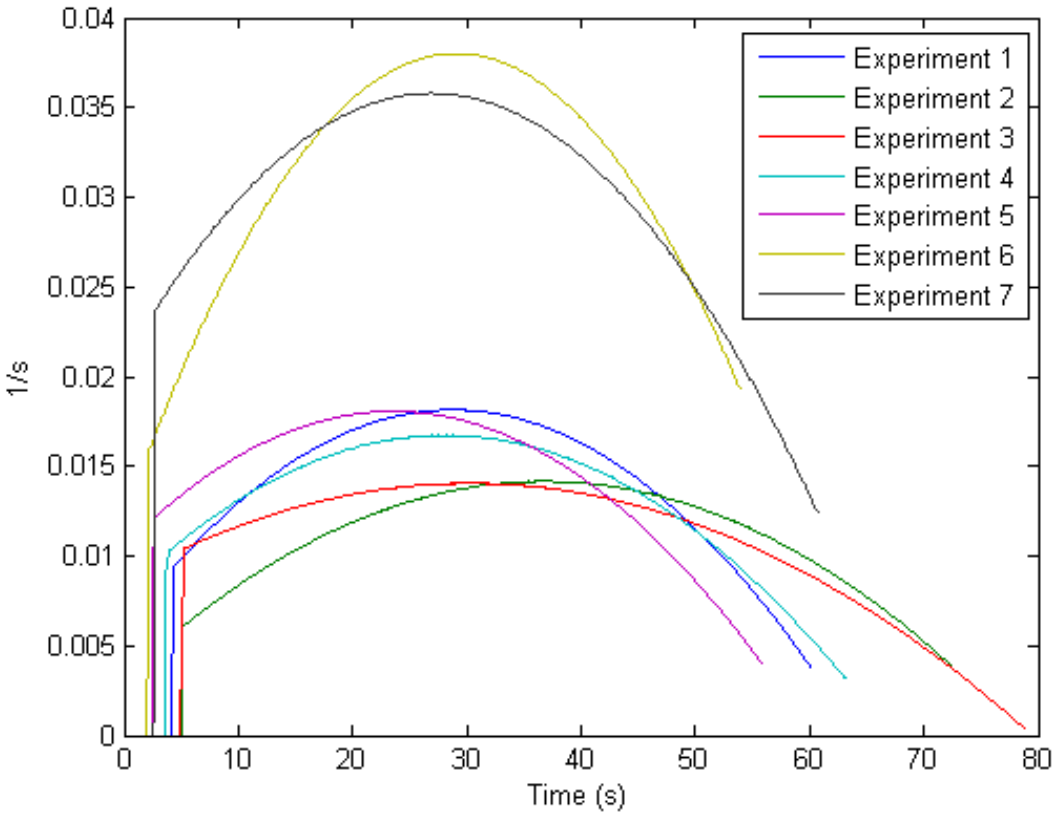


**Figure 51. Dimensionless draining rate.**

# CALCULATIONS

### Estimation of methane in the flame

The main objective of the project is to analyze the composition of the gas released into the flame. In the previous sections it was explained that this gas has methane and water, but not the quantity of each at every instant of the combustion.

The estimation of the methane released from the hydrate is assumed to be homogeneous throughout all the process and follows the molar ratio of the methane hydrate sample. In other words, the dissociation process releases methane and water at a constant ratio. Therefore, using the differential weight measurements and the percentage of methane of the sample it is possible to calculate the methane released:

$$Mass\ of\ CH_4\ (t) = [Initial\ mass\ hydrate(t_0) - Mass\ sample\ (t)] * Percentage\ CH_4\ hydrate$$

This assumption is reasonable because the experiments had shown that the combustion reaches a quasi-steady state where the behavior of the combustion is constant.

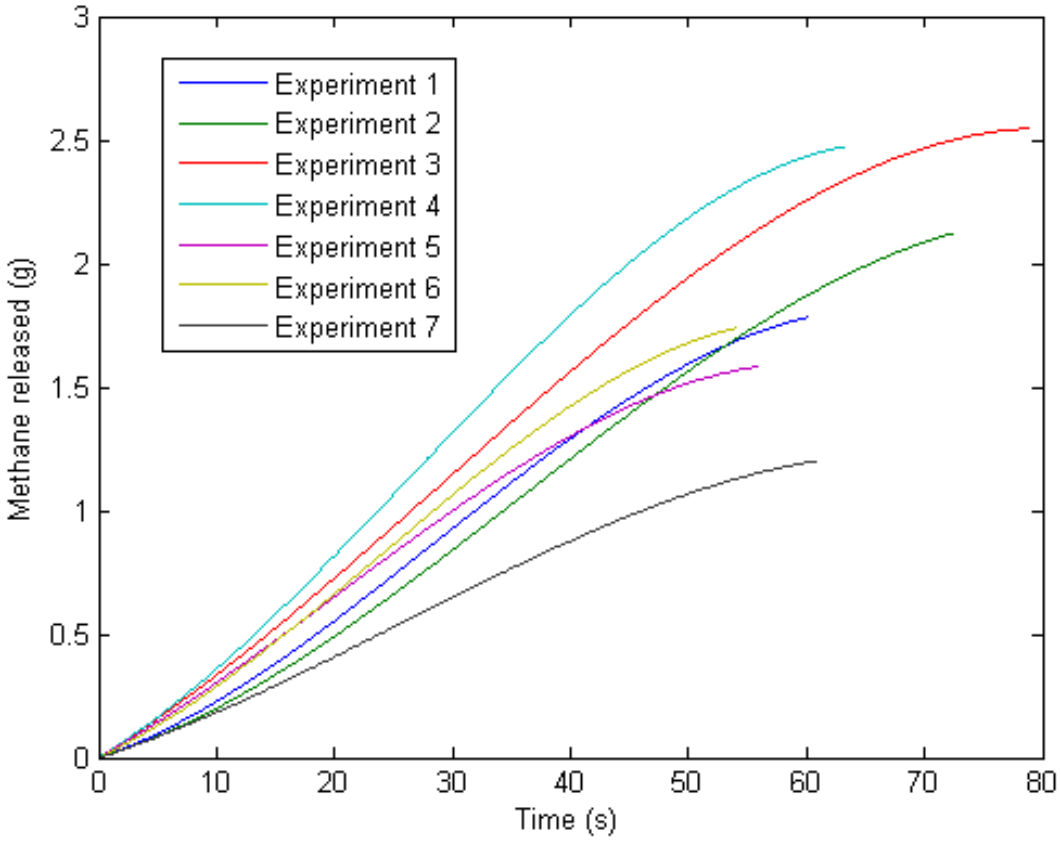


**Figure 52. Methane released during combustion.**

As seen in Figure 52, the shape of the methane released is the same as the dissociation because it is only a percentage of it, but is important to realize that the methane content and release are very similar in all the experiments. This evidence can be seen more easily in Figure 53 by the dimensionless results.

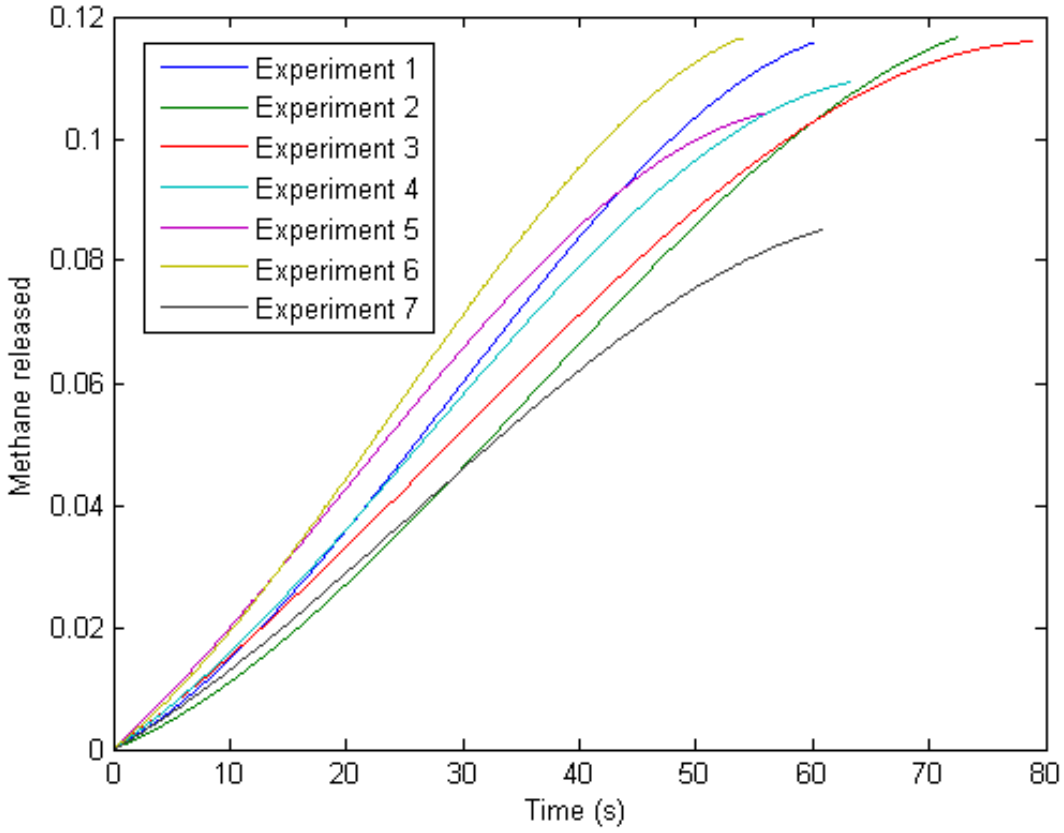


**Figure 53. Fractional methane released.**

**Water evaporated**

With the methane calculated, it is possible to estimate the water evaporated by simply determining the difference of the masses.

$$Mass\ water\ evaporated\ (t) = Mass\ dissociated\ (t) - Mass\ of\ CH_4\ (t)$$

or

$$Mass\ water\ evaporated\ (t) = Initial\ mass\ hydrate(t_0) - Mass\ sample\ (t) - Mass\ of\ CH_4\ (t) - Water\ drained\ (t)$$

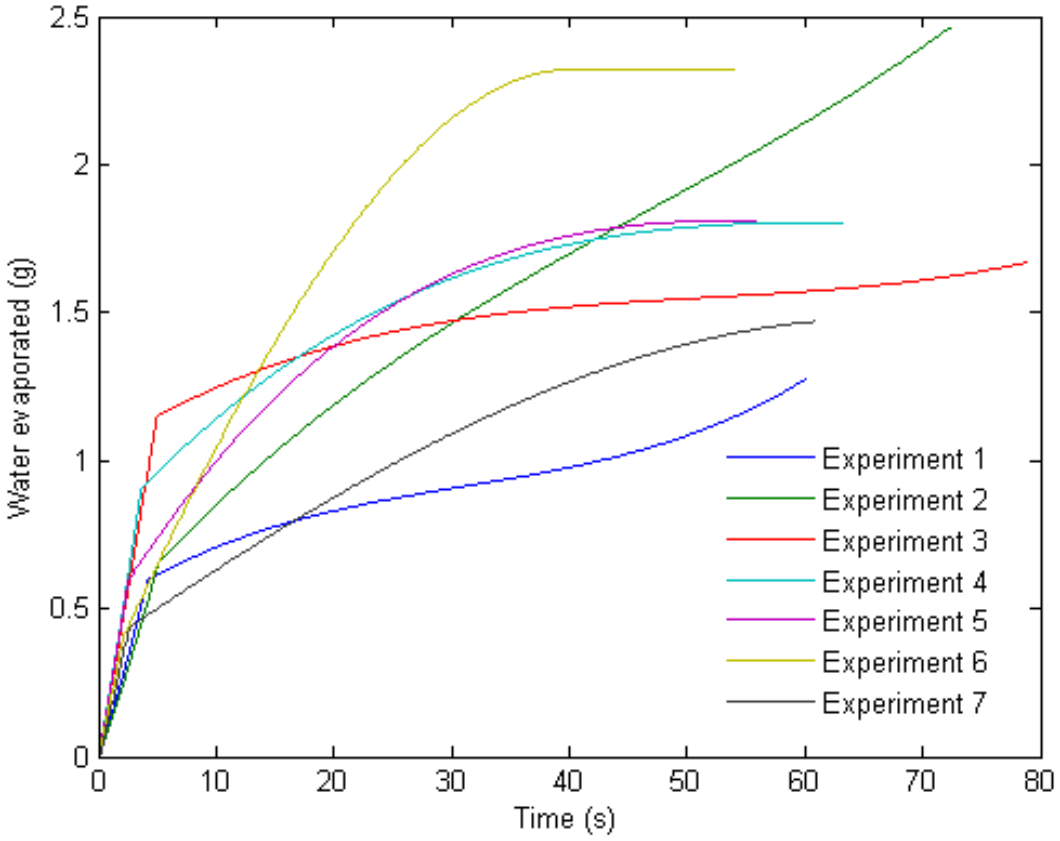


**Figure 54. Water evaporated during combustion.**

As Figure 54 shows, the water content in the flame varies throughout the different experiments due to the different percentage amount of water, although it is possible to compare their qualitative behavior. There are two main periods during the combustion; during the first 3-5 seconds, there is a large amount of vapor water in the flame and a second period where the water evaporated increases at a relatively constant rate, i.e., during the quasi-steady burning period.

Figure 55 is the same as Figure 54 except with dimensionless units. The variation of experiments is still appreciable.

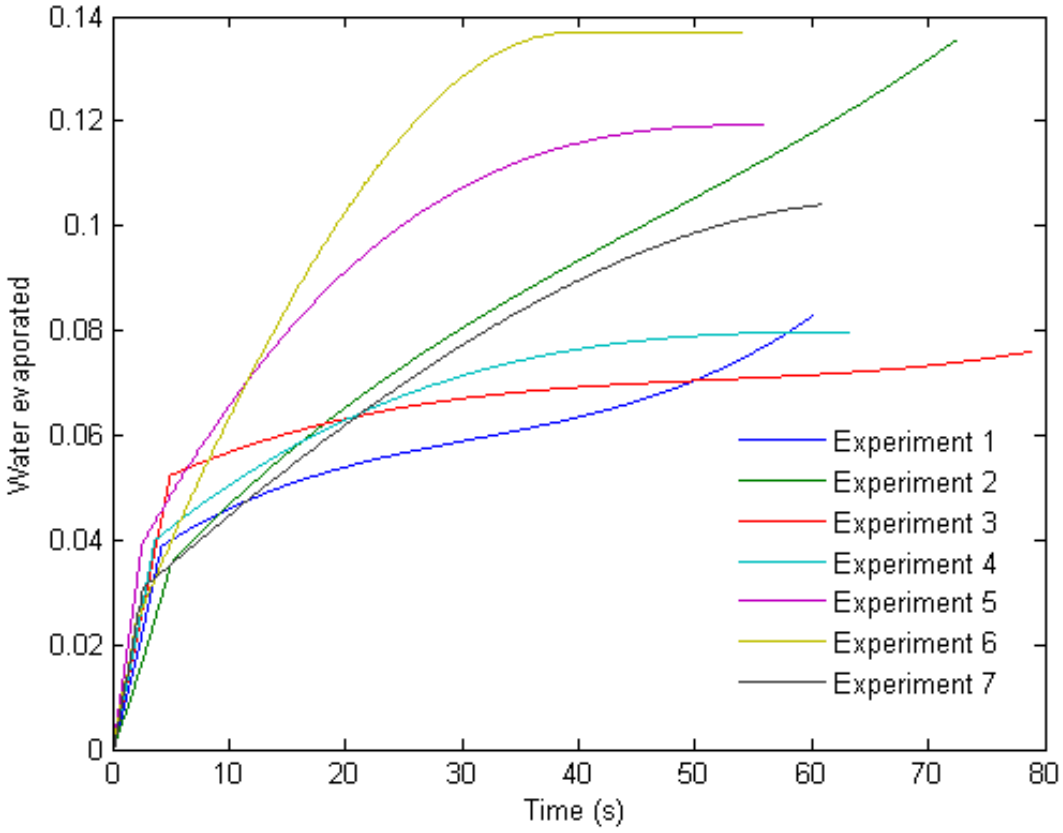


**Figure 55. Fractional water evaporated.**

**Flow rate of methane released**

The flow rate of the methane, Figure 56 and Figure 57, is the rate at which the methane is released from the hydrate. It is calculated by the time derivative of the methane released.

$$Methane\ flow\ rate\ \left({}^{g}/_{s}\right) = \frac{d(Mass\ methane\ released\ (t))}{dt}$$

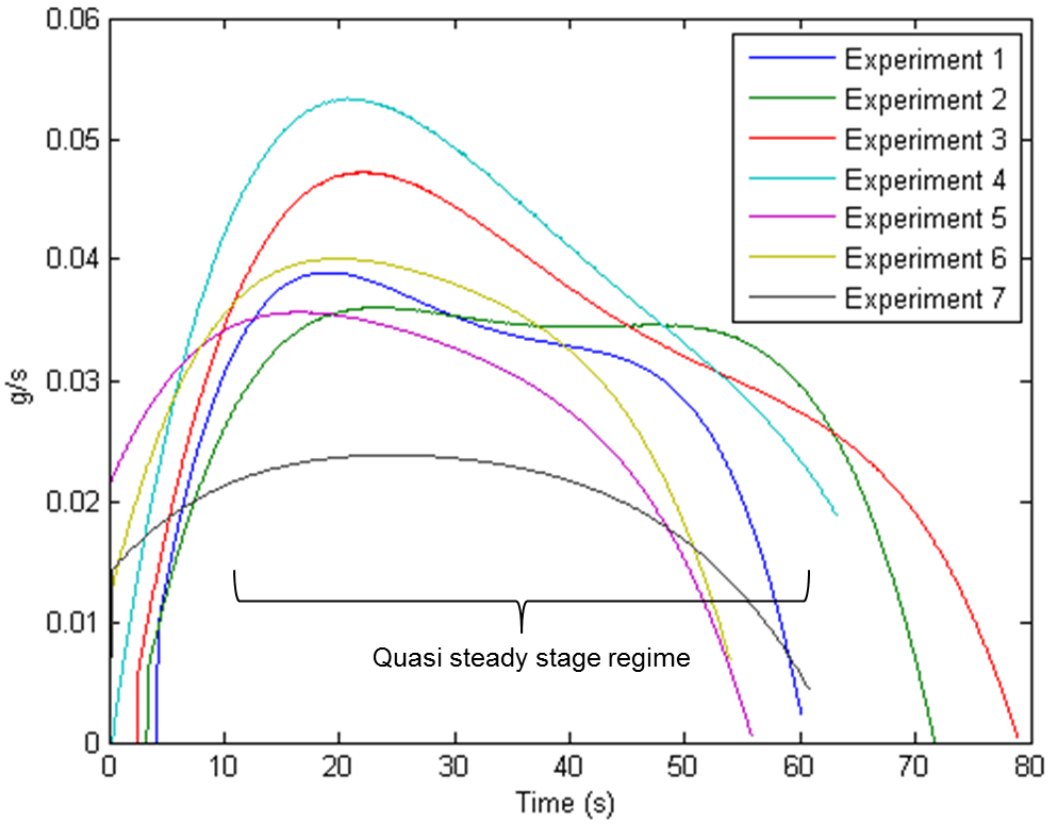


**Figure 56. Methane flow rate released.**

As seen in Figure 56, they all have the same general behavior. There is a first stage between 0 and 20 seconds where the methane released increases rapidly to its peak, a second stage where this value either stays steady or decreases slowly, and the final stage where the gas is released at a low rate until the sample is gone. For comparing the results, it is useful to use dimensionless units. In Figure 57 it is possible to see the variability of the samples, while in 5 experiments the quasi-steady state fractional loss rate is $2x10^{-3}$ $s^{-1,}$ one at $3.5x10^{-3}$ $s^{-1}$ and another one at $5.5x10^{-3}$ $s^{-1}$.

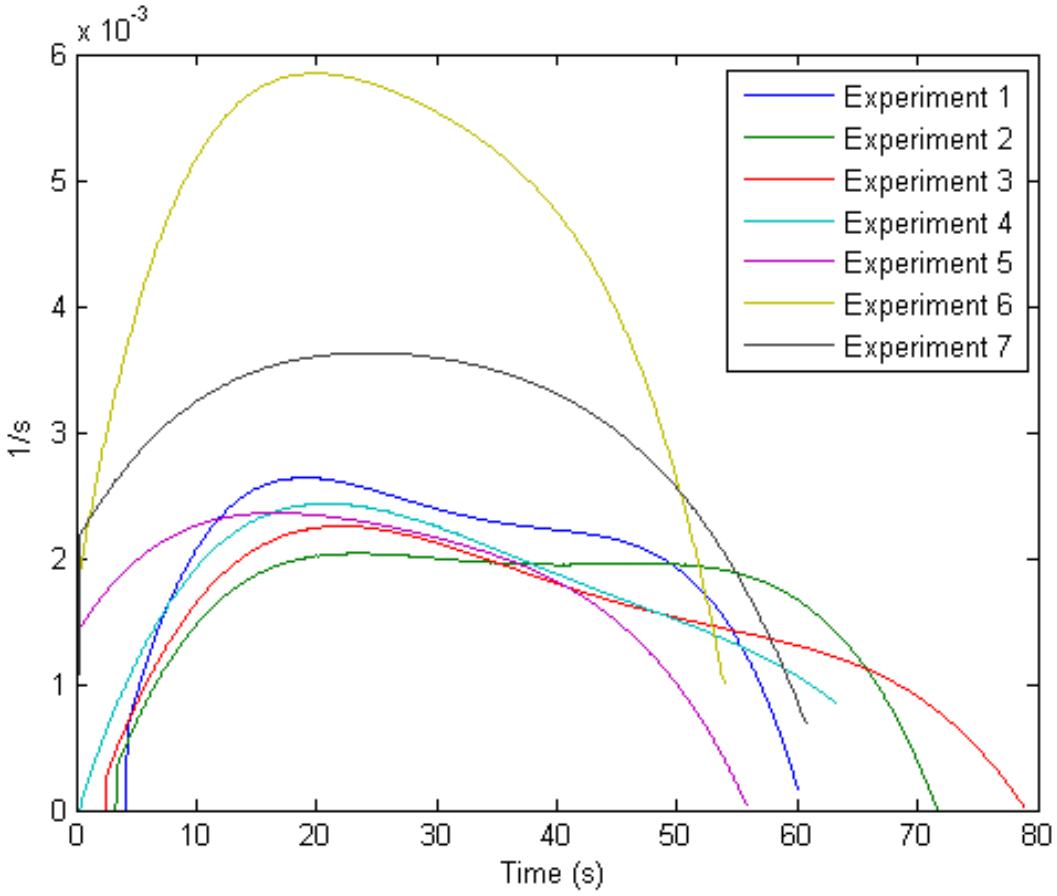


**Figure 57. Dimensionless methane flow rate released.**

**Flow rate of water evaporated**

The flow rate of the water evaporated, Figure 58, is the velocity at which the water evaporated is released from the hydrate. It is calculated by the time derivative of the water evaporated.

$$Water\ evaporated\ flow\ rate\ \left({}^{g}/_{s}\right) = \frac{d(Mass\ water\ evaporated\ (t))}{dt}$$

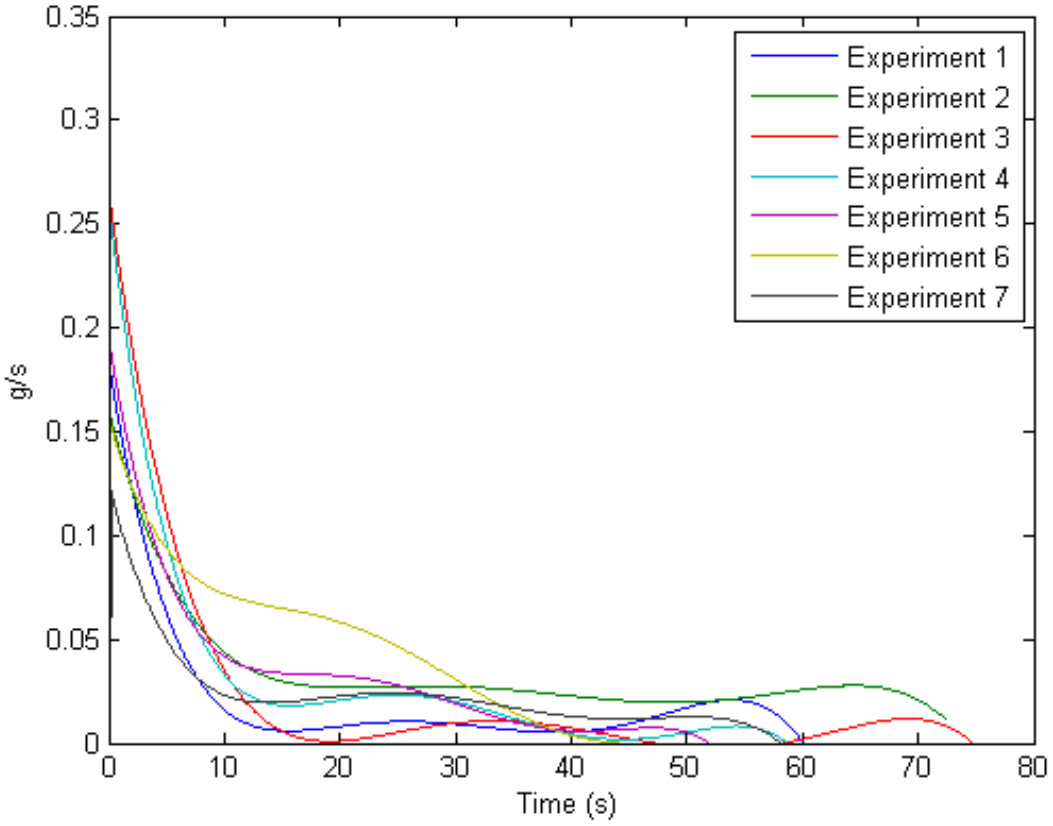


**Figure 58. Water evaporated flow rate.**

In Figure 58 and Figure 59, the initial high rate of water vapor generation can be seen during the first 3-5 seconds. This is followed by the quasi-steady state phase with some oscillations due to the non-homogeneity of the process compare to the calculations, the real combustion is not homogenous and small variations produce these oscillations in the calculations of the water evaporated flow rate. This error is expected with the assumption of homogeneity of combustion.

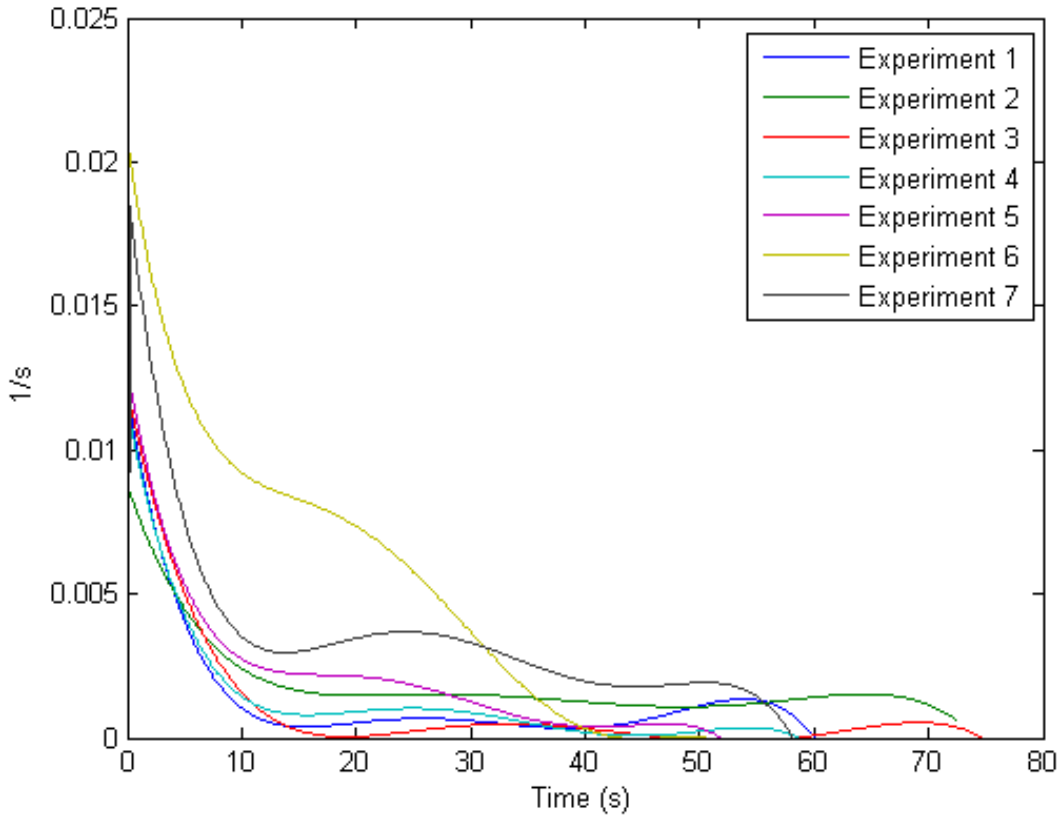


**Figure 59. Dimensionless water evaporated flow rate.**

**Molar ratio of water evaporated versus methane released**

The molar ratio of the water evaporated and methane released, Figure 60, is very important because it describes the composition of the flame and determines the temperature, heat release and sustainability of the flame. There is a computationally determined maximum ratio of water/methane content in the flame in the steady-state of approximately 2, as other work from the laboratory shows [23] , which is more than is seen in natural burning of hydrates. Hence, calculating the molar ratio during combustion is essential to demonstrate that the combustion can be sustained with the amount of water evaporated during the process.

During the first seconds, before steady-state, the content of water evaporated is much larger than the methane as explained in previous section. It cannot be compared to the limits of the flame sustainability because this phase is not in the steady-state and is governed by other properties of the combustion. After this time, the molar ratio decreases rapidly to the

zone that is steady but the amount of water decreases until the end of the combustion. In the experiments, this value varies from 0.5 to 1.5 with an average of 0.8841 with a deviation of ±0.441.

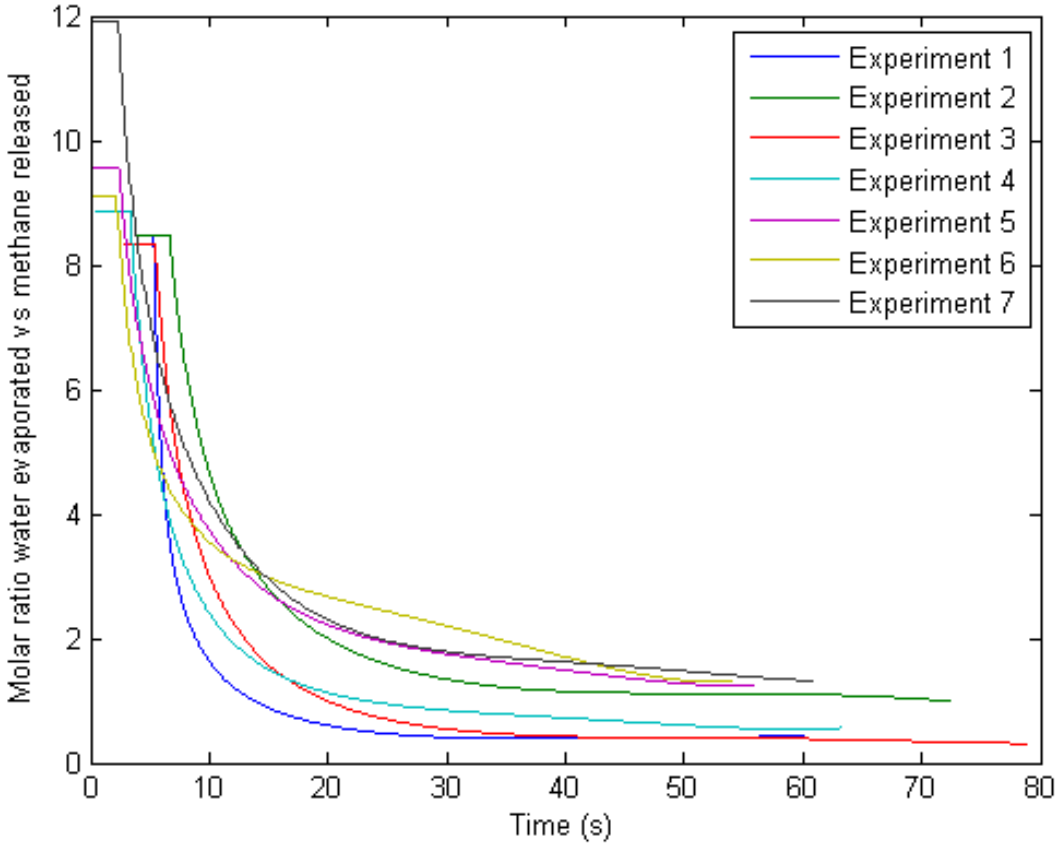


**Figure 60. Molar ratio of water/methane during combustion of the hydrates.**

**Surface measurements**

To have a better understanding of the quasi-steady state and real comparison between the different experiments and further energy model, the hydrate exposed surface is estimated to relate all the previous calculations to the surface. The flame is enclosing the entire sample therefore the surface is the area of the cylinder. In this way, it is possible to extrapolate the results obtained to all the hydrate samples, independently of the size. The surface is determined by the video of the combustion and analyzed using the ImageJ software to determine the diameter and length of the cylinder during different stages of combustion, assuming that the cylindrical shape is conserved all the time. In Figure 61, different stages

of the measurements are shown; initial hydrate without ignition, steady-state phase at 30 seconds, and the final phase at 50 seconds. Measurements were taken every 5 seconds during two experiments of different size; the first one used a sample 6 cm long by 2 cm diameter and the second one was 7.5 cm long by 2.5 cm diameter. They both have the same regression result; therefore it is assumed that both samples burn with the same surface area regression.

**Figure 61. ImageJ measurements of the area of the hydrate during combustion.**

The measurement showed in the following graphs is for the second sample, 7.5x2.5 cm. The first sample looks very similar to the second one.

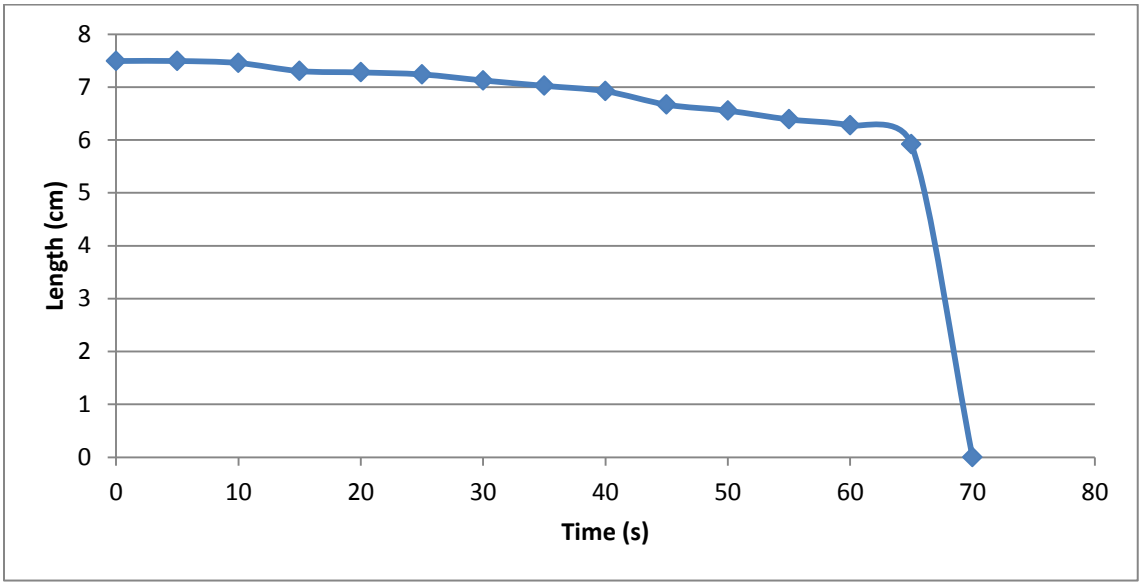


**Figure 62. Length of the 7.5x2.5 cm hydrate sample during combustion.**

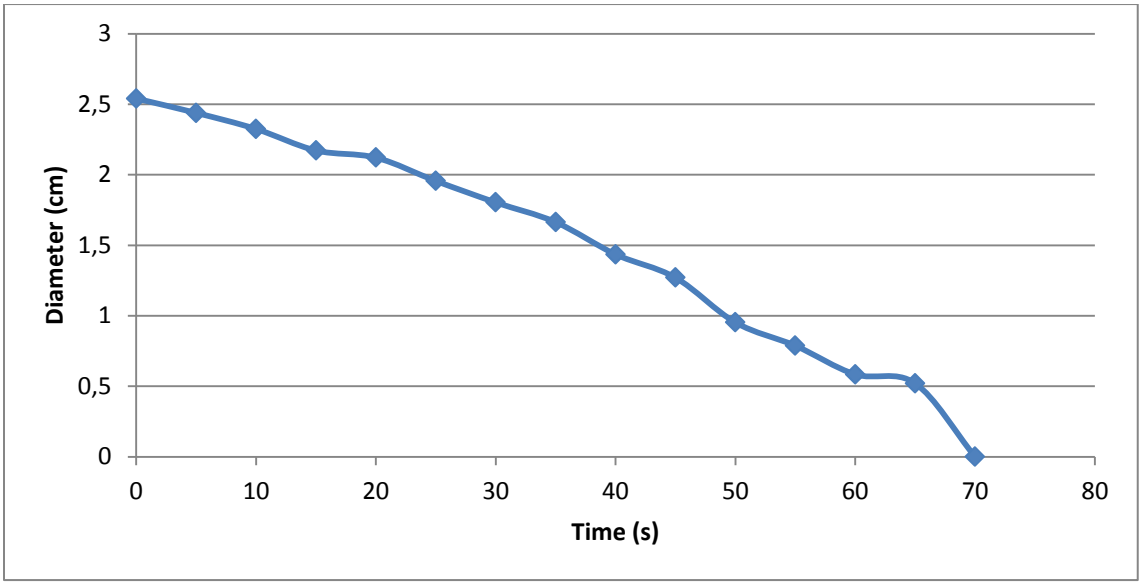


**Figure 63. Diameter of the 7.5x2.5 cm hydrate sample during combustion.**

From Figure 62 and Figure 63 it is possible to see that the hydrate shrinks at the same rate of approximately 0.36mm/s during combustion and the length decreases very slowly during the first 65 seconds at 0.23 mm/s; it then decreases at 12 mm/s the last 5 seconds, when the sample is almost gone.

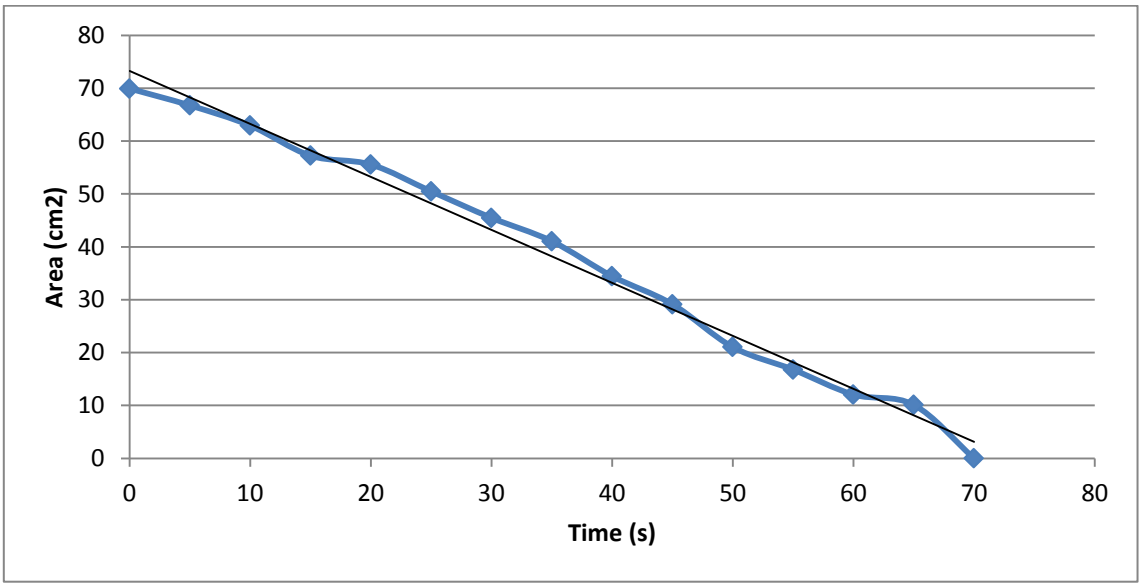


**Figure 64. Surface area of 7.5x2.5 cm hydrate sample during combustion.**

Using the data from the measurements the surface area of the hydrate is calculated and it is

possible to see from Figure 64 that it can be approximated by a linear regression line. At the end of the combustion the surface of the samples is variable, not uniform and very small, therefore the last 15% of the surface calculation is deleted because it does not show fairly the properties of the combustion.

**Hydrate dissociation rate per surface**

The dissociation rate per surface is obtained by dividing the dissociation rate by the surface area.

$$Dissociation\ rate\ per\ surface\ (t)\left[\frac{g}{s\ m^2}\right] = \frac{Dissociation\ rate\ (t)\ \left[\frac{g}{s}\right]}{Surface\ area\ (t)\ [m^2]}$$

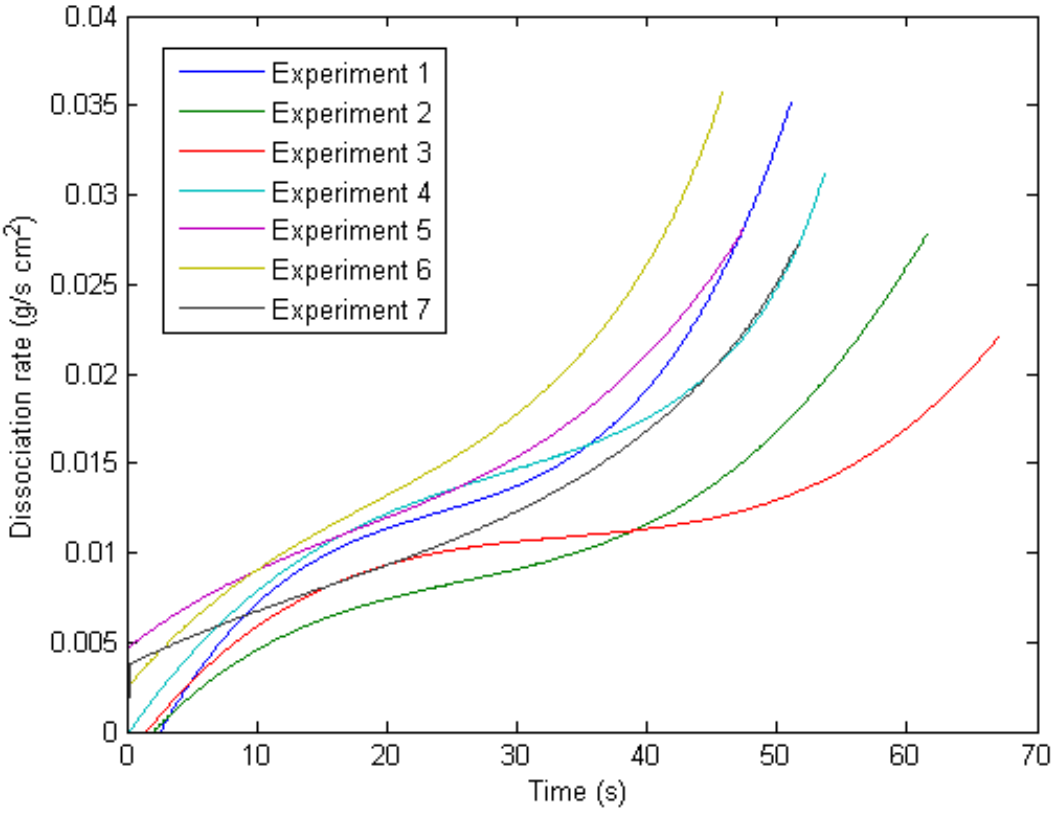


**Figure 65. Dissociation rate per unit surface area.**

As shown in Figure 65, it is appreciable to see the steady-state of combustion between 10 and 40 seconds, coinciding with the homogeneity of the flame and surface. It varies, but approximately the dissociation rate during quasi-steady state is 0.0125 g/s*cm$^2$ with a

variation of ±0.0025.

The explanation for low dissociation rate during the first 10 second is because the combustion is not in the steady-state. There is an exponential increase of the dissociation rate at the end of the process due to the deformation of the surface of the hydrate and homogeneity of the flame. For these reasons, the experiments show that the dissociated rate during the quasi-steady state is fairly constant and that is possible to explain the characteristics of the combustion process.

**Burning rate per surface**

The burning rate per surface is obtained dividing the burning rate by the surface.

$$Burning\ rate\ per\ surface\ (t)\left[\frac{g}{s\ m^2}\right] = \frac{Burning\ rate\ (t)\ \left[\frac{g}{s}\right]}{Surface\ area\ (t)\ [m^2]}$$

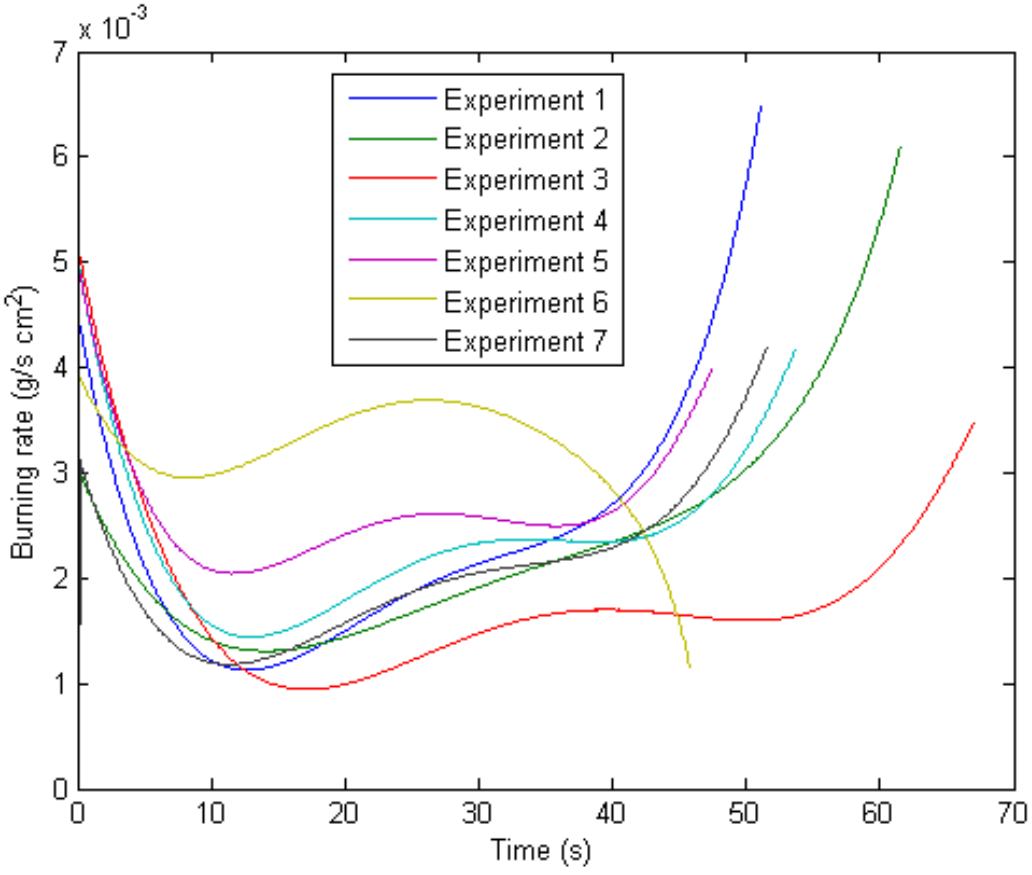


**Figure 66. Burning rate per unit surface area.**

Figure 66 shows the variability of the burning rate due to the fact that the release of methane is not continuous, but it follows approximately a rate of 2.5 mg/ s*cm$^2$ during the quasi-steady state. What is remarkable about the burning rate is the proximity between the experiments although they have quite different global characteristics. The increase at the end of the combustion is due to that the samples are very small and they do not have a regular shape, therefore the surface cannot be approximated correctly.

**Draining rate per surface**

The draining rate per surface is obtained dividing the draining rate by the surface.

$$Draining\ rate\ per\ surface\ (t)\left[\frac{g}{s\ m^2}\right] = \frac{Draining\ rate\ (t)\ \left[\frac{g}{s}\right]}{Surface\ area\ (t)\ [m^2]}$$

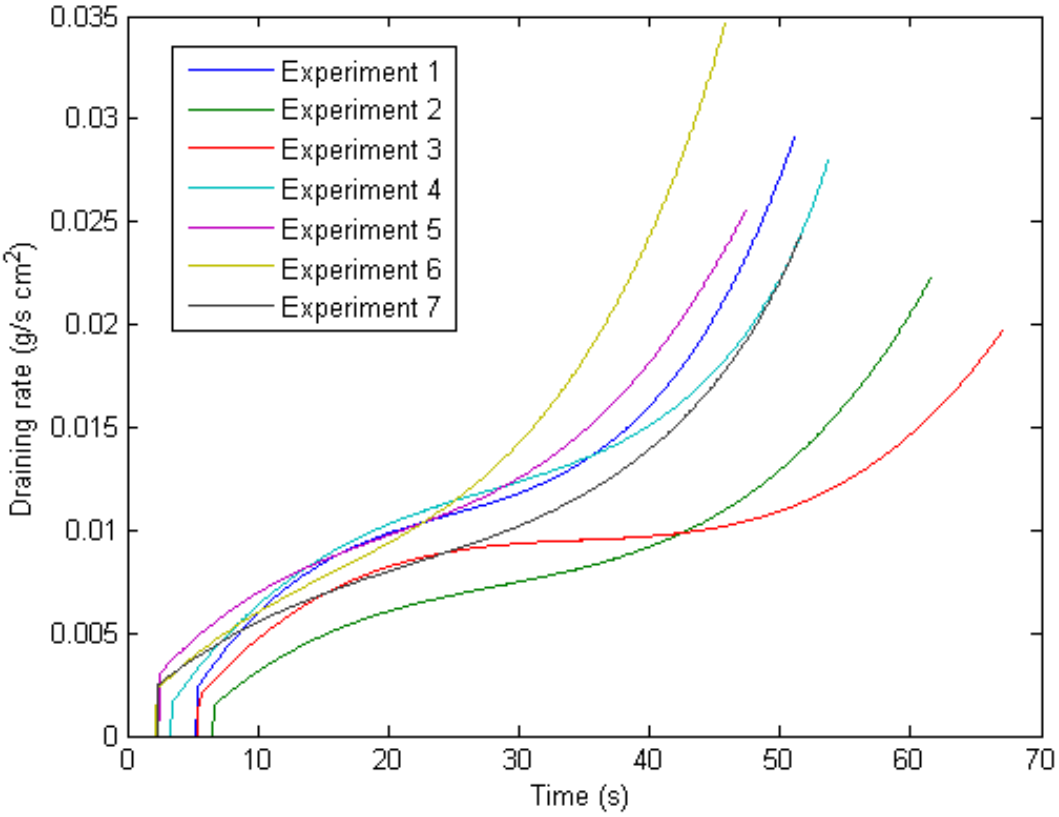


**Figure 67. Draining rate per unit surface area.**

In Figure 67, the similarity of the draining rate throughout the experiments is appreciable and the different stages of the combustion. During the first seconds, the water is not

draining because of the mesh and melting time. After approximately 5 seconds, the water starts draining and reaches the quasi-steady state with a draining rate around 0.01 g/s*cm$^2$. As in the other calculations, the exponential increase at the end of the combustion is due to the deformation of the sample, since at the end of the combustion the shape is no more cylindrical and the sample is split in very small pieces of hydrate.

**Flow rate of methane released per surface**

The flow rate of methane released per surface is obtained dividing the flow rate of methane by the surface.

$$Flow\ rate\ methane\ released\ per\ surface\ (t)\left[\frac{g}{s\ m^2}\right] = \frac{Flow\ rate\ methane\ (t)\ \left[\frac{g}{s}\right]}{Surface\ area\ (t)\ [m^2]}$$

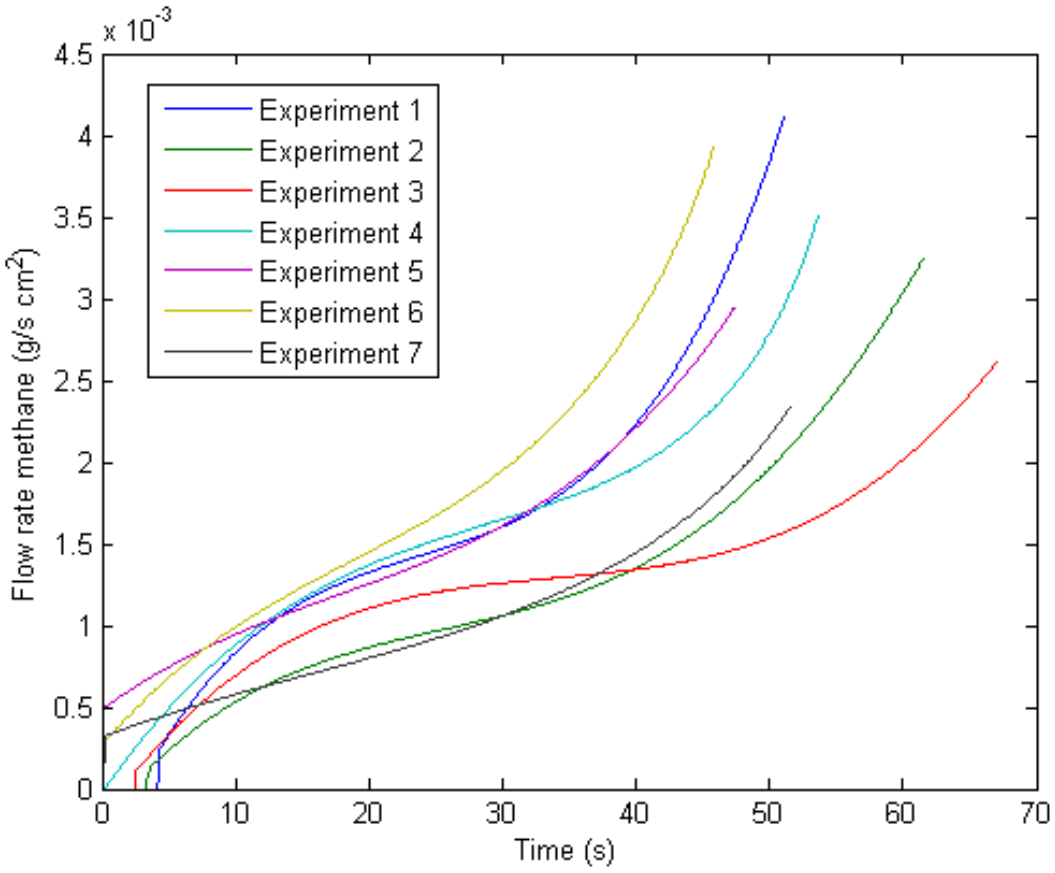


**Figure 68. Flow rate methane released per unit surface area.**

From Figure 68 it can be extrapolated that the methane released during the quasi-steady

state is approximately 1.25 mg/s*cm$^2$ with a variation of ±0.25 mg/ s*cm$^2$. This value is a very useful one with regards to considering methane hydrates as a fuel source. For typical heat of combustion of 50 MJ/kg for methane, the burning rate results indicate that you can obtain 62.5 W/cm$^2$ of active fuel surface.

**Flow rate water evaporated per surface**

The flow rate of water evaporated per surface is obtained by dividing the flow rate of methane by the surface area.

$$Flow\ rate\ water\ evaporated\ per\ surface\ (t)\left[\frac{g}{s\ m^2}\right] = \frac{Flow\ rate\ water\ evaporated\ (t)\ \left[\frac{g}{s}\right]}{Surface\ area\ (t)\ [m^2]}$$

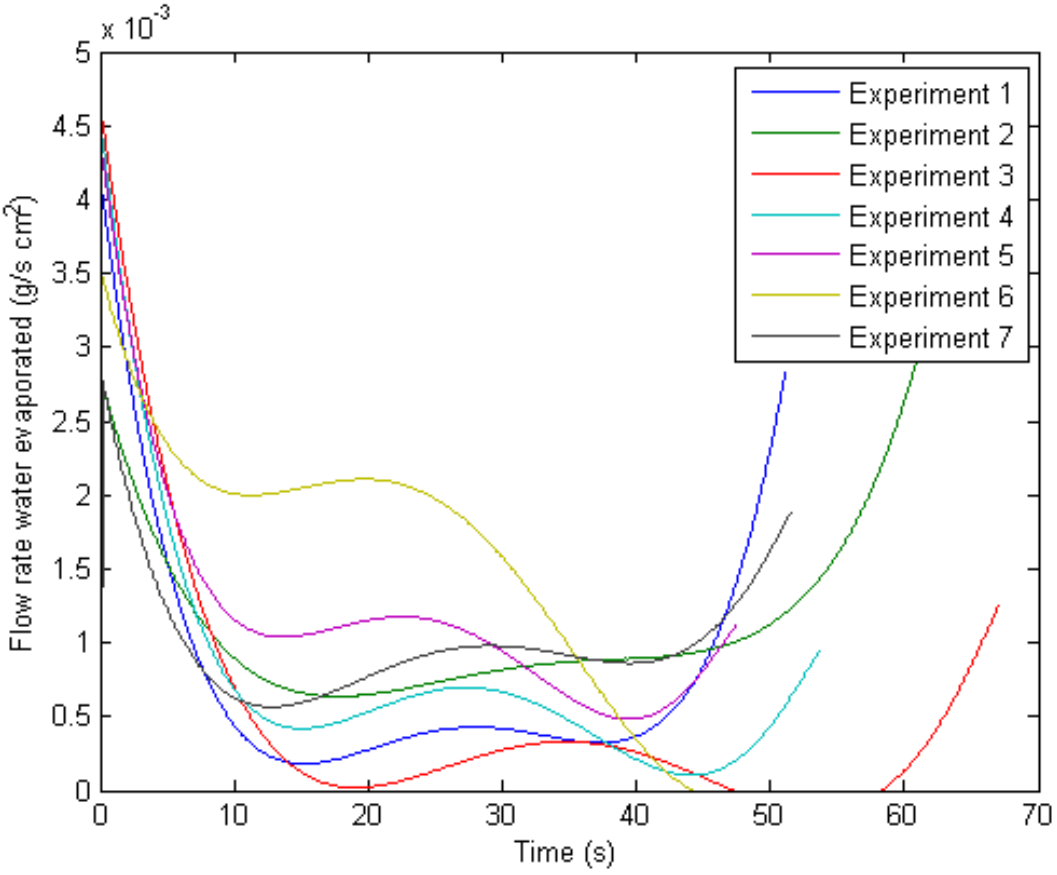


**Figure 69. Flow rate water evaporated per unit surface area.**

The flow rate of water evaporated, Figure 69, shows that hydrates have a very complex composition and, although for study and calculations they are treated as homogenous, they have a variable behavior.

In spite of that fact, it is possible to estimate the quasi-steady state at around 1.25 mg/ s*cm$^2$ of water evaporation per unit surface area as the average of the oscillations.

**Average steady-state**

In previous chapter, the dissociation, burning rate, draining rate and molar ratio between water evaporated versus methane were estimated during the quasi-steady state. Hence these values are used for the energy model to determine the heat transfer values.

**Table 5. Average flow rates and molar ratio water evaporated vs. methane.**

| | |
|---|---|
| Average dissociation rate, ($\dot{m}_s$) [kg/s m$^2$] | 0.125 |
| Average burning rate, ($\dot{m}_g$) [kg/s m$^2$] | 0.025 |
| Average draining rate, ($\dot{m}_d$) [kg/s m$^2$] | 0.1 |
| Average molar ratio, (α) | 0.8841 |

The resulting liquid/solid surface regression rate is:

$$regression\ rate\ = \frac{\dot{m}_s}{\rho_{hydrate}} = 0.14\ mm/s$$

## ENERGY MODEL

From these experiments it becomes clear that there is an important relationship between heat flux from the flame, the amount of water that was released, and the ratio of water evaporated to methane released. In order to understand that process better a simplified planar one-dimensional steady-state energy balance of hydrate combustion is created to account for these behaviors.

In this way, it is possible to calculate how much of the thermal energy obtained from burning the gas released in the hydrate flame is used to melt the hydrate and evaporate the water in the dissociated zone.

### One dimensional planar model

This model includes three different phases: solid (which is the hydrate, with the ice-like structure cages and the methane trapped), liquid (which is the water melted) and gas (which is composed of methane and water vapor). The schematic of the model illustrated in Figure 70.

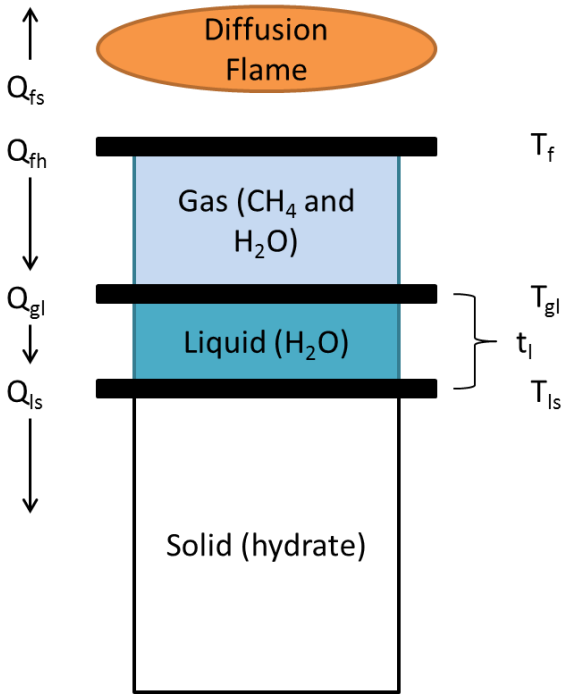


**Figure 70. Schematic 1-D planar model of the methane hydrate heat transfer.**

The flame provides heat flux to the surroundings $Q_{fs}$ and transmits the rest toward the hydrate $Q_{fh}$. This heat flux goes through the gas layer, that has thickness $t_l$, to the liquid layer $Q_{gl}$ and finally into the hydrate $Q_{ls}$.

The solid hydrate phase is assumed to be semi-infinite for this analysis, which is a good practical assumption because the thermal transport in hydrate is very poor so there is no influence of the distant boundary. There are three interfaces: the flame sheet at temperature $T_f$, the gas-liquid boundary with water boiling temperature $T_{gl}$, and the liquid-solid boundary, with hydrate dissociation temperature $T_{ls}$, which is the water melting temperature. This problem is similar to a moving boundary problem or a three-phase Stefan problem [14] with some realistic simplifications with the heat transport in the phases.

The governing equations are energy and mass balances at each interface. Starting from the solid/liquid interface, it is assumed that the hydrate has a constant dissociation temperature $T_{ls}$ and latent heat of fusion $L_f$, which includes the effects of the caged methane on the dissociation. The heat flux per unit area into the hydrate $Q_{ls}$ includes the heat of fusion and the sensible heat of increasing the temperature of the hydrate from its initial temperature $T_i$ to the dissociation temperature:

$$Q_{ls} = \dot{m}_s(L_f + c_{ps}(T_{ls} - T_i)$$

where $c_{ps}$ is the specific heat of the hydrate and $\dot{m}_s$ is the dissociation rate of the hydrate per surface area. The thermal conductivity of the hydrate is very low so it is assumed that all the energy is used to heat and melt the hydrate layer and no heat is transferred into the solid. It is assumed that the liquid phase has a constant thermal conductivity $k_l$ and the thickness of the layer is very thin, therefore heat transfer through the liquid can be considered to occur only by conduction. The convection may be important, but it can be adjusted with the conductivity. Radiation is neglected because hydrate flames have very low radiance because they have no soot, they are relatively cold, and the albedo of a component with similar optical properties of the hydrates like snow is 0.9, which reflects most of the radiation.

$$Q_{ls} = k_l \frac{(T_{gl} - T_{ls})}{t_l}$$

Regarding the liquid/gas interface, the heat flux per unit area incorporates the latent heat of vaporization $h_{fg}$, the sensible heat to increase the temperature of the liquid that is evaporating to the boiling point $T_{gl}$, and the liquid that is draining to the draining temperature $T_d$. Adding the heat flux into the hydrate solid, the heat flux per unit area of the liquid/gas interface is:

$$Q_{gl} = \dot{m}_g \alpha (h_{fg} + c_{pl}(T_{gl} - T_{ls}) + \dot{m}_d c_{pl}(T_d - T_{ls}) + Q_{ls}$$

where $c_{pl}$ is the specific heat of water, $\dot{m}_g$ is the burning rate of the hydrate per surface area, $\dot{m}_d$ is the draining rate per surface area and $\alpha$ is the mass fraction of the gas released that is vapor, since the methane has no latent heat associated. The heat transfer from the flame into the liquid layer is estimated to occur by convection only:

$$Q_{gl} = h_g(T_f - T_{gl})$$

where $h_g$ is the effective convective heat transfer coefficient.

Finally, for the flame/gas interface, the sensible heat to increase the gas from the boiling point to the flame temperature $T_f$ is added to the heat flux into the liquid layer to get the heat flux per unit area of the flame/gas interface.

$$Q_g = \dot{m}_g(c_{pg}(T_f - T_{ls}) + Q_{gl}$$

where $c_{pg}$ is the specific heat of the gas.

The heat generated by the flame is determined by the mass portion of methane that goes into the flame and the heat of combustion for methane and air $\Delta H_c$:

$$Q_f = (1 - \alpha)\dot{m}_g \Delta H_c$$

This combustion heat is diffusing outward toward the surroundings to heat the incoming oxidizer and inward toward the hydrate to heat the fuel and vapor, along with that heat required to dissociate the hydrate.

The mass balance is defined so that all the mass that is dissociated from the hydrate goes into gas or liquid water:

$$\dot{m}_s = \dot{m}_g + \dot{m}_d$$

One of the outcomes of the model is the fraction of combustion needed to maintain the dissociation and release of methane.

$$fraction\ combustion = \frac{Q_g}{Q_f}$$

The physical properties needed for the analysis are tabulated in Table 6.

**Table 6. Physical properties used for the model.**

| | |
|---|---|
| Thermal conductivity of water, ($k_l$) [kW/m K] | $0.6x10^{-3}$ |
| Hydrate heat of fusion, ($L_f$) [kJ/kg] | 333 |
| Water heat of evaporation, ($h_{fg}$) [kJ/kg] | 2260 |
| Specific heat of water, $c_{pl}$ [kJ/kg K] | 4.186 |
| Specific heat of hydrate, $c_{ps}$ [kJ/kg K] | 2.11 |
| Specific heat of gas (nitrogen/steam/methane), $c_{pg}$ [kJ/kg K] | 2 |
| Flame temperature, ($T_f$) [K] | 1750 |
| Boiling temperature water, ($T_{gl}$) [K] | 373 |
| Temperature water drained, ($T_d$) [K] | 300 |
| Hydrate dissociation temperature, ($T_{ls}$) [K] | 273 |
| Initial temperature hydrate, ($T_i$) [K] | 265 |
| Hydrate density, ($\rho_{hydrate}$) [kg/m$^3$] | 900 |

The values used for the hydrate heat of fusion and the specific heat are the values of ice, which are very close to the hydrate properties. The real values of thermal properties for the hydrates are still under discussion over the past years and needs more validation [16-18].

At the same time, the flame temperature is estimated from other studies [15] , the initial temperature of the hydrate is the temperature of the hydrate when is taken out from the vessel and the temperature of the water drained is measured.

With the dissociation rate, the heat flux through the solid/liquid layer is and the water layer thickness:

$$Q_{ls} = \dot{m}_s(L_f + c_{ps}(T_{ls} - T_i) = 43735\frac{W}{m^2}$$

$$Q_{ls} = k_l\frac{(T_{gl} - T_{ls})}{t_l} \rightarrow t_l = k_l\frac{(T_{gl} - T_{ls})}{Q_{ls}} = 0.0014\,m = 1.4\,mm$$

After that, the heat flux through liquid/gas and the convective heat transfer coefficient are determined:

$$Q_{gl} = \dot{m}_g\alpha(h_{fg} + c_{pl}\left(T_{gl} - T_{ls}\right) + \dot{m}_d c_{pl}(T_d - T_{ls}) + Q_{ls} = 88399\ \frac{W}{m^2}$$

$$Q_{gl} = h_g\left(T_f - T_{gl}\right) \rightarrow h_g = \frac{Q_{gl}}{\left(T_f - T_{gl}\right)} = 64.2\frac{W}{m^2\,K}$$

Next, the heat flux to the gas is calculated:

$$Q_g = \dot{m}_g(c_{pg}\left(T_f - T_{ls}\right) + Q_{gl} = 157250\ \frac{W}{m^2}$$

The heat from the flame is:

$$Q_f = (1 - \alpha)\dot{m}_g\Delta H_c = 627260\frac{W}{m^2}$$

And the heat flux to the surroundings is:

$$Q_{fs} = Q_f - Q_g = 470010\ \frac{W}{m^2}$$

Therefore, the fraction of the combustion that is used to dissociate the hydrate and heat the gas and liquids is:

$$fraction\ combustion = \frac{Q_g}{Q_f} = 0.2507 \rightarrow 25.07\%$$

Only 25% of the combustion heat would be needed to maintain the steady release of methane and a steady burn. The energy balance analysis confirms that the experiments sustain the steady-state and the flame thanks to the drainage of water. The hydrate could produce 470 kW/m$^2$ from the methane released. These results are not exact for every experiment, are only a reference using the average of the experiments. Hence, the validity of the results is more qualitatively rather than quantitative. As an example, the fraction of combustion heat used for the dissociation of the hydrate is 25%, but it can be ±10% depending on the gas released, water thickness layer or the mass fraction of the gas that is methane.

**Water layer thickness**

Another method to find the parameters for the energy model is determining the water layer thickness to determine all the values as a function of this thickness. To do so, the liquid layer is considered as a laminar open channel uniform flow [19] and the equations of motion are applied, under the assumptions that the cylindrical shape of the hydrate can be approximate by an inclined flat plane of 45º and the water draining flow is laminar and steady. This simplification can be seen in Figure 71.

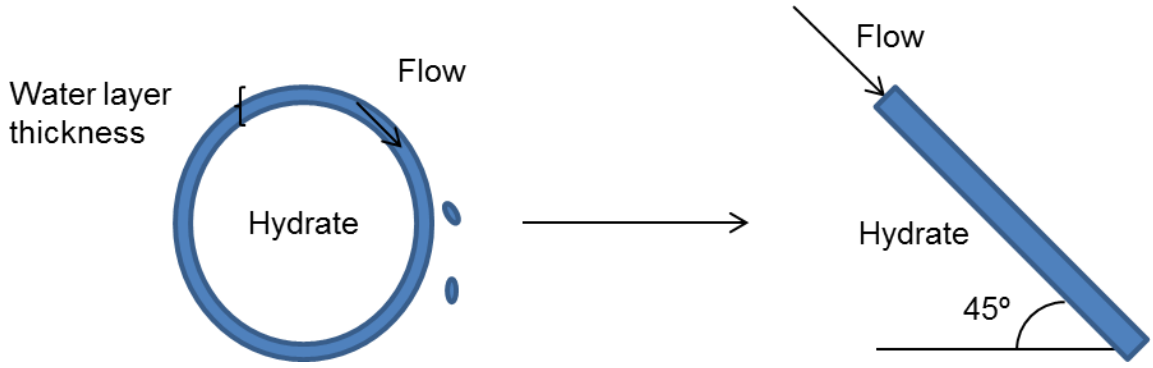


**Figure 71. Model simplification of the water drained flow.**

To determine the thickness, the volumetric flow of the sample is needed, and from Figure 50 the draining rate during the steady state is 0.25 g/s.

$$Volume\ flow = q = Water\ drained\ \left[\frac{g}{s}\right] * \frac{1}{density\ water\ \left[\frac{g}{m^3}\right]} = 0.25 * 10^{-6}\frac{m^3}{s}$$

Once the volume flow is known, the thickness of the water layer is calculated by the following formula:

$$thickness\ layer\ [m] = h = \sqrt[3]{\frac{3 * q * \mu}{\rho * g * W * \sin\alpha}}$$

where $\mu$ is the dynamic viscosity of water, $\rho$ is the density of water, $W$ is the width of the hydrate sample and $\alpha$ is the angle of the plane, with the values in Table 7.

**Table 7. Values properties water layer.**

| | |
|---|---|
| Dynamic viscosity water at 300 K, (μ) [kg/s m] | $1.002 * 10^{-3}$ |
| Density of liquid water at 300 K, (ρ) [kg/m$^3$] | 998.2 |
| Width hydrate cylinder, (W) [m] | 0.06 |

$$h = 0.00015\ m = 0.15mm$$

Using this simplification and method, the water layer thickness is 10 times smaller than the method used before. The rest of the energy balance analysis is calculated based on that value.

$$Q_{ls} = k_l \frac{(T_{gl} - T_{ls})}{t_l} = 400000 \frac{W}{m^2}$$

$$\dot{m}_s = \frac{(L_f + c_{ps}(T_{ls} - T_i)}{Q_{ls}} = 1.14 \frac{kg}{s\ m^2}$$

Experiments had shown that approximately 80% of the dissociated mass goes as water drained and 20% released as a gas.

$$\dot{m}_d = 0.912 \frac{kg}{s\ m^2}$$

$$\dot{m}_g = 0.228 \frac{kg}{s\ m^2}$$

$$\alpha = 0.4982$$

The rest of the values are:

$$Q_{gl} = \dot{m}_g \alpha (h_{fg} + c_{pl}(T_{gl} - T_{ls}) + \dot{m}_d c_{pl}(T_d - T_{ls}) + Q_{ls} = 806190 \frac{W}{m^2}$$

$$h_g = \frac{Q_{gl}}{(T_f - T_{gl})} = 585.47 \frac{W}{m^2 K}$$

$$Q_g = \dot{m}_g (c_{pg}(T_f - T_{ls}) + Q_{gl} = 1434102 \frac{W}{m^2}$$

$$Q_f = (1 - \alpha)\dot{m}_g \Delta H_c = 5720600 \frac{W}{m^2}$$

$$Q_{fs} = Q_f - Q_g = 4286498 \frac{W}{m^2}$$

$$fraction\ combustion = \frac{Q_g}{Q_f} = 0.2507 \rightarrow 25.07\%$$

Although the final result of the fraction of heat that goes to dissociate the hydrate is the same as the previous method, the values of the flow rates and heat fluxes are one order of magnitude higher than using experimental flow rates.

Physically, the hydrate dissociation rate cannot be 1.14 kg/s $m^2$ because it will represent losses of 5 g/s in the sample of the experiments, and a complete dissociation of the hydrate in 3 seconds.

$$Dissociation\ sample = \dot{m}_s * Surface\ hydrate \approx 5 \frac{g}{s}$$

$$Combustion\ time = \frac{Mass\ hydrate}{Dissociation\ sample} \approx 3\ seconds$$

Moreover, the regression rate of the solid/liquid layer is too fast for a cylinder of 2 centimeter diameter.

$$regression\ rate\ = \frac{\dot{m}_s}{\rho_{hydrate}} = 1.3\ mm/s$$

There is another reason to reject the theory of the laminar open channel uniform flow by analyzing the value of the heat that the hydrate could produce. $Q_{fs}$ is approximately 4.29

$MW/m^2$, a very high value that suggests that the model is not the correct one.

An option to adjust this model to reality and analyze if it could be acceptable is to determine the angle inclination of the plane based on the water layer thickness calculated from the average flow rates of the experiments. The volume flow is proportional to the slope of the channel; therefore the inclination of 45º must be reduced.

$$\sin\alpha = \frac{3 * q * \mu}{\rho * g * W * h^3} = 0.00052$$

$$\alpha = 0.03°$$

Even though the model was adjusted to the flow rates, physically has no sense to simulate the slope of the cylinder as a channel of 0.03º inclination, since it is a flat plane. It appears, therefore, that the porous hydrate surface does not behave as a solid smooth surface with a thin liquid film.

For these reasons, the model of laminar open channel uniform flow are not effective for hydrate simulations, and the energy balance is calculated only with the flow rates of the experiments.

**Liquid water layer thickness**

Using the measurements and calculations explained above, the energy model can be computed along with the combustion of hydrates using the dissociation rate per surface, Figure 65, the burning rate per surface, Figure 66, the draining rate per surface, Figure 67, and the properties and temperature the of hydrate, Table 6.

The thickness calculated is presented in Figure 72. It is interesting that during the first phase of the combustion this layer is very thick related to the thickness of the diameter of the cylinder. This might suggest that during the first 5 seconds the value is not the correct one. The explanation for this error is that during this phase the process is not in the quasi-steady state region and cannot be computed with the energy balance model designed for the steady-state. Despite this fact, what it is shown is that during the first second the liquid layer is bigger, that is because the hydrate starts dissociating after it is depressurized. Then, the outer layer is converted into liquid and an icy layer since the methane is released, but

the liquid is not drained and there is no water evaporated, therefore all the water stays on the outer layer of the hydrate. Once the hydrate is ignited, the heat creates evaporation and water flow, decreasing the thickness of the layer to the steady state, shown in the figure after 10 seconds of the ignition point. There is some variability throughout the experiments, but the calculated water layers are all between 1 and 2 mm thick.

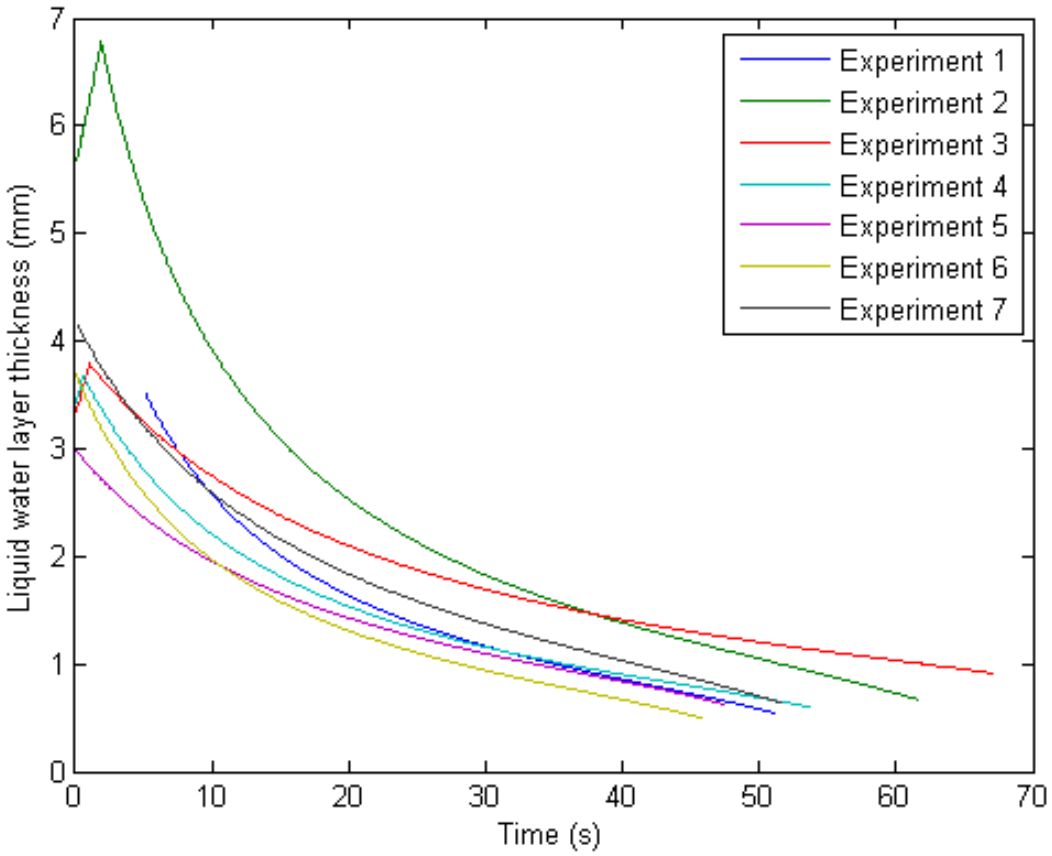


**Figure 72. Liquid water layer thickness.**

**Heat needed to dissociate hydrate**

The heat needed to dissociate the hydrate includes the heat flow for the gas phase, heat flow of the liquid water layer and the heat flow of the solid phase. In Figure 73 it is seen that this heat flow is fairly constant around 50 and 100 kW/m$^2$, which is a little bit lower than the value calculated above (which was approximately 150 kW/m$^2$). Only in two experiments there is a big increase of this value at the end of the process, due to the non-uniformity of the shape that might splitted into small pieces and the linear approximation of the surface is

affected.

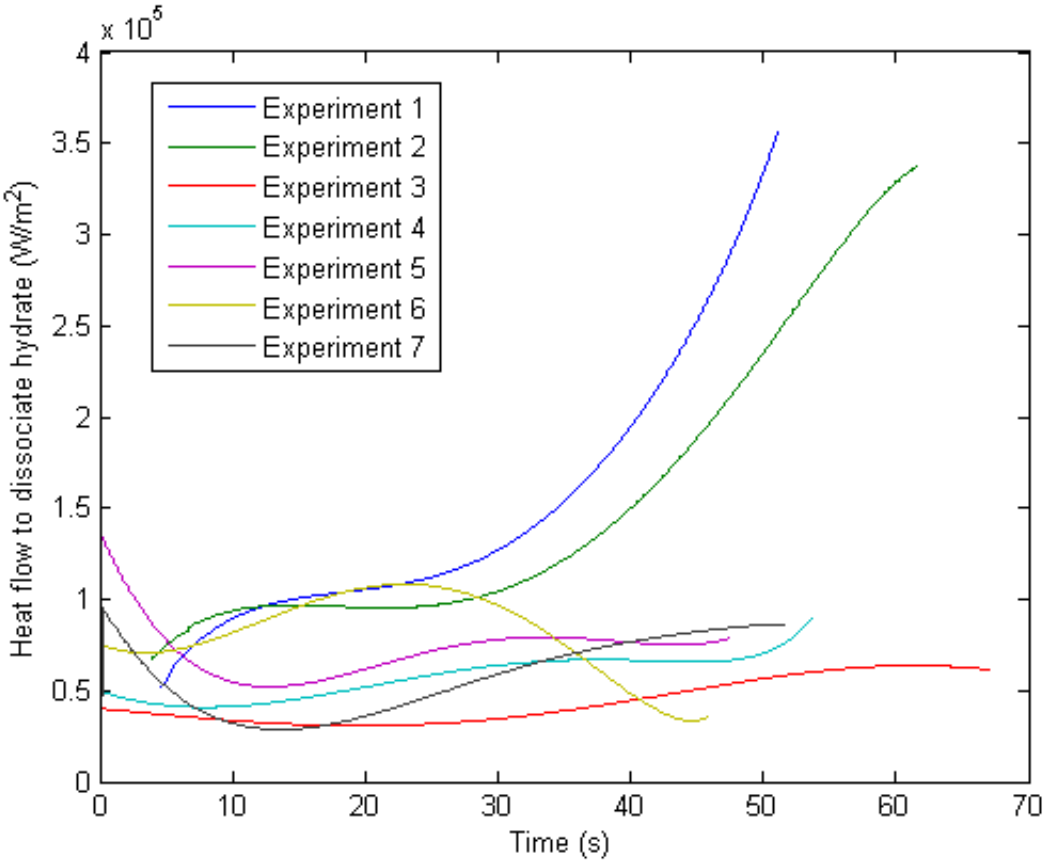


**Figure 73. Heat flow needed to dissociate the hydrate.**

**Heat flux of the flame**

The heat of the flame is produced by the methane released from the hydrate. The value increases along the process from around 200 kW/ $m^2$ at the beginning to 500 kW/$m^2$. The reason for this increase is that although the surface area of the hydrate is decreasing, the flow rate per surface of methane is not decreasing at the same rate as the surface. The quasi-steady state is fairly seen in Figure 74 between 10 and 30 seconds.

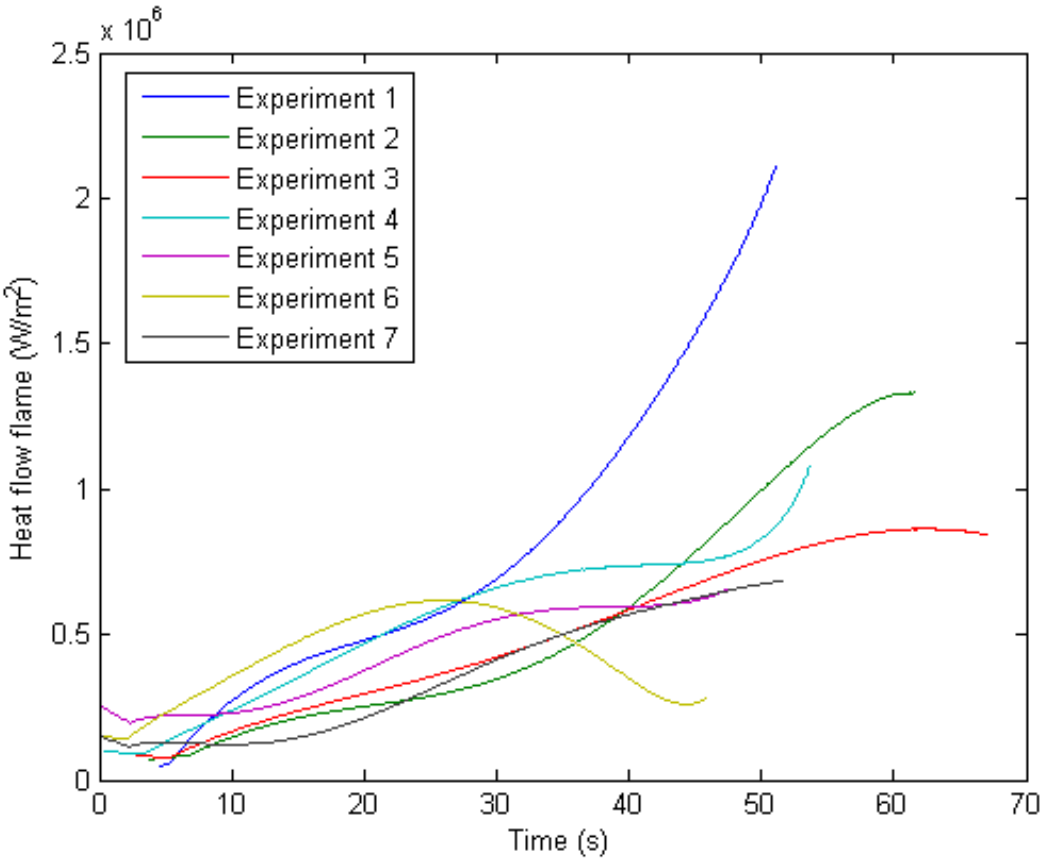


**Figure 74. Heat flow of the hydrate flame.**

**Fraction of combustion heat used to dissociate the hydrate**

The fraction of combustion heat used to dissociate the hydrate is shown in Figure 75. Because in the first second of the combustion the gas released has much more water than methane, all the heat of the flame during this period is needed to dissociate the hydrate and the value is close to one. After 10 seconds, the fraction moves to the quasi-steady state which ranges between 10% and 30% in the different experiments.

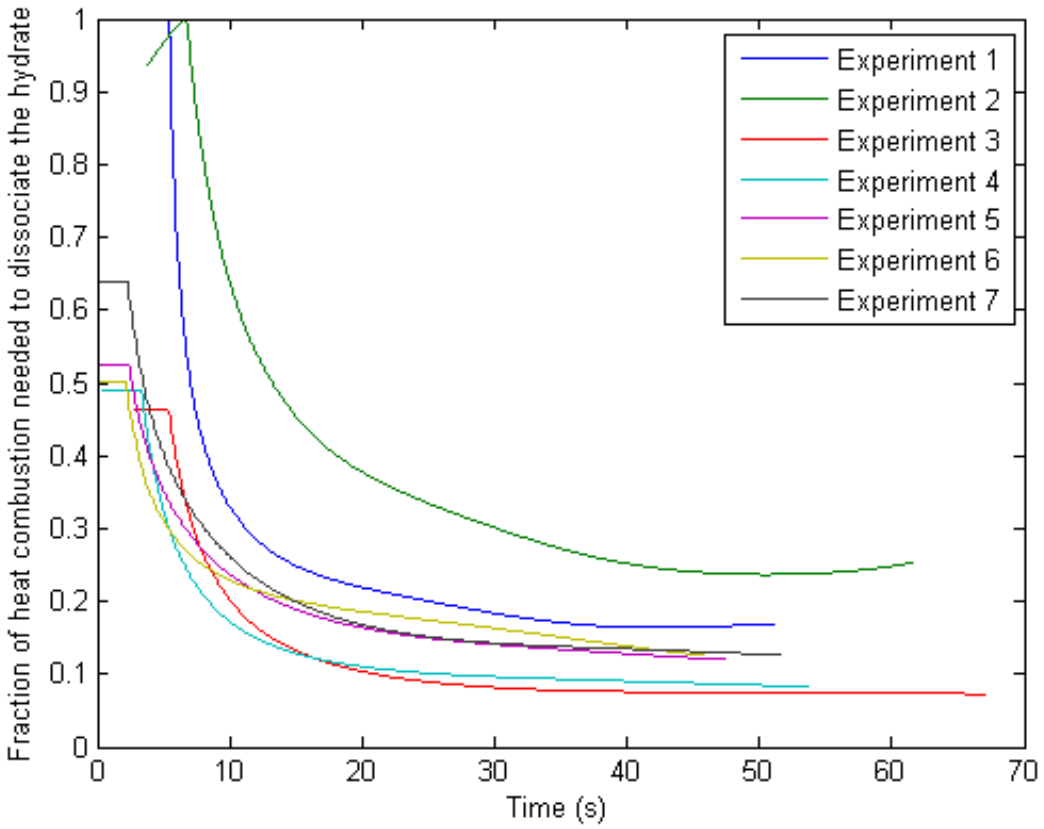


**Figure 75. Heat of combustion fraction needed to dissociate hydrate.**

**Heat flow of the flame to the surroundings**

Subtracting the heat flux for dissociation to the heat flux of the flame, the heat flux to the surroundings is obtained. This is the energy that is released by the methane combustion. From Figure 76 it is possible to see that this energy is increasing from 100 kW/m$^2$ during the first moments, into 400 kW/m at the quasi-steady state region. The explanation of that increase is the same as the above calculations that the surface area decreases faster than the flow rate of methane per surface.

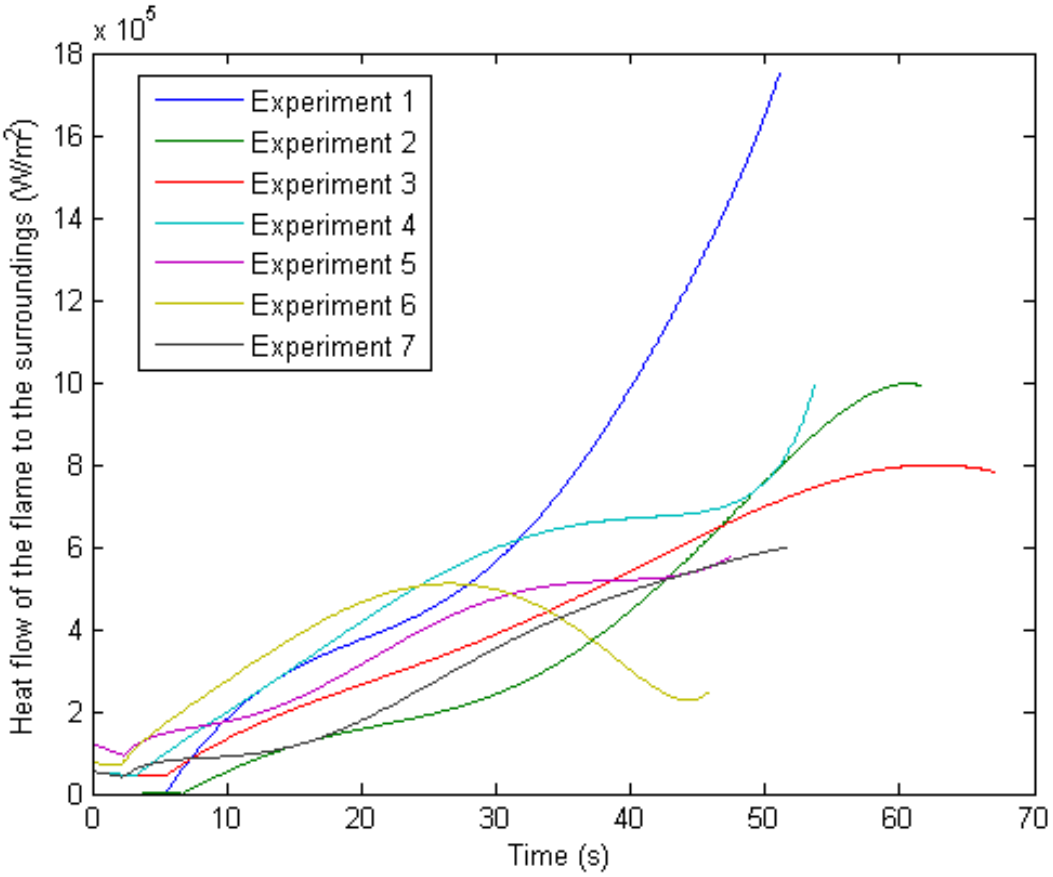


**Figure 76. Heat flow of the flame to the surroundings.**

**Adiabatic flame temperature**

Another property of hydrate combustion is the temperature of the flame. In this project, no direct measurements of this temperature in the experiments are done, but other work [15] measured temperatures around 1700-1800 K.

With the present experiments and measurements, the temperature of the flame can be estimated by modelling the flame as a constant-pressure flame and calculating the adiabatic flame temperature [20] .

This theory says that if a fuel-air mixture burns adiabatically at constant pressure, the standardized enthalpy of the reactants at the initial state is equal to the standardized enthalpy of the product at the final state.

$$H_{reac}(T_i, P) = H_{reac}(T_{ad}, P)$$

Evaluating this quantity requires knowledge of the composition of the combustion products. For the methane hydrate the stoichiometric methane-water-air mixture at 1 atm and the initial reactant temperature of 298 K is used to determine the temperature. Therefore, the adiabatic flame temperature is only considering the gas portion of the methane hydrate combustion, not the dissociation heat.

$$CH_4 + n\,H_2O + 2(O_2 + 3.76N_2) \rightarrow CO_2 + (n+2)H_2O + 7.52N_2$$

where *n* is the molar ratio of water evaporated versus methane of the flame. The calculation makes the following 4 assumptions:

1. The combustion is complete, which means that the product mixture consist of only $CO_2$, $H_2O$ and $N_2$. All the methane reacts in the chemical reaction.
2. The product mixture enthalpy is estimated using constant specific heats evaluated at 1300 K (≈0.5 ($T_i$ + $T_{ad}$)), where $T_{ad}$ is estimated at 2300 K (≈1750/0.75).
3. The flame temperature is estimated as 75% of the adiabatic temperature because there is heat extracted for dissociation.
4. The value used for the molar ratio of water evaporated versus methane is the average of the experiments, n=0.8841.

**Table 8. Properties species methane hydrate combustion.**

| Species | Enthalpy of Formation at 298 K, $\bar{h}^{\circ}_{f,i}$ (kJ/kmol) | Specific heat at 1300 K, $\bar{c}_{p,i}$ (kJ/kmol K) |
|---|---|---|
| $CH_4$ | -74831 | - |
| $CO_2$ | -393546 | 56.984 |
| $H_2O$ | -241845 | 45.027 |
| $N_2$ | 0 | 34.113 |
| $O_2$ | 0 | - |

The enthalpy of the reactants is:

$$H_{reac} = \sum N_i \bar{h}_i = N_{CH4}\bar{h}_{CH4} + N_{H2O}\bar{h}_{H2O} + N_{N2}\bar{h}_{N2} + N_{O2}\bar{h}_{O2}$$

$$H_{reac} = 1 * (-74831) + 0.8841 * (-241845) + 2 * 0 + 7.52 * 0 = -288646\ kJ$$

And for the products:

$$H_{prod} = \sum N_i \bar{h}_i = N_{CO2}\bar{h}_{CO2} + N_{H2O}\bar{h}_{H2O} + N_{N2}\bar{h}_{N2}$$

where $\bar{h}_i$ is

$$\bar{h}_i = \bar{h}^{\circ}_{f,i} + \bar{c}_{p,i}(T_{ad} - 298)$$

$$H_{reac} = 1 * [-393546 + 56.984(T_{ad} - 298)] + 2.8841 * [-241845 + 45.027(T_{ad} - 298)] + 7.52 * [0 + 34.113(T_{ad} - 298)]$$

The value of $T_{ad}$ is determined by equating $H_{reac}$ to $H_{prod}$.

$$T_{ad} = 2108\ K$$

The difference between the adiabatic flame temperature and the real temperature of the flame is due to the part of the heat of combustion needed for dissociating the methane hydrate cake. This heat includes the heat of fusion of the hydrate, the heat of vaporization of the water that is going to the flame and the heat capacity of the water drained. This value was computed before with the energy balance, and therefore the adiabatic flame temperature is multiplied by the proportion part of heat that is used for the flame to be adjusted to the real flame and its losses.

$$T_f = 0.75 * T_{ad} = 1581\ K$$

Comparing this result with the obtained in the previous work [15] the difference is slightly more than 100 K that considering the assumptions and the variability of the experiments is fairly reasonable.

Computing the flame temperature during the combustion process for the experiments, Figure 77, there is a difference between a minimum of 1550 K to 2050 K, with an average of 1822 K at the peak temperature. The big range shows the high dependency on the water content in the gas released and the difference by the assumption that the temperature of the

flame is the fraction of the heat combustion needed for dissociating.

It is appreciable that the temperature at the beginning of the process is lower due to the high content of water in the flame. This statement is also true looking at the color of the flame because the brightness at the beginning suggests a lower temperature than in the quasi-steady state.

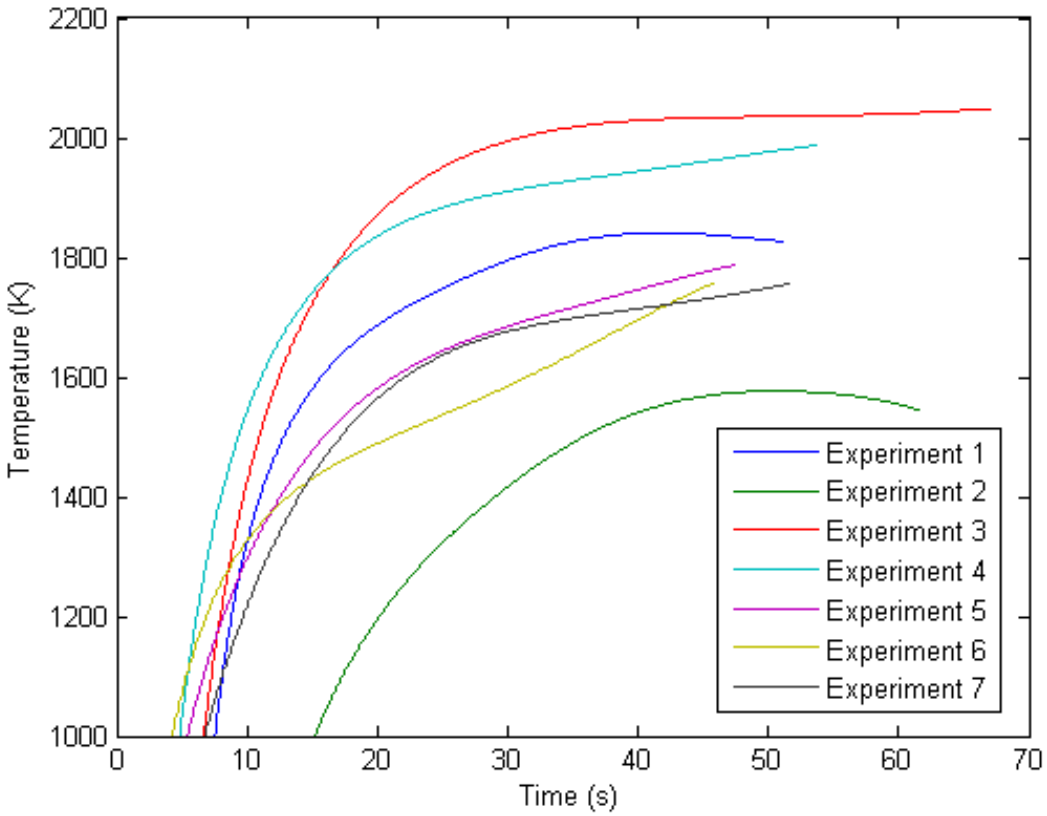


**Figure 77. Adiabatic flame temperature based on water content of experiments.**

## SUMMARY

The process followed for the formation of methane hydrates successfully forms samples that are fairly repeatable with uniform shape that burn completely until full dissociation. The clathration achieved is between 75% and 90% after 3 minutes of depressurization, suggesting a clathration level better than 90% at the end of the formation process, considering that natural formation takes years for full clathration, these results are promising for a formation time around 24 hours. The complexity of the hydrates causes the different degree of clathration and variability of the results.

The combustion of the methane hydrates is represented in Figure 33. The methane from the hydrate is released and it feeds the flame. The water is either melted and drained or evaporated to the flame. Based on the photographs of the process, the flame has an ignition and initial phase where the flame shape is unsteady and tall, and the flame color is bright with elevated water. Following this initial phase, the flame diminishes and transforms to a bluish color at what it can be considered as the quasi-steady state until all the hydrate is dissociated.

The natural dissociation of the hydrates shows that during the time between depressurization and ignition of the methane hydrate, there is a release of methane that cannot be controlled but is considered for the calculations. The natural dissociation rate is exponentially decreasing. Therefore it is very important to have a fast process to avoid losses. In order to reduce the dissociation, the samples can be cooled down with dry ice to 240K, at this temperature the methane hydrate auto-sealed and did not have losses.

From the collected data of the experiments, around 81% by mass of the methane hydrate goes to water melted, 11% as methane released, and 8% as water evaporated at the end of the combustion process. It is important to drain the water melted in order to maintain the combustion reaction because if all the water were to evaporate, the temperature of the flame would decrease to a point that the reaction is not sustainable and the flame extinguishes leaving hydrate cake remaining with methane content. The proportion of products remains during the quasi-steady state, with a dissociation rate approximately of 12.5 $mg/s*cm^2$, burning rate 2.5 $mg/s*cm^2$, and draining rate 10 $mg/s*cm^2$.

Assuming that the molar ratio of the sample is constant throughout all the combustion is it possible to estimate the water evaporation content during the process by differentiation of masses. This value confirms that naturally burning hydrate flames evaporate only a small fraction of the water in the original sample. During the first seconds of the combustion, the water content in the flame is around 90% of the total content, above the level of sustainability of the adiabatic flame temperature, suggesting that the ignition and initial temperature is fairly insensitive to the water content. Once the combustion is steady, the molar ratio of water versus methane in the flame stabilizes between 0.5 and 1.5, depending on the degree of clathration, and in this case the molar ratio is inside the limits of sustainability.

A simplified one dimensional planar three phase energy model represented in Figure 70 establishes the relationship between the heat flux from the flame and the heat flux of dissociation. This energy balance is only valid for the steady-state region with constant water layer thickness. It estimates that approximately 25% of the combustion heat is needed for dissociation, with a regression rate of the hydrate of 0.14 mm/s that could produce 470 $kW/m^2$ from the methane released by the hydrate.

Finally, the adiabatic flame temperature of the flame is estimated by assuming a methane-air-water combustion reaction and that the temperature is the percentage of heat released to the surroundings. This flame temperature varies significantly with the different experiments between 1550 K and 2050 K, depending on the water content and methane released heat flux, but these calculations of the temperature are in the same range as the temperature measured previously for the hydrate flame [20] .

# CONCLUSIONS

Methane hydrates are an interesting field of study and they may be a promising fuel due to the large amounts of methane they contain. Their direct combustion behavior is studied in this project and their unique structure makes them a very challenging fuel problem due to their multi-phase characteristics.

In this thesis, it is shown that is possible to form methane hydrates in the laboratory that burn completely and they are fairly reproducible, with the same shape and internal structure. This is the most difficult aspect of the hydrate combustion experiments. The clathration achieved (i.e., the amount of methane trapped relative to the theoretical maximum), is above 90% of the ideal saturated methane hydrate, based on the inverse regression of the dissociation. For the cylindrical samples (2 cm diameter 6 cm long) tested, the combustion reaches a quasi-steady state regime 10 seconds after ignition during which the key combustion characteristics are determined. Analysis of the data determined the dissociation rate to be approximately 12.5 mg/s $cm^2$ and 20% of the dissociated mass is released as a gas, giving a burning rate of 2.5 mg/s $cm^2$. Estimates from the differential mass measurements, and assuming the hydrates are homogenous, show that the gas composition released from the hydrate has a molar ratio of methane to water between 0.5 and 1.5, inside the limits of flame stability determined in other work.

The energy balance model showed that during steady-state burning around 25% of the energy released by the flame is needed for dissociating the methane hydrate and that the regression rate is 0.14 mm/s. The energy from the hydrate flame to the environment is approximately 470 $kW/m^2$. Finally, calculating the flame temperature with corrections for the real losses yields estimates between 1550-2050 K, showing the high dependency of the flame temperature on the water vapor content.

## FURTHER WORK

The studies of methane hydrate combustion are still in their early stages. Future experiments will include combustion at high pressure to reproduce the ocean depth environment where the methane hydrates are located. Furthermore, direct measurement of the species composition of the hydrate flames and flame temperatures are planned to confirm the results of the present project.

## REFERENCES


[1]. *Energy Resource Potential of Methane Hydrate*. National Energy Technology Laboratory. (2011).

[2] E.D Sloan, C.A. Koh, *Clathrate Hydrates of Natural Gases*, CRC Press/Taylor&Francis, Boca Raton, FL, (2008).

[3] L.A. Stern, S.H. Kirbyl, W.B. Durham, S. Circone, W. Waite, in: M.D Max (ed.), *Natural Gas Hydrate in Oceanic and Permafrost Environments*, Kluwer Academic Publishers, Massachusetts, (2000), 323-348.

[4] J. Long, E.D Sloan, International Journal Thermo physics, 17, (1996).

[5] R.L. Christiansen, E.D Sloan, *Mechanisms and kinetics of hydrate formation*, (1994), 283-305.

[6] U. Krasslan, E. Uluneye, Journal of Petrolium Science and Engineering, (2002).

[7] D.D. Link, E.P. Ladner, H.A. Elsen, C.E. Taylor, Fluid Phase equilibria 211(1) (2003) 1-10.

[8] W. Lin, J.Chen, *Effect of surfactant on the formation and dissociation kinetic behavior of methane hydrate*, State Key laboratory of Heavy Oil Processing, University of Petroleum, Beijing, (2004).

[9]. E. Chassafière, *Metastable methane clathrate particle as a source of methane to the martian atmosphere*, Paris, France (2009).

[10]:J.Warntz, U.Maas, R.W.Dibble. Combustion. Physical and chemical fundamentals, modeling and Simulation, Experiments, Pollutant Formation, 4$^{th}$ edition, Heidelberg, Germany.

[11] M. Roshandell. *Experimental and Theoretical Studies of the Methane Hydrate Combustion*. University of California Irvine, (2013).

[12] A. Yokozeki. *Methane Gas Hydrates Viewed through Unified Solid-Liquid-Vapor Equations of State*. (March 2004).

[13] J. Santacana Vall, *Automated measurements in a hydrate flame*, Senior Project, Universitat Politècnica de Catalunya, Spain, (2013).

[14] H.S. Carslaw, J.C. Jaeger, *Conduction of Heat in Solids*, Clarendon Press, Oxford, (1959).

[15] R. Padilla, M. Minniti, D. Jaimes, J. Garman, D. Dunn-Rankin, and T.K. Pham, *Thin Filament Pyrometry for Temperature Measurements in Fuel Hydrates Flames and Non-premixed Water-Laden Methane-Air Flames*, Paper 070LT-0361, US Combustion Meeting, Park City, Utah, May 20-23, (2013).

[16] R.P. Warzinski, I.K. Gamwo, E.J. Rosenbaum, E.M. Myshakin, H. Jiang, N.J. English, and D.W. Shaw, *Thermal Properties of methane hydrate by experiment and modeling and impacts upon technolog*y, Proceeding fot he 6th International Conference on gas Hydrates, Vancouver, Canada, July 6-10, (2008).

[17] W. Waite, L.A. Stern, S.H. Kirbyl, W.J. Winters, and D.H. Mason, *Simultaneous determination of thermal conductivity, thermal diffusivity and specific heat in sI methane hydrate,* Geophysical Journal International, (2007), 169:767-774.

[18] E.J. Rosenbaum, N.J.Englishm J.K. Johnson, D.W. Shaw, and R.P. Warzinski, *Thermal conductivity of methane hydrate from experimental and molecular simulation*, Journal of Physical Chemistry B, (2007) 11:13194-13205.

[19] J.E.A. John, and W.L Haberman, *Introduction to Fluid Mechanics*, Prentice-Hall, Inc., Englewood Cliffs, New Jersey, second edition (1980), 305-308.

[20] S.R. Turns, *An introduction to Combustion Concepts and Applications*, McGraw Hill, third edition, 33-36.

[21] J.A. Abbondondola, E.B. Fleischer, K.C. Janda, *Propane Clathrate Hydrate Formation Accelerated by Xenon,* Journal of Physical Chemestry, (2009).

[22] Photograph courtesy of the U.S. Geological Survey.

[23] R. Padilla, V. Ricchiutti, S. Karnani, D. Dunn-Rankin, *Structure and extinction of water-laden methane/air non-premixed flames*, 3th International Symposium on Combustion, (August 2014), PROCI-D-13-01177R1.

[24] J. Botimer, P. Taborek, S. Karnani, D. Dunn-Rankin, *The effect of surfactant on the formation and combustion of methane hydrates*, APS March Meeting (2014), D34.00002.

[25] Image courtesy of the National Research Council of Canada.

[26] K. Kitamura, K. Nakajo, T. Ueda, *Proceedings of the Fourth International Conference on Gas Hydrates*, Yokohama, Japan, (2002).

[27] M. Iwata, T. Ueda, *Proceedings of the Fourth International Conference on Gas Hydrates*, Yokohama, Japan, (2002).

[28] Y. Nakamura, R. Katsuki, T. Yokomori, R. Ohmura, T. Ueda, *Proceedings of the Sixth International Conference on Gas Hydrates*, Vancouver, Canada, (2008).

[29] Y. Maruyama, M. Fuse, T. Yokomori, R. Ohmura, S. Watanabe, T. Iwasaki, W. Iwabuchi, T. Ueda, *Experimental investigation of flame spreading over pure methane hydrate in a laminar boundary layer*, Proceedings Combustion Institute. 34 (2013) 2131-2138.

[30] S. Takeya, T. Ebinuma, T. Uchida, J. Nagao, H. Narita, *Journal of Crystal Growth,* 237-239,379-382, (2002).

[31] T. Uchida, I.Y. Ikeda, S. Takeya, T. Ebinuma, J. Nagao, H. Narita, *Journal of Crystal Growth,* 237-239,383-387, (2002).

[32] V. Nakoryakov, S.Y. Misyura, S. Elistratov, A. Y. Manakov, and A. Shubnikov. *Journal of Engineering Thermophysics*, 22 (2): 87-92, 2013a.

[33] V. Nakoryakov, S. Y. Misyura, S. Elistratov, A. Y. Manakov, and A. Sizikov. *Journal of Engineering Thermophysics*, 22 (3): 169-173, 2013b.

[34] A. A. Trafimuk, N. V. Cherskiy, and V.P. Tsarev, *The gas-hydrate sources of hydrocarbons,* Priroda 1 (1979): 18-27.

[35] R. D. McIver, R.F. Meyer, and J.C. Olson, *Long Term Energy Resources*, Vol. 1 Pitman, Boston, (1981).

[36] Y. F. Makogon, *Perspectives for the oil and gas industry in the world. Gazovaya Promishlennost (Gas Industry)*, Moscow, Russia, (1984).

[37] J. S. Gundmundsson, A. Borrehaug, *Proceedings Second International Conference on "Gas Hydrates",* Toulouse, France, (1996), 415.

[38] K. J. Landa Research group, University of California, Irvine.

[39] Y. Park, D.Y. Kim, J.W. Lee, D.G. Huh, K.P. Park, J. Lee, and H. Lee, *Sequestering carbon dioxide into complex structures of naturally occurring gas hydrates*, Proceedings f the Natural Academy of Sciences, (2006).